Evaluation of infiltration efficiencies in vegetated swales through SWMM and single ring infiltrometer tests

- A numerical and field experimental study

Masters Thesis

Water and Environmental Engineering

Aalborg University

10TH of June 2022

Alex Arberg & Mathias Åbo Godskesen

AALBORG UNIVERSITY
STUDENT REPORT

Department of the Built Environment
Water and Environmental Engineering
Thomas Mannsvej 23
9220 Aalborg East

Title:

Evaluation of infiltration efficiencies in vegetated swales through SWMM and single ring infiltrometer tests

Project:

Masters Thesis

Project period:

February 1st - June 10th 2022

Project group:

aarber17@student.aau.dk

mgodsk17@student.aau.dk

Participants:

Alex Arberg
Mathias Åbo Godskesen

Supervisors:

Søren Liedte Thorndal - AAU

Co-supervisor:

Anders Badsberg Larsen - Niras
Jasper Vagner Jensen - Niras

Number of pages: 85
Appendix: 14
Ended: 10/06/2022

Abstract:

I dette afgangsspeciale undersøges infiltrationseffektivitet i trug. Trug benyttes ofte som anlæg til Lokal Afledning af Regnvand (LAR) og derfor i sammenhæng med andre LAR anlæg, blandt andet forsinkelse- eller nedsivningsbassiner. Under dimensioneringen af trug, som ofte anlægges med længdefald, medregnes infiltrationen af regnvand oftest ikke, da dette i den nuværende danske praksis ikke inkorporeres. Igennem projektforløbet er der udført enkelt-rings infiltrometer tests, hvor resultaterne fra disse inkluderes som inputparametre i den numeriske modellering. Den numerisk modellering er udført i programmet SWMM, som står for Storm Water Management Model. Numeriske simuleringer af både syntetisk og historisk regn benyttes til at undersøge overordnede infiltrationseffektiviter i et generelt model-setup, hvor der benyttes Hortons infiltrationsligning, samt til at undersøge de fysiske test-lokationer. Resultaterne indikerede at trug er effektive til at reducere hverdagsregnhændelser, som er målt i den historiske regnserie, hvor effektiviten var henholdsvis 42% i Marshalls Allé og 52% i Skjoldet. De viste yderligere at trug er ineffektive til at reducere syntetiske høj-intense regnhændelser, hvor effektiviteten var hendholdsvis 6,6%-7,4% i Marshalls Allé som blev modelleret med en 10-års 10-minutters regn, og 8,6%-10,9% i Skjoldet som blev modelleret med en 100-års 10-minutters regn. Resultaterne viser yderligere at inkluderingen af Hortons infiltrationsligning samt trugets længdefald påvirker den generelle infiltrationseffektivitet. Derfor foreslår forfatterne at en revurdering af den nuværende praksis er nødvendig baseret på de fremsatte resultater.

Table of Contents

Preface

This Master Thesis project was made as a 10^{th} semester project for Water and Environmental Engineering at Aalborg University, from the 1^{st} of February to the 10^{th} of June 2022. The central topic of this project is *Infiltration efficiencies in swales*. The report aims to investigate the infiltration loss in vegetative swales at two field locations of Marshalls Allé, Aalborg East and Skjoldet, Svenstrup South and evaluate the current swale dimensioning practice. The thesis structure is presented in Figure 1.

The authors would like to thank our supervisor, associate professor Søren Liedtke Thorndahl from the Department of the Built Environment, for his guidance and supervision during the project. Furthermore, we would like to thank our co-supervisors, Anders Badsberg Larsen and Jasper Vagner Jensen from NIRAS Aalborg, for their early input and constructive ideas for shaping our Master Thesis in the direction of problems discussed in practical engineering. We would also like to thank associate professor Franz Tscheikner-Gratl and PhD candidate Vincent Pons from the Department of Civil and Environmental Engineering at the Norwegian University of Science and Technology for their time and ideas for implementations and model setup in EPA SWMM 5.1. A special thanks to Kevin Casipillai at Ramboll for discussing and clarifying possible solutions of SWMM for model setup and data processing. Finally, a special thanks go to John Keller and Kristian Hougaard for making possible field measurements at Marshalls Allé and Svenstrup South.

The report utilises the Harvard Style referencing method. In this method, an associated reference is placed at the end of a sentence.

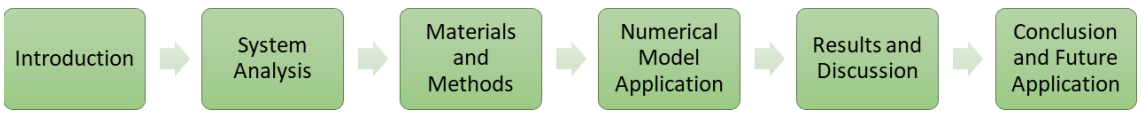

Figure 1. Flow diagram for the thesis structure.

Glossary of terms

CDS - Chicago Design Storm
EPA - Environmental Protection Agency
GSD - Grain Size Distribution
IPCC - Intergovernmental Panel on Climate Change
K - Hydraulic Conductivity
K_s - Saturated Hydraulic Conductivity
LID - Low Impact Development
OM - Organic Matter
RMSE - Root Mean Squared Error
SRI - Single Ring Infiltrometer
SuDS - Sustainable Drainage System
SVK - The Water Pollution Committee of The Society of Danish Engineers
SWMM - Storm Water Management Model
USDA - United States Department of Agriculture

Part I

Introduction

The following part introduces the concept of sustainable drainage systems and why they are highly used, focusing on vegetative swales. The current swale dimensioning practice is presented, highlighting strengths and weaknesses associated with a simplified dimensioning practice. A literature review of previous empirical swale infiltration studies is given to indicate the span of infiltration efficiencies, followed by the thesis statement of this master thesis.

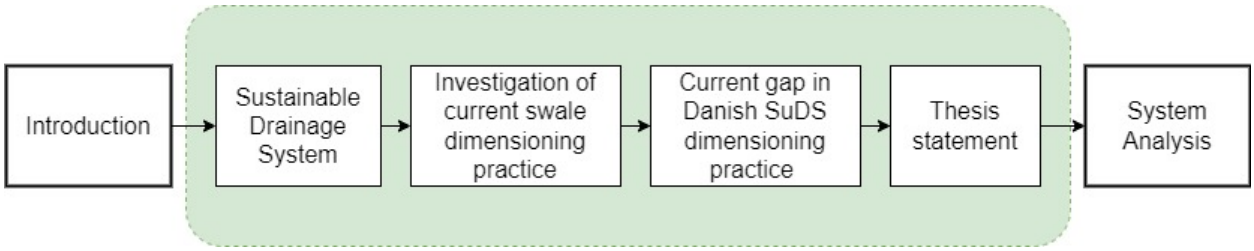

Sustainable Drainage System

1

Since the 1960s, urbanisation has led to approximately 90% of the Danish population being located within cities. Expanding cities pressure the existing drainage systems' capabilities since the systems have to handle larger volumes of waste- and rainwater, which potentially can exceed the dimensioned criteria. In addition to urbanisation, climate change is increasingly causing more extreme weather with longer dry periods and intense rainfall [Trenberth, 2011]. Based on the RCP 8.5 scenario from the latest report (AR6) from the Intergovernmental Panel on Climate Change (IPCC), the annual rainfall percentage will rise upwards of 10-20% by the year 2100, as seen in Figure 1.1 [EEA, cited January 2022].

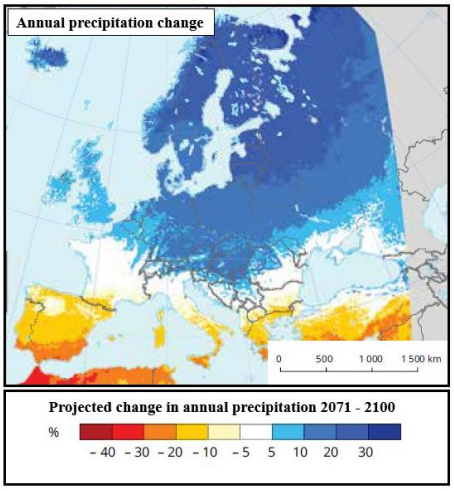

Figure 1.1. Annual percentage rain change towards 2100, based on the IPCC RCP 8.5 scenario.

Impervious surfaces within the urbanised landscape replace natural vegetation capable of infiltrating, delaying and storing rain, resulting in less evapotranspiration and infiltration, thereby increasing the total surface runoff as seen in Figure 1.2. The projected rise in estimated annual rainfall increases the requirements for capacity in existing drainage systems, resulting in overflow events degrading the water quality of recipients while increasing flooding events such as seen in the 2021 flash flood in the Rhineland-Palatinate region of Germany [Shafique et al., 2018; UN, cited January 2022]. Increased focus on measures of urban climate adaptation is required to encounter adverse urban water-related problems.

One method of urban climate adaptation is the application of Sustainable Drainage Systems (SuDS) or Low Impact Development (LID).

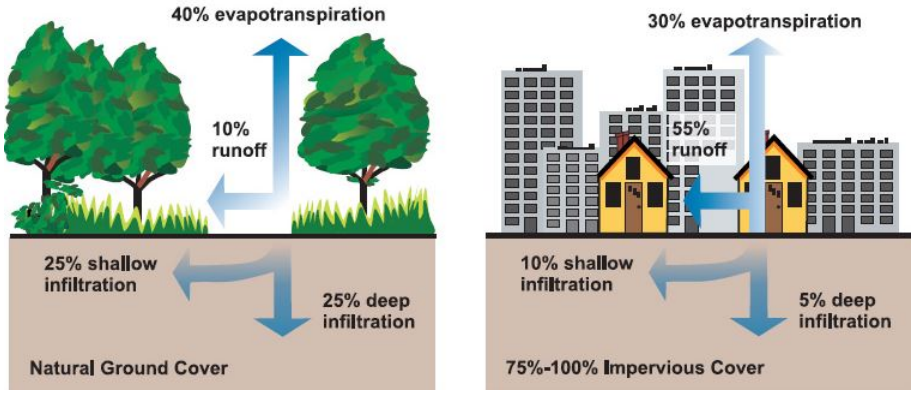

Figure 1.2. Result of bigger impervious areas in the urban areas. Edited from [United States Environmental Protection Agency, 2003].

The purpose of SuDS can be categorised into three primary purposes [Rujner et al., 2016]:

1. Convey urban runoff
2. Reduce runoff volumes and discharges by infiltration
3. Enhance runoff quality by filtration and settling

SuDS are often applied to one another, increasing the climate adaptation strategy for the given area. Mainly vegetative swales are applied for transporting surface water from one SuDs-element to the next.

1.1 Vegetative swales

Vegetative swales are typically a grass-covered depression implemented with the purpose of delaying, transporting and decreasing nonpoint source pollution from surface runoff water [Aalborg Kommune, Miljø- og Energiforvaltningen, 2016b; Rushton, 2001]. Swales are typically designed to contain water during rain events and drain within 2-3 days of the rain event through infiltration. A 10-year statistical rain event is the applied minimum for swale dimension but with a general expectancy of a 30-year event [Aalborg Kommune, Miljø- og Energiforvaltningen, 2016b,a]. The design of a swale can vary significantly from a simple excavated ditch to more complex designs with specific grain-size distributions of soil filter material such as sand gravel and drainage pipes (fig. 1.3).

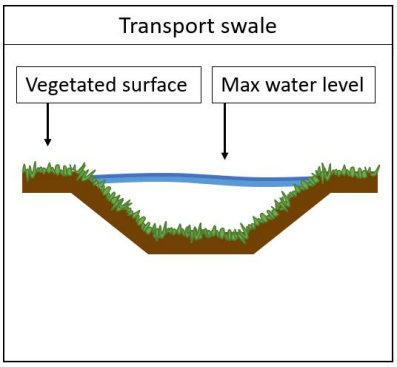

Figure 1.3. Depiction of a transport swale, excluding infiltration.

Precise dimensioning of swales to a certain dimension giving rain event is a challenge to execute in practice due to a variety of factors influencing the infiltration rate, such as:

- Rainfall intensity
- Soil water content
- Maintenance history
- Vegetative cover
- Longitudinal slope
- Erosion and sedimentation
- Groundwater table height
- Hydraulic conductivity

Especially the soil's ability to transport water, namely the hydraulic conductivity, is often applied as a direct measurement for determining the accumulated infiltration [Rawls et al., 1993]. The spatial variability in soil properties, such as the hydraulic conductivity, results in the saturated hydraulic conductivity being applied to describe the infiltration rate of the entire swale. This leads to varying accuracy in applied infiltration rate, due to unsaturated conditions dominating the swale system.

1.2 Investigation of current swale dimensioning practice

The current practice in Denmark when dimensioning vegetative swales is to dimension the swale as a detention basin with a constant seepage rate through the use of the SuDS dimensioning spreadsheet, created by The Water Pollution Committee of The Society of Danish Engineers (SVK) [Arnbjerg-Nielsen and Sørup, 2019]. The spreadsheet applies a statistical-box rain when dimensioning the required volume of a swale, applying a 20% increase in volume to the SuDS to account for coupled rain events. According to Gregersen et al. [2015], application of the SVK spreadsheet generally leads to well dimensioned SuDS. However, the general assumptions lead to systematic effects resulting in an overestimation of the actual required SuDS volume [Arnbjerg-Nielsen and Sørup, 2019]. Two main assumptions applied in the SVK spreadsheet are:

1. Constant seepage rate
2. 0% longitudinal swale slope

The combination of the two assumptions results in an inaccurate interpretation of the natural system, with varying seepage/infiltration rates, while implementing 0% slope results disregards water transport.

Therefore, an investigation of the current assumptions regarding swale slope and infiltration method is needed to determine the potential infiltration occurring within vegetated swales when implementing swale slope and water transport, as seen in Figure 1.4

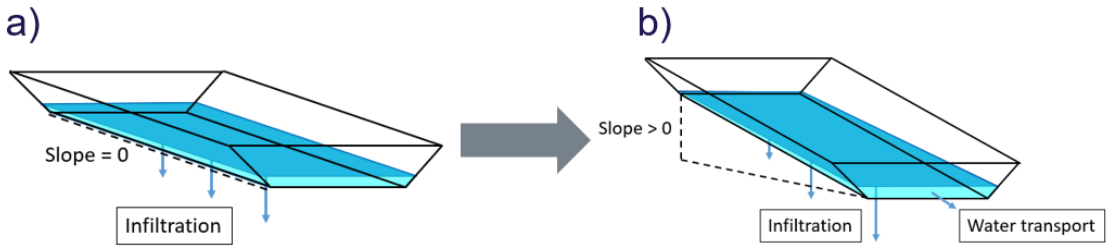

Figure 1.4. Conceptual understanding of a swale within the current practice of the SVK Spreadsheet (a), and a revised conceptual understanding of a swale.

1.3 Current gap in Danish SuDS dimensioning practice

Despite the general acceptance and application of the SVK spreadsheet, it is argued by the authors that the current practice applies an outdated modelling technique able to dimension simple SuDS; however, lacking the following abilities:

- Swale slope and therefore water transport
- Infiltration method including unsaturated and saturated conditions

The current application allows for a constant infiltration with no transport, resulting in 100% infiltration efficiencies and long emptying times when dimensioned in the SVK Spreadsheet. Previous research investigating the performance of grassed swales as an infiltration practice underlines that the assumption of 100% infiltration efficiency is invalid (tab. 1.1).

Table 1.1. Rainfall runoff volume reduction in percentage, from different grass swale systems and varying rainfall intensities.

Reference	Infiltration Efficiency (%)	Location
[Shafique et al., 2018]	40-75	Seoul, Korea
[Rushton, 2001]	33-87	Florida, USA
[Rujner et al., 2016]	40-55	Luleå, Sweden
[Davis et al., 2012]	59	Maryland, USA
[Jensen, 2004]	75	Copenhagen, Denmark

The considerable variance in infiltration rates and efficiencies results in uncertainties for decision-makers, such as consulting engineering firms, when applying an infiltration rate for the dimensioning and planning of vegetative swales. Weiss et al. [2010] therefore suggests that each swale investigated should be tested individually since a general relation is difficult to attain when determining the infiltration capacity of a swale. Numerical modelling is applied in many reaches of complex system analysis, however, within SuDS dimensioning, a simple practice is withheld. An investigation of swale infiltration efficiencies with the application of a numerical modelling program can increase the current practice's accuracy.

1.4 Choice of modelling program: Stormwater Management Model

In urban drainage modelling, rainfall-runoff and infiltration are typically estimated by coupling infiltration and surface runoff models. This can include the complex Richard's equation as an infiltration model, while more simplified infiltration models often are applied, such as the Horton's and Green-Ampt models. The simplified models are favoured due to their relatively simple parametric input while also requiring less computational power. The surface runoff models can be equally complex such as the Saint-Venant equations for two-dimensional surface flow. The fully dynamic Saint-Venant equations can be, however, computationally heavy requiring significant computational power, which is why a simplified surface runoff model such as the one-dimensional kinematic wave approximation often is applied [Nielsen et al., 2020].

The U.S. Environmental Protection Agency has developed a dynamic rainfall-runoff model allowing for simulations for single and long-term events. The Stormwater Management Model (SWMM) allows for the evaluation and implementation of LID controls, such as vegetative swales, capable of capturing surface runoff and providing detention, infiltration, and evapotranspiration. The LID module is applied to model and investigate infiltration effects by implementing a dynamic numerical model compared to the current SVK spreadsheet.

Currently, there is a gap in easily and readily usable models in the private sector of engineering firms, which ensures the dimension of swales as a SuDS while accounting for infiltration during water transport. Therefore, a revised proposal for a swale dimensioning practice is needed, resulting in a model more complex than the current SVK spreadsheet while still being applicable for practical engineering purposes.

Thesis Statement 2

The perception of swales being either a water transport system exclusively or capable of infiltrating all run-on is, in reality, invalid since a continuous infiltration process occurs. Varying infiltration rates are based on factors such as rain intensity, initial soil water content, hydraulic conductivity and swale slope. Including the infiltration process in swale dimensioning will, in principle, allow for smaller swale dimensions or connected SuDS.
In Denmark, however, local municipalities do not recommend including infiltration in swale dimensioning [Aalborg Kommune, Miljø- og Energiforvaltningen, 2016b]. This recommendation is based on the large, spatial and temporal variability in hydraulic conductivity.

This master thesis will therefore investigate:

How does the current practice of swale dimensioning, with the use of the SVK spreadsheet, compare to a fully distributed model in SWMM implementing swale slope and Horton's infiltration?

To advance the understanding of swale infiltration, single-ring-infiltrometer measurements are applied to evaluate a coupled surface runoff- and infiltration model, intended to represent a more accurate dimensioning practice than the current SVK spreadsheet. The Storm Water Management Model (SWMM) is applied to investigate the current neglection of water transport and the use of an infiltration method allowing for time-varying rainfall, infiltration models and Low Impact Development (LID) implementation.

The thesis statement will be investigated through the following questions:

- Is it possible to couple measured infiltration data with a model set up in SWMM, allowing to model both synthetic and historical rain and evaluate the current dimensioning practice based on infiltration efficiency?
- Can a general model setup in SWMM enable understanding of input parameters, allowing a revision of the current swale dimensioning practice?

Part II

System analysis

The following part is comprised of a thorough analysis and presentation of fundamental processes and natural parameters influencing infiltration in swales. Furthermore, relevant theory regarding infiltration models and a comparison of the Horton's and Green-Ampt method will be given. Finally, theory regarding modelling of water transport in swales is elaborated through the Saint Venant equations and Manning formula.

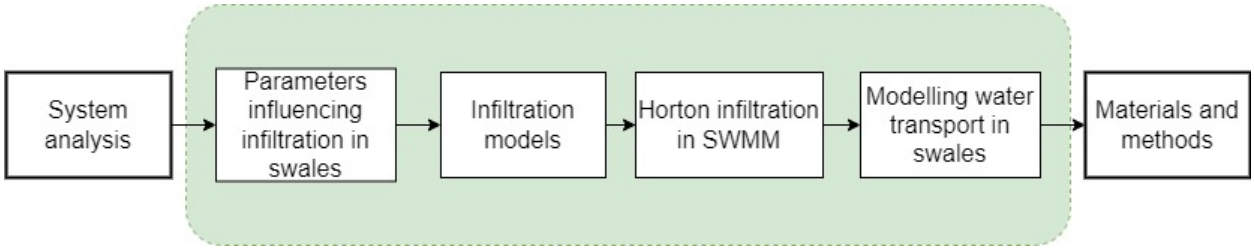

Parameters influencing infiltration in swales 3

Investigating influencing parameters on infiltration in swales can typically start by understanding rain and how different rain events affect infiltration. The duration and intensity of the rain event will govern infiltration over time. When investigating infiltration in swales, understanding local and spatial variability in soil properties is also a crucial parameter. The infiltration capacity depends on several morphological properties, such as the grain size distribution and volume fraction of water, air and solids. A commonly used descriptor of a soil's ability to transmit water, thus an indication of infiltration capacity, is the hydraulic conductivity correlated to the soil morphological properties and the soil water content.

In the following chapter, an elaboration of factors influencing infiltration in swales will be given, enabling a thorough understanding and capability to assess and interpret infiltration data.

3.1 Rainfall intensity

Generally, there is two types of rain. Synthetic rain and historically measured rain. Within synthetic rain two types commonly used is Box rain and Chicago Design Storm (CDS) rain. The three types of rain can be seen in the conceptual Figure 3.1.

Rainfall intensity is determined as the average rainfall rate for a specific duration and a known statistical return period. The historical rainfall intensity generally varies based on duration and return period; why a short historical rain will have a higher intensity than a long, given its the same statistical return period.

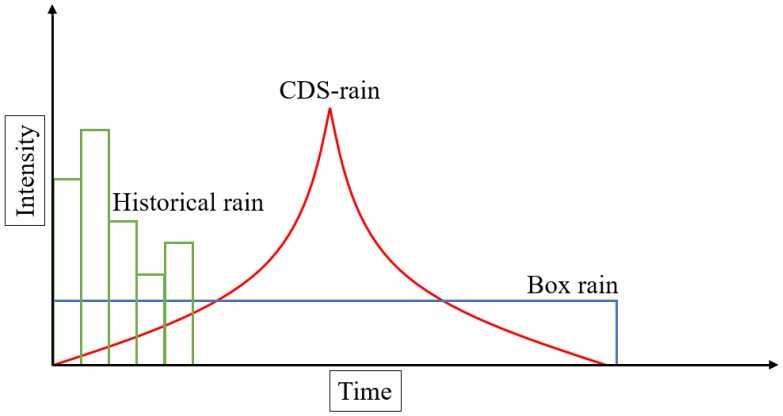

Figure 3.1. Conceptual figure showing different categories of rain, including historical rain series (green), CDS-rain (red) and box-rain (blue).

Historical rain series are measured rain events varying in intensity, reflecting the physical nature of rain, where the intensity depends on spatial and temporal variability. Historical rain series are often applied when cross-checking existing and planned SuDS and whether the SuDS will uphold a given service level, determined by an acceptable amount of overflows.

CDS rain or box rain is often used when dimensioning sewer systems or SuDS-elements. The constructed rain series has potential when historical rain series are too short, or no data is available [Winther et al., 2011]. They are often coupled with local climate factors that will simply enlarge the rain event with higher intensity overall. This climate projection factor is, however, a subject of great discussion and is being investigated on how to accurately climate project historical rain series [Winther et al., 2011,p. 277].

When dimensioning swales as transport swales without ongoing infiltration, the peak intensity of the dimension-giving rain will affect the size of the swale and, often, the SuDS element in conjunction. However, peak flow and total volume decrease when incorporating infiltration.

3.2 Soil Morphology

Generally, the most conductive soils at saturation are those in which large and continuous pores constitute most of the overall pore volume. In contrast, the least conductive are the soils in which the pore volume consists of numerous micropores (<30 µm) [Loll and Moldrup, 2000]. Characterisation of the soil is therefore helpful to properly understand infiltration in swales.

An experimental method of characterising the soil can be conducted via grain size distribution (GSD). Through GSD, soil particle size classes are defined to investigate the soil composition which highly influences the saturated hydraulic conductivity and allows an understanding of the soil composition of sand, clay and silt [Loll and Moldrup, 2000,page 5] as seen in Figure 3.2.

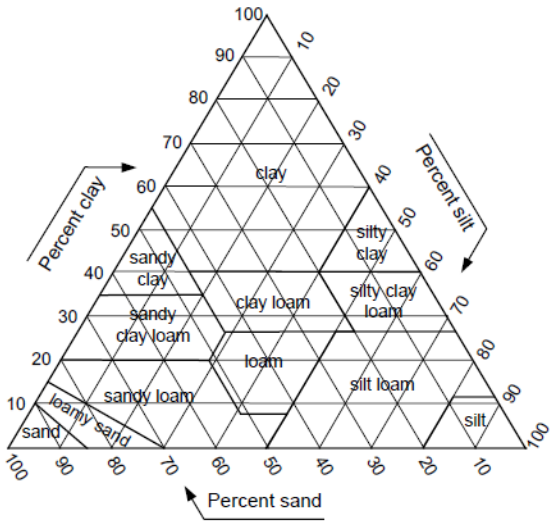

Figure 3.2. Textural triangle defining soil textural classes Loll and Moldrup [2000].

Furthermore, a soils organic matter (OM) content should also be investigated. The OM has a similar size to clay particles and has a substantial ability to retain water in the soil. OM can hold upwards of 5 times the water compared to clay minerals. This is caused by its surface charge, altering the soil structure and creating soil pores increasing the saturated hydraulic conductivity and thereby infiltration rate. [Loll and Moldrup, 2000].

Another process influencing the pore composition is aggregation. Aggregation occurs, e.g. when the soil dries out, causing the soil to "draw close" to the remaining water, creating bigger pores, called macropores [Loll and Moldrup, 2000]. Macro pores are often a term used to characterise pores in the range of 30 - 3000 µm. Likewise, the macropores can also be created from plant roots dwindling or animals burrowing through the soil [Loll and Moldrup, 2000]. Changes in soil structure will affect the soil volume ratio of solids, air and water, thus the infiltration capacity.

3.2.1 Soil as a three phase system

Considering the soil as a three phase system (fig. 3.3), it can be divided into three specific parts, consisting of:

- Water
- Air
- Solids

A soil's infiltration capacity is determined by the volume ratio of water, air, and solids. Depending on the soil composition an unsaturated soil with little water content will infiltrate larger volumes of water than saturated soil. This is caused by the air filled pores within the unsaturated soil being filled with infiltrating water initial, resulting in an initial infiltration rate. As the soil matrix becomes saturated, the infiltration rate reaches the infiltration capacity.

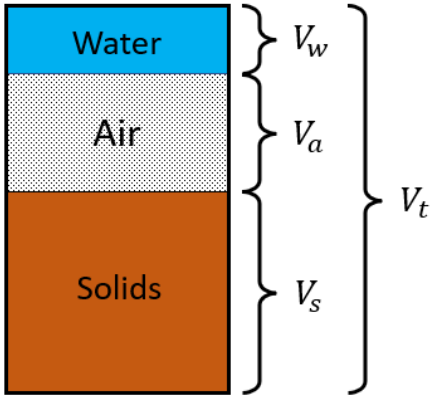

Figure 3.3. Figure showing the three parts of soil. The volume of water is denoted by V_w, the volume of air by V_a, the volume of solids by V_s, while the total soil column is denoted by V_t. Modified from [Loll and Moldrup, 2000]

Characterisation of the soil phase system, is done based on soil bulk density (eq. 3.1), porosity (eq. 3.2), and water content (eq. 3.4).

Dry bulk density expresses the ratio of mass to volume. It greatly depends on soil structure, with higher bulk densities being observed with increasing depth as a result of compaction [Loll and Moldrup, 2000].

$$\rho_b = \frac{M_s}{V_t} \tag{3.1}$$

Where,

ρ_b	dry bulk density	$[g \cdot cm^{-3}]$
M_s	Mass of solids	$[g]$
V_t	Total volume	$[cm^3]$

Construction of swales will often be affected by these phenomena caused by the construction phase, where industrial machines alter the soil structure, e.g. as a result of compression.

The bulk density is found to determine a soil sample's porosity, which is the remaining fraction of the soil volume.

The porosity is an essential soil parameter in infiltration since it is the percentage of void space within the soil column.It is the volume in which water and air are trapped and thus contributing to water transport during saturated conditions. The porosity of the soil can be determined by the intact samples used for bulk density and is shown in equation 3.2.

$$\phi = 1 - \frac{\rho_b}{\rho_s} \tag{3.2}$$

Where,

ϕ	Porosity	$[cm^3 \quad \text{pores} \cdot cm^{-3} \quad \text{soil}]$
ρ_b	Dry bulk density	$[g \cdot cm^3]$
ρ_s	Mean bulk density	$[g \cdot cm^3]$

If a direct method for the porosity determination is not available, an indirect approach can be applied.

3.2.2 Indirect method for porosity using grain size distribution

An indirect method for estimating the porosity using the uniformity coefficient from the GSD can be applied, as seen in equation 3.3. Equation 3.3 was found after extensive analysis and proved accurate for sandy sediments [Blohm, 2016]. The uniformity coefficient describes the relation between d_{10}, which is the diameter of the 10^{th} lowest percentile obtained from GSD and the d_{60}, which is the diameter of the 60^{th} percentile in the GSD.

$$\phi = 0.255 \cdot (1 + 0.85^U) \tag{3.3}$$

Where,

U	Uniformity coefficient	[-]

The physical phase distribution of particles, water and air directly influences the hydraulic conductivity, e.g., if a soil consists of 40% particles, water can only flow in the remaining 60%. The most conductive soils at saturation are those in which large and continuous pores constitute most of the overall pore volume. In contrast, the least conductive are soils consisting of numerous micropores. A soil's ability to transmit water is thereby affected by the total porosity [Loll and Moldrup, 2000].

3.2.3 Soil moisture

In relation to swale dimensioning and infiltration calculations, soil moisture is a key parameter. As seen in equation 3.4, the soil moisture, or relative water content depends on the volumetric water content.

$$\theta = \frac{V_w}{V_t} \tag{3.4}$$

Where,

θ	Water content	$[cm^3 \ \text{H}_2\text{O} \cdot cm^{-3} \ \text{soil}]$
V_w	Volumetric water content	$[cm^3 \ \text{H}_2\text{O} \cdot cm^{-3} \ \text{soil}]$
V_t	Total volume	$[cm^3 \ air \cdot cm^{-3} \ soil]$

Initial soil water content is essential to include when modelling infiltration since the infiltration rate will vary depending on the initial water content. If the soil is near

saturation at the start of a rain event, runoff will occur substantially quicker than if the soil is completely dry.

Varying soil water content is not applied in the current dimensioning practice of swales, which applies saturated conditions. The neglection of an initially higher infiltration rate is thereby omitted, potentially resulting in an underestimation of the accumulated infiltration. The application of soil water content for the determination of varying hydraulic conductivities should therefore be incorporated in a swale dimensioning practice.

3.3 Hydraulic conductivity

One of the most commonly used parameters applied in soil science and infiltration modelling is the hydraulic conductivity [Rawls et al., 1993]. In the following sections, the hydraulic conductivity will be elaborated upon.

3.3.1 Darcy's law

Darcy's law describes how water flow occurs in the direction of decreasing potential energy levels, with the water flux being proportional to the energy gradient. The proportionality factor between flux and energy gradient is the hydraulic conductivity, and the hydraulic gradient is expressed as the change in head over a given flow length. Darcy's law is thereby only dependent on the pressure difference, with an assumption of constant permeability and steady flow conditions [Rawls et al., 1993].

Saturated hydraulic conductivity

During saturated soil conditions, the main driving force for infiltration is gravity. The composition of the soil will also directly impact the saturated hydraulic conductivity, and thereby the infiltration of water through the soil, as seen in equation 3.5.

$$v = -K_s \cdot \frac{\Delta H}{\Delta l} \tag{3.5}$$

Where,

v	Darcy velocity	$[m \cdot s^{-1}]$
K_s	Saturated hydraulic conductivity	$[m \cdot s^{-1}]$
ΔH	Pressure difference	$[m]$
Δl	Length difference	$[m]$

Darcy's law is originally applied for saturated sandy soil, but can also be used to describe water flow in unsaturated soils.

Unsaturated hydraulic conductivity

In unsaturated soils, the hydraulic conductivity is not a constant but increases rapidly with increasing water content, thus becoming a function of the water content or pressure potential (suction). Sandy soils, which drain more rapidly, will thus show a more significant decrease in hydraulic conductivity with decreasing water content than, e.g. clay related to

the large pores (>30 µm) draining first. During unsaturated soil conditions, gravity's influence on infiltrating water becomes minimal, while suction is the driving force of infiltration.

$$v = -K \cdot (\frac{d\psi}{dz} - 1) \tag{3.6}$$

Where,

v	Darcy velocity	$[m \cdot s^{-1}]$
K	Unsaturated hydraulic conductivity	$[m \cdot s^{-1}]$
$d\psi/dz$	Hydraulic gradient	$[m \cdot m^{-1}]$

The Darcy equations presented above can estimate the hydraulic conductivity through direct methods, such as infiltrometer tests. The distinction between direct and indirect methods will be presented in the following.

3.3.2 Direct and indirect methods for determining hydraulic conductivity

The hydraulic conductivity should preferably be estimated through direct methods such as infiltrometer tests or constant head setup using intact soil samples in the laboratory. Ahmed et al. [2015] observed the spatial variability of the saturated hydraulic conductivity to vary two orders of magnitude, within the same test section alone, based on infiltrometer tests.

Multiple in-situ experiments, therefore, give a more accurate estimate of the hydraulic conductivity since such methods apply the soil intact, investigating the natural soil texture and morphological properties. Typical ranges of the saturated hydraulic conductivity from different soil textural classes is seen in Table 3.1, highlighting the uncertainty of applying a single saturated hydraulic conductivity value when describing a complex system with varying conditions.

Table 3.1. Typical ranges of saturated hydraulic conductivity given for soil texture classes [Loll and Moldrup, 2000,p. 36].

Soil texture	K_s range $[m \cdot s^{-1}]$
Gravel	3E-04 - 3E-02
Coarse sand	9E-07 - 6E-03
Medium sand	9E-07 - 5E-04
Fine sand	2E-07 - 2E-04
Silt	1E-09 - 2E-05
Clay	1E-11 - 4E-09

Such empirical formulae estimating the hydraulic conductivity as a function of grain size include USBR, Kozeny-Carman and the Nielsen model, seen in Table 3.2 [Carrier, 2003; Nielsen et al., 2018].

The saturated hydraulic conductivity model should always depend on the available input parameters regarding the soil of investigation. Parameters known to influence the saturated

hydraulic conductivity should therefore be applied, if known, to estimate a more accurate value than a model which does not include said parameter.

Models such as USBR and Kozeny-Carman are two classical models regularly applied for sandy soils when determining the saturated hydraulic conductivity. The idea behind a more complex model, such as the Nielsen model, is to apply the total porosity to account for soil compaction, which reduces the saturated hydraulic conductivity and OM, which may contribute to higher saturated hydraulic conductivity [Nielsen et al., 2018]. Criteria regarding the empirical equations region of validity also determine the choice of the saturated hydraulic conductivity model. Further description of the empirical equations is given in Appendix E.

Table 3.2. Presentation of three empirical saturated hydraulic conductivity models and their region of validity.

Method	Equation	Intended use
USBR [Blohm, 2016]	$K_s = \beta \cdot \frac{g}{v} \cdot d_{20}^{2.3}$	U < 5 $0.06mm \leq d_{10} \leq 2mm$
Kozeny-Carman [Carrier, 2003]	$K_s = \beta \cdot \frac{\rho g}{u} \cdot \frac{n^3}{(1-n)^2} \cdot d_{10}^2$	$d_{10} \leq 3mm$ Silts, sands, and gravelly sands
Nielsen [Nielsen et al., 2018]	$K_s = A \cdot \phi \cdot (\frac{CS+B \cdot FS}{CL+R_D \cdot OM})_{NC}^{P}$	Only valid for very sandy soils with $< 10\%$ fine particles (clay + OM)

A drawback of applying the saturated hydraulic conductivity models is the considerable uncertainty associated with simplifying a complicated system with varying conditions, such as the soil matrix, as described previously with the magnitude of difference in the saturated hydraulic conductivity. This is because swales are designed to drain within 2-3 days, resulting in the infiltration being governed mainly by the unsaturated hydraulic conductivity during smaller rain intensities [Aalborg Kommune, Miljø- og Energiforvaltningen, 2016b]. The transition from unsaturated to saturated conditions is often hard to determine accurately, and soils will often be somewhere between these conditions, depending on rain and weather prior to measurement.

3.4 Wetted Perimeter

When dimensioning swales exclusively or partly for infiltration, the drainage period prolongs over time as the infiltration area decreases with lowering water level (fig. 3.4).

As swales are often designed for transportation along the longitudinal slope, water will naturally run 'downstream' while simultaneously infiltrating, affecting the max water level caused by water transportation. In the SVK spreadsheet, a constant infiltration area equal to the total surface area of the swale is assumed. This application of a constant wetted perimeter is, as such, incorrect and will lead to wrongful accumulated infiltration estimates in swales when utilising the SVK spreadsheet.

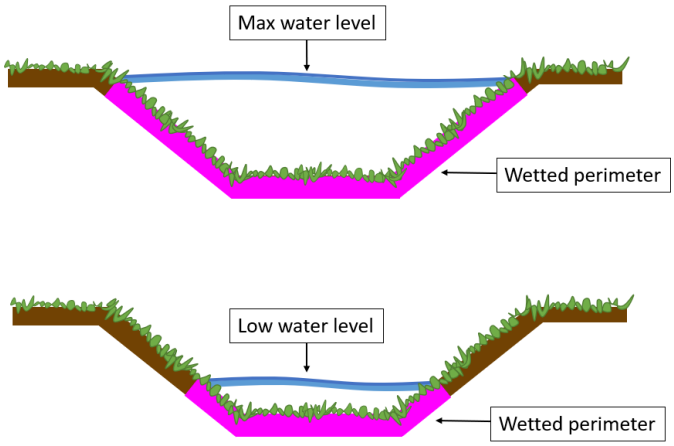

Figure 3.4. The effect of water level in regards to the wetted perimeter in the cross section of a swale. The wetted perimeter will decrease with decreasing water level.

The wetted perimeter fluctuates based on the current water level in the swale, which directly influences the overall area in which infiltration can occur. The accumulated infiltration in a swale depends on the total wetted area and is also influenced by physical soil properties, which determine the infiltration capacity. The following section will elaborate on parameters influencing the infiltration capacity, such as soil morphology, soil matrix composition, and soil water content. This is done to establish how varying soil conditions affect a swale's ability to infiltrate rainwater.

3.4.1 Swale Slope

The longitudinal swale slope affect water velocity, thereby indirectly the infiltration. Fox et al. [1997] conducted experiments trying to determine the relationship between slope and infiltration rate in soil and had conducted a 'meta-study' of articles and investigations to establish knowledge of previous fieldwork investigating slope and infiltration rate. Fox et al. [1997] found a decrease in infiltration as a result of an increase in slope in their experimental analysis.

Similarly, in the meta-study they carried out, reports had also been published, stating no relationship between slope increase and infiltration rate change. They did, however, report studies which had found contradicting results, stating the infiltration increases with increasing slope. Fox et al. [1997] introduced the effect of rilling on topsoil as the reason for increased infiltration with a slope angle increase.

The article by Fox et al. [1997], generally highlights the uncertainties related to the relationship between slope angle and infiltration rate change in the real world, as soil parameters also vary greatly, which may affect infiltration in different soils.

When modelling infiltration in swales using a modelling program, the slope effect can be isolated, indicating what impact the increase of slope in swales could have when constructing swales with SuDS purposes.

3.5 Infiltration stages

The infiltration process can be divided into infiltration behaviour stages (fig. 3.5), describing the decline in infiltration capacity when a rainfall intensity (I) occurs over the soil with a saturated hydraulic conductivity, and an infiltration capacity (f_c).

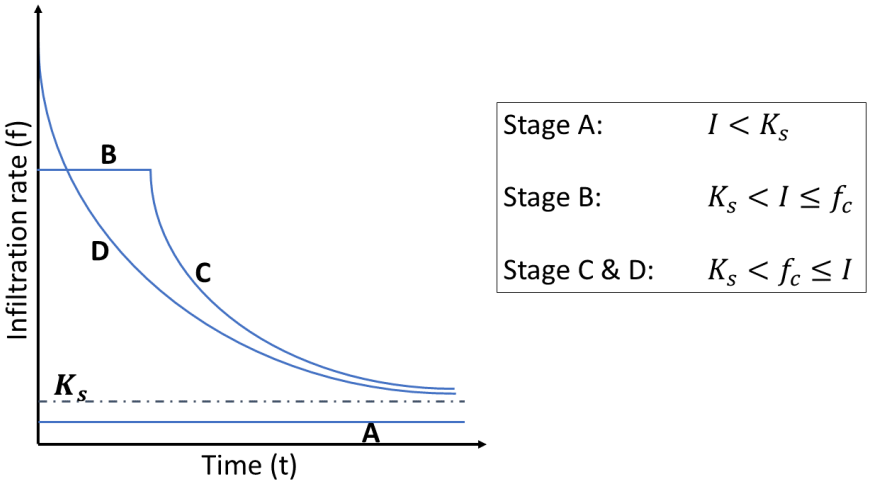

Figure 3.5. Description of infiltration stages, based on Mein and Larson [1973].

An initial period occurs during most rainfall events where all rainfall infiltrates the soil (stages A & B). The infiltrating water volume decreases the soil's ability to infiltrate water until the infiltration rate reaches the infiltration capacity or hydraulic conductivity (stages C & D). Stage D assumes ponded water at time 0, not accounting for stage B. Curve D is how the empirical Horton infiltration model describes the infiltration rate over time, as compared to the combination of curves B and C, such as the physical Green-Ampt infiltration model [Mein and Larson, 1973]. The dotted line corresponding to the saturated hydraulic conductivity represents a constant seepage infiltration rate or seepage rate, such as the SVK spreadsheet utilises.

The infiltration rate decreases from the onset of rain event, when the rainfall event exceeds the infiltration rate, until infiltration capacity is reached. An increase in infiltration rate can, however, also occur during dry periods.

3.5.1 Recovery of infiltration rate

Regeneration of the infiltration capacity naturally occurs as the soil water content decreases until the next rain event. The time of drainage varies dependent on soil texture, structure and weather conditions [Rossman, 2016a]. The water retained after drainage, held with soil micropores, is termed field capacity and represents the soil's maximum water-holding capacity.

Fully understanding soil drainage is complex and often varies depending on local variability in soil structure and weather conditions. A conceptual illustration of the infiltration capacity regeneration, as a function of time, can be seen in Figure 3.6, where the dry period in between rain events will lead to an increase in infiltration capacity.

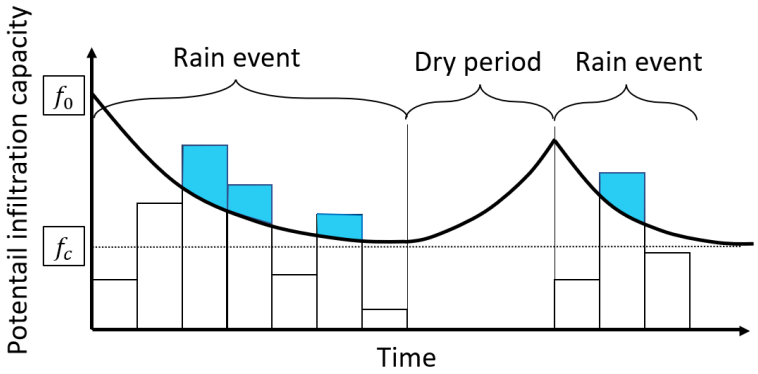

Figure 3.6. Conceptual figure illustrating regeneration of infiltration capacity in dry periods.

The implementation of soil regeneration within infiltration models is important when modelling and analysing infiltration in swales, due to the potential infiltration capacity being directly influenced by antecedent soil moisture. The effect of soil moisture therefore influences the accumulated infiltration, resulting in varying total infiltration volumes for corresponding rain intensities (fig. 3.6).

Mathematical descriptions are the basis of numerical models applying infiltration equations in varying complexity. In the following chapter, the Horton and Green-Ampt infiltration models are presented to understand the implementation of infiltration in numerical hydrologic simulations.

Infiltration models 4

Infiltration models describe the infiltration of water into the soil column based on varying complexity and input parameters, ranging from physical to fully empirically based models. Most infiltration models are derived from the complex Richard's equation, which is a partial differential equation describing one-dimensional vertical flow in an unsaturated soil [Rawls et al., 1993]. The complexity of Richard's equation is beside the chosen modelling tool capabilities and project purpose, which is why less complex models are applied for describing infiltration capacities. The general computational scheme of the infiltration models applied can be seen in Figure 4.1.

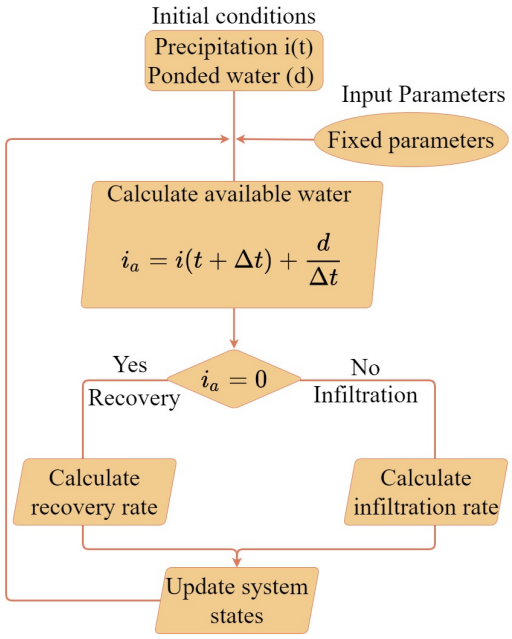

Figure 4.1. General computational scheme applied by SWMM for solving infiltration equations. i_a is the available water and i is the rain. Modified from Parnas et al. [2021].

In the following section, a brief description of the Horton's and Green-Ampt infiltration models is presented. A comparison of the model and application is given to determine an infiltration model for the purpose of investigating swale infiltration efficiencies. Finally a detailed description of the chosen model is given and how it is implemented in SWMM.

4.1 Horton's infiltration

Horton's infiltration describes the reduction in infiltration capacity of a soil over time and is described in equation 4.1 [Rossman, 2017; Winther et al., 2011]. The parameter values in Horton's infiltration equation are based on empirically collected data, such as infiltrometer tests, thereby disregarding any physical significance to soil parameters. Horton infiltration is based on the assumption that the equation is only applicable if the rainfall intensity exceeds the infiltration capacity.

$$f_p = f_c + (f_0 - f_c) \cdot e^{-k_d \cdot t_p} \tag{4.1}$$

Where,

f_p	Potential infiltration capacity	$[m \cdot s^{-1}]$
f_c	Saturated infiltration capacity	$[m \cdot s^{-1}]$
f_0	Initial infiltration rate	$[\mathrm{m} \cdot s^{-1}]$
k_d	Decay constant of the infiltration	$[s^{-1}]$
t_p	Time	$[s]$

The concept of Horton's infiltration is highlighted in Figure 4.2, where infiltration and runoff volume is seen.

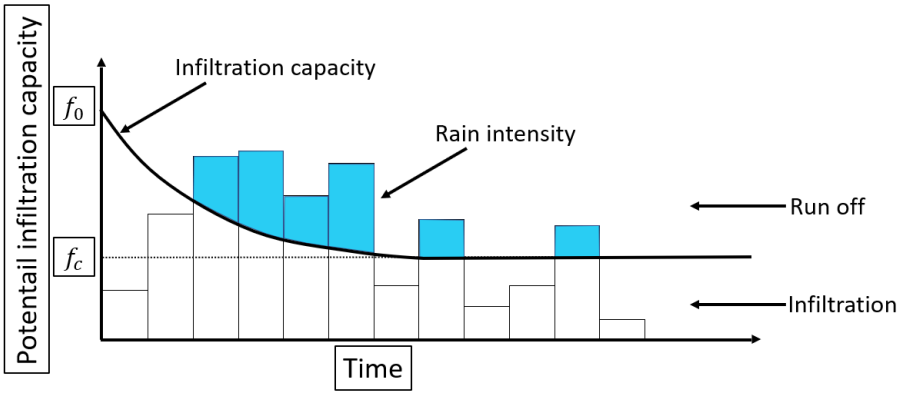

Figure 4.2. Conceptual model of Horton's infiltration, based on potential infiltration capacity and elapsed time.

Infiltration begins with the initial infiltration rate (f_0) decreasing towards the infiltration capacity (f_c). Rain with intensities higher than infiltration capacity will thus result in runoff from permeable areas. If the rainfall intensity does not exceed the infiltration capacity, the decay in infiltration capacity will follow the same decay rate, regardless of rainfall intensity resulting in a small rain intensity reducing the infiltration capacity equally as a large rain intensity would.

4.2 Green-Ampt infiltration

The Green-Ampt model developed for ponded infiltration into a homogeneous soil with uniform initial water content is derived from Darcy's law [Rawls et al., 1993]. The method is based on a physically-based model allowing coupling of physical soil parameters to

describe the infiltration process, compared to the Horton's method [Rawls et al., 1993]. Green-Ampt infiltration can therefore be applied to determine the potential infiltration in varying soil types as a function of the saturated hydraulic conductivity, capillary suction (ψ_{wf}) and the initial moisture deficit.

The Green-Ampt equation is based on several assumptions, including piston flow, sharp wetting front in the soil, a homogeneous soil, constant soil water potential at the wetting front and a uniform saturation in the wetted zone. Some of these assumptions are illustrated in Figure 4.3, where a conceptual model of the Green-Ampt infiltration is shown.

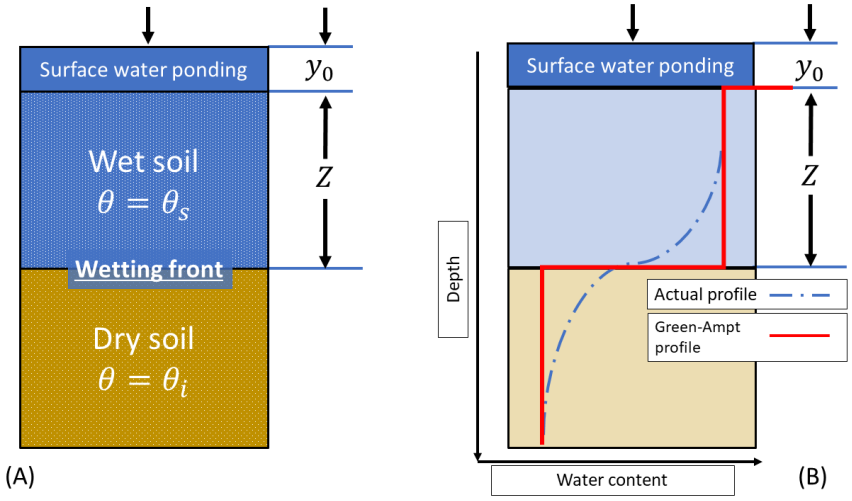

Figure 4.3. (A) Conceptual model of Green-Ampt model, modified from Rawls et al. [1993]. (B) Infiltration profile for the Green-Ampt model, modified from Kale and Sahoo [2011]. θ_s is the saturated water content while θ_i is the initial water content (dry conditions).

The revised formulation of Green-Ampt developed by Mein and Larson [1973] expressing a two-stage infiltration model during a constant rainfall event, including surface delay effects during infiltration [Mein and Larson, 1973]. The Green-Ampt-Mein-Larson model applies two equations for describing infiltration (eq. 4.2 and 4.3). Equation 4.2 computes the potential infiltration before saturation, and equation 4.3 describes infiltration at soil saturation. In SWMM the two equations are basis for determining if saturation has occurred with an increasing time increment. This is solved by equation 4.3, with the potential infiltration equal to the rainfall rate, to validate if the value exceeds the actual cumulative infiltration (F).

$$f_p = K_s[1 + \frac{\psi_s \, \theta_d}{F}] \tag{4.2}$$

Where,

f_p	Potential infiltration	$[m \cdot h^{-1}]$
K_s	Saturated hydraulic conductivity	$[m \cdot h^{-1}]$
ψ_s	Soil-water potential at wetting front	$[m\ H_2O]$
θ_d	Initial moisture deficit $(\theta_s - \theta_i)$	$[m^3\ soil \cdot m^{-3}\ H_2O]$
F	Cumulative infiltration	$[m]$

$$F_s = \frac{K_s \, \psi_s \, \theta_d}{i - K_s} \tag{4.3}$$

Where,

F_s	Potential infiltration at saturation	$[m]$
i	Rainfall rate	$[m \cdot h^{-1}]$

Estimates for the saturated hydraulic conductivity and ψ_{wf} have been collected from measurements of approximately 5000 soils in the United States by Rawls et al. [1993], which are widely applied in modelling programs such as SWMM [Rossman, 2016a]. An empirical relation (eq. 4.4) for calculating the suction head has been used. The relation is based on nonlinear regression from average values of Rawls et al. [1983] for the determination of the suction head by its relation with the hydraulic conductivity, presented in Appendix D.

$$\psi_s = 0.0016 \cdot K_s^{-0.327} \qquad (R^2 = 0.89) \tag{4.4}$$

Where,

ψ_s	Capillary suction at wetting front	$[m]$
K_s	Saturated hydraulic conductivity	$[m \cdot s^{-1}]$

4.3 Infiltration efficiency comparison

The following results highlight the discrepancy between the Horton's and Green-Ampt infiltration methods. The results are based on two swales, each with a connected road in conjunction. The swale and road properties such as area, width and slope are identical according to values presented in Table 4.1. The only difference is the choice of infiltration method.

Table 4.1. Applied standard values for the model setup in SWMM for road and swales.

Subcatchment values	Road	Swale
Area $[m^2]$	300	75
Width [m]	50	1.5
Slope [%]	2.5	0.5

Values applied for the comparison of Horton's and Green-Ampt infiltration methods are based on values presented in Table 4.2. Average values obtained from three swale sections at Marshalls Allé are applied as Horton input parameters. Applied input Green-Ampt values correspond to average saturated hydraulic conductivity from Marshalls Allé, suction is based on the determined power function relating the saturated hydraulic conductivity and suction (app. D). Finally, the soil moisture deficit is obtained from a standard soil value corresponding to sandy soil from Rossman [2016a].

Table 4.2. Applied standard values for the model setup in SWMM for Horton's and Green-Ampt infiltration method. Average values are applied from measured values at Marhslls Allé.

Horton's parameters			**Green-Ampt parameters**		
f_c	8.8E-06	$[m \cdot s^{-1}]$	K_s	8.8E-06	$[m \cdot s^{-1}]$
f_0	6.6E-05	$[m \cdot s^{-1}]$	ψ	0.071	$[m]$
T_d	2.79	$[h^{-1}]$	θ_d	0.34	$[/]$
k_d	3.36	$[/]$			

In general, it can be observed that the Horton infiltration produces higher infiltration peak values compared to the Green-Ampt method (fig. 4.4). Horton infiltration produces higher infiltration values during low rain intensities compared to the Green-Ampt method since rain intensity needs to exceed the infiltration capacity for Horton's method. The Horton's decay rate remains constant regardless of the rainfall intensity, resulting in higher infiltration values (fig. 4.4). Despite the Green-Ampt method having lower infiltration rate peaks, the total infiltration time for Green-Ampt exceeds the Horton infiltration, thus resulting in a total infiltrated volume closely corresponding to the Hortons.

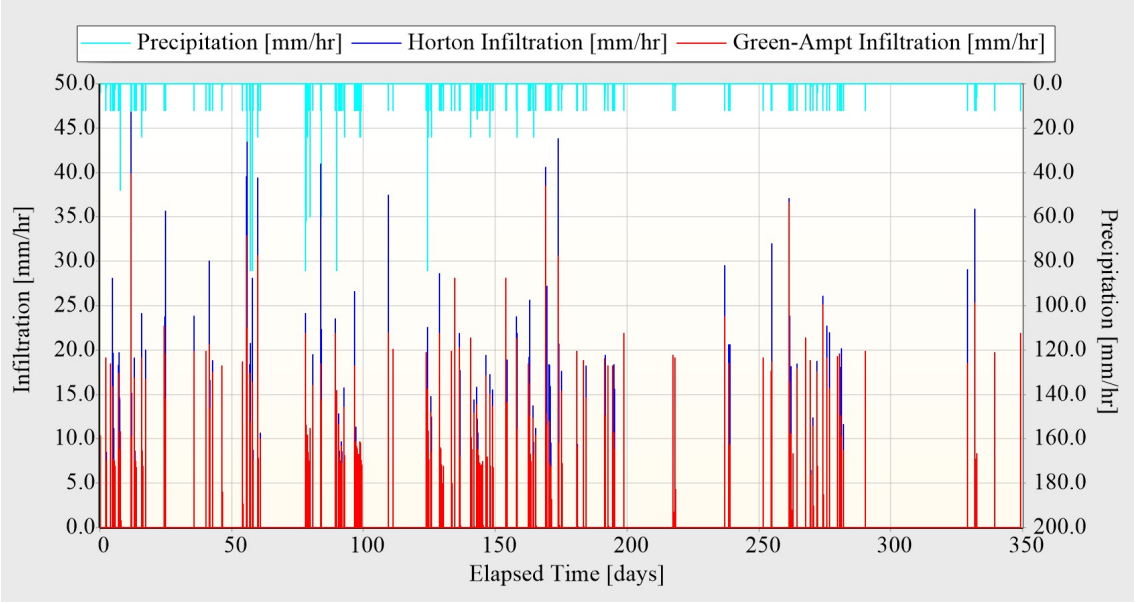

Figure 4.4. Comparison of the Horton's (blue) and Green-Ampt (red) infiltration method, based on a 1-year historic rain series (light blue).

From Table 4.3 the infiltration efficiencies for each infiltration method are compared based on a 1- and 10-year historic rain period from the Svenstrup series. Despite Horton's producing higher infiltration rates, a discrepancy of approximately 2% points in infiltration efficiencies for both events for Green-Ampt and Horton are observed.

Table 4.3. Runoff coefficient for Horton's and Green-Ampt infiltration method. Results are based on a 1 and 10-year historic event.

Infiltration efficiency	**1-year**	**10-year**
Swale (Horton infiltration)	67.7%	71.4%
Swale (Green-Ampt infiltration)	65.6%	69.6%

The difference in infiltration efficiencies between the two methods can not be determined to arise from a methodical or input variation. Further investigation requiring calibration and validation data would be required, to determine such discrepancies. The input values applied for the Green-Ampt model only relate to the calculated saturated hydraulic conductivity, where an empirical relation has been used for the determination of suction and the soil moisture deficit, increasing the uncertainty of fitting input values for describing the swales of investigation.

Horton's method is argued of being a more practical approach than Green-Ampt, based on minimum input requirements, yet increasing complexity in infiltration description compared to current the practice. The initial investigation of swale infiltration performance for Horton's and Green-Ampt infiltration, indicate a minimal variation in total infiltration, why the Horton's infiltration model has been chosen for further analysis when modelling infiltration for two field locations.

Horton infiltration in SWMM

5

Within the original Horton's method, the actual infiltration is determined as the minimum value of the infiltration capacity or rainfall intensity (eq. 5.1). Within the SWMM model setup the actual infiltration will be the minimum value of the infiltration capacity or runoff from the roadside plus the rainfall intensity.

$$f(t) = min[f_p(t), i(t)] \tag{5.1}$$

Where,

$f(t)$	Actual infiltration	$[m \cdot s^{-1}]$
i	Rainfall intensity	$[m \cdot s^{-1}]$

SWMM, which applies an integrated form of Horton's equation, calculating the cumulative infiltration capacity, instead of an infiltration rate to account for the of constant decay regardless of rainfall intensity (eq. 5.2).

$$F(t_p) = \int_0^{t_p} f_p \, dt = f_c \cdot t_p + \frac{(f_0 - f_c)}{k}(1 - e^{-k_d t_p}) \tag{5.2}$$

Where,

$F(t_p)$	Cumulative infiltration capacity at time t_p	$[m]$

The implementation of equation 5.2 can be visualised in Figure 5.1, with the cumulative infiltration capacity (F) at time t_p.

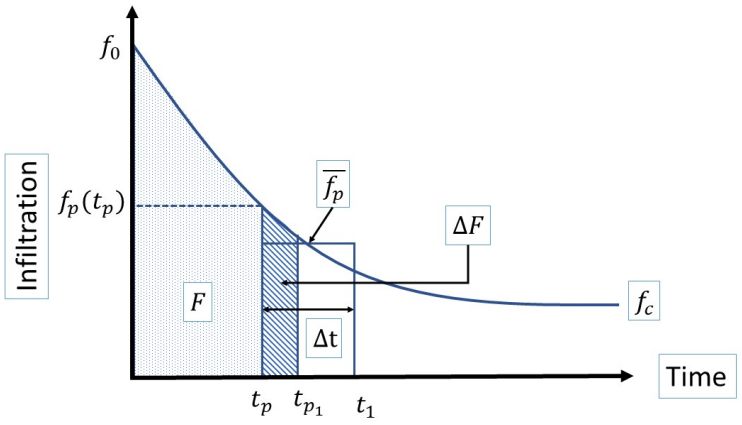

Figure 5.1. A conceptual representation of Horton infiltration in SWMM, applied as cumulative infiltration (F) as the area under the Horton curve. Modified from Rossman [2016a].

It is assumed that the actual infiltration has been equal to the infiltration capacity (f_p) over all time steps. When the infiltration is below the infiltration capacity the cumulative infiltration becomes equal to the rain intensity (eq. 5.3).

$$F(t) = \int_0^t min[f_p, i]\, dt \tag{5.3}$$

Where,

$F(t)$	Cumulative infiltration	$[m]$
f_p	Potential infiltration capacity	$[m \cdot h^{-1}]$
i	Rain intensity	$[m \cdot h^{-1}]$

The two equations (eq. 5.2 and 5.3) are applied by SWMM to define time (t_p) along the Horton curve at which the next infiltration capacity value can be found ($f_p(t_p)$). The cumulative infiltration (F) is thus updated with actual infiltration ($f(t)$) over the current time step, with t_p being the only unknown (eq. 5.2). Once the next t_P is known, the infiltration capacity (f_p) for the next time step can be found (eq. 4.1).

5.1 Recovery of infiltration rate

During coupled rain events SWMM applies a recovery rate to calculate the increase of the infiltration rate during dry weather. This is applied with Horton's method when a subcatchment is dry, thus having no rain and ponded surface water. Equation 5.4 is applied to calculate the hypothetical recovery curve.

$$f_p = f_0 - (f_0 - f_c)e^{-k_r(t-t_w)} \tag{5.4}$$

Where,

k_r	Coefficient for recovery curve	$[s^{-1}]$
t_w	Hypothetical projected time at which $f_p = f_c$ on the recovery curve	$[s]$

5.1.1 Regeneration Coefficient

For Horton's method, an estimate of drying time T_{dry} is applied instead of applying a recovery coefficient (k_r). Drying time states the time for a fully saturated soil to recover its maximum infiltration rate, thereby going from a fully saturated soil to a completely dry soil after a rain event ends. Literature values vary greatly, dependent on factors such as soil texture, evapotranspiration and soil percolation. Such factors are, however, not included in the recovery expression in SWMM but replaced by an empirical approach whenever a subcatchment is dry - thereby receiving no rain or having ponded surface water [Rossman, 2016a]. Rossman [2016a] state rapid drying times, corresponding to a couple of days, for well-drained porous soils, while 7-14 days for heavier clayey soils.

The Green-Ampt method determines the recovery time solely on an empirical relationship dependent on the soil's saturated hydraulic conductivity (eq. 5.5).

$$T_{dry} = \frac{3.125}{\sqrt{K_s}} \tag{5.5}$$

Where,

T_{dry}	Drying time of soil	[days]
K_s	Saturated hydraulic conductivity	[inches $\cdot h^{-1}$]

For consistency in comparison of regeneration coefficients between the two infiltration models, equation 5.5 is applied for the determination of T_{dry} for both models.

The implementation of soil regeneration is important when modelling and analysing infiltration in swales. This is because the potential infiltration capacity is directly influenced by the period leading up to a rain event for coupled rain series or historical rain events. Initial soil water conditions will thus be crucial to whether runoff occurs quickly or slowly (fig. 3.6).

5.2 Computational scheme for Horton infiltration

An overview of the infiltration capacity and infiltration recovery computations, is given in Figure 5.2 with input variables presented in Table 5.1. At the beginning of each time step the available rainfall rate (i_a) is calculated, followed by the criteria of "wet weather" or "dry weather".
If a dry surface is present then the infiltration rate is updated based on a given recovery rate (k_r). During rainfall or ponding water the cumulative infiltration volume is determined based on eq. 5.2 for time t_p and $t_p + \Delta t$. An infiltration rate is then computed, based on the average cumulative infiltration volume in each time step.
SWMM then computes the actual infiltration rate (f_t) as the minimum value of the infiltration capacity (f_p) and available rainfall (i_a). The time (t_p) is then updated with the the integral form of Horton's equation. SWMM then updates the model states re-running the model until simulation end [Rossman, 2016a].

Table 5.1. Overview of variables and constants at the start of each time step for the Horton infiltration method [Rossman, 2016a].

Abbreviation	Parameter explanation	Unit
i	Rainfall rate	$[m \cdot s^{-1}]$
d	Depth of ponded surface water	$[m]$
t_p	Equivalent time on the Horton curve	$[s]$
f_0	Initial infiltration rate	$[m \cdot s^{-1}]$
f_c	Infiltration capacity	$[m \cdot s^{-1}]$
k_d	Infiltration capacity decay coefficient	$[s^{-1}]$
k_r	Infiltration capacity recovery coefficient	$[s^{-1}]$

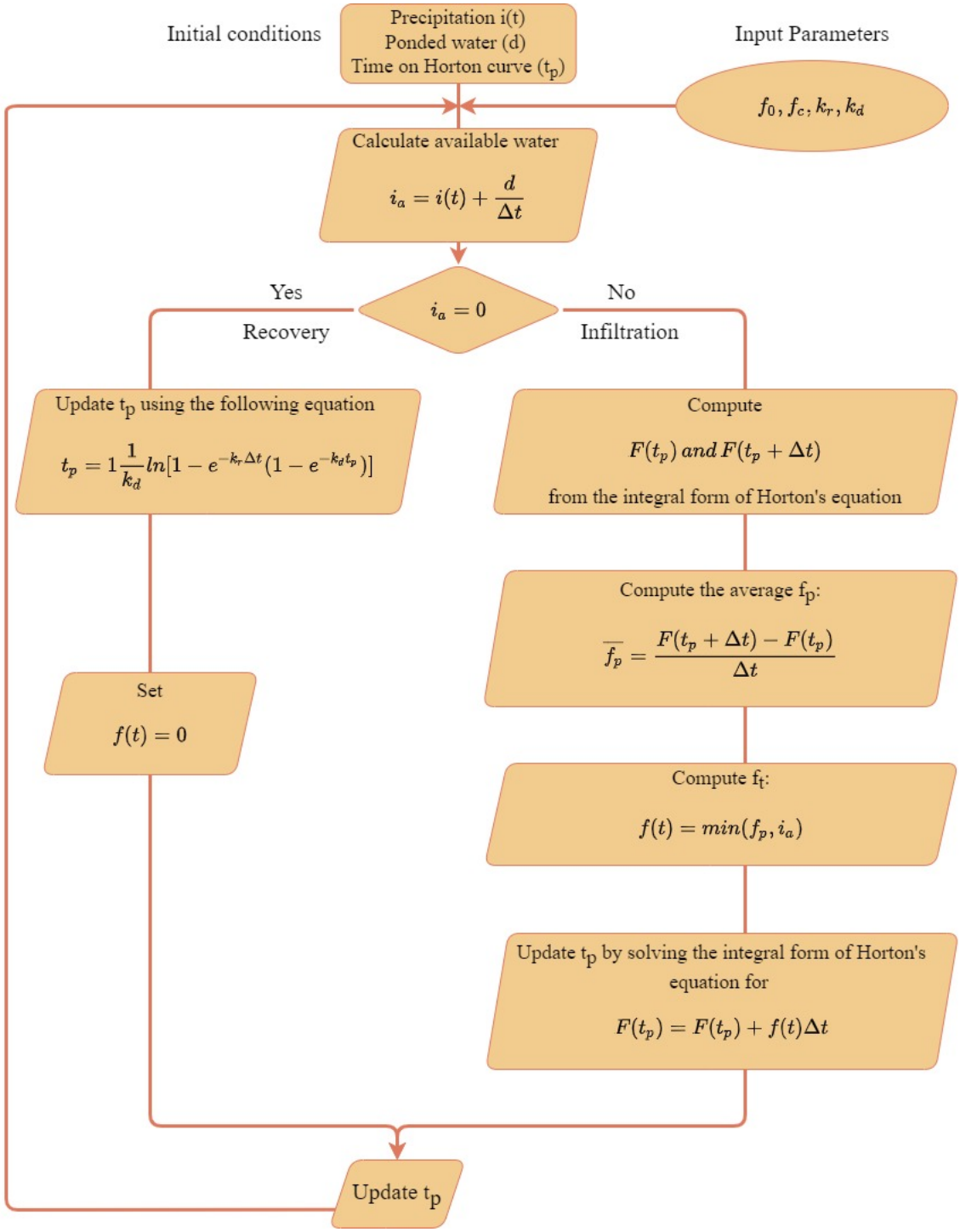

Figure 5.2. A computational scheme of Horton infiltration for each subcatchment in SWMM, within a single time step. Modified from Parnas et al. [2021].

Modelling Water transport in Swales 6

The description of water transport in swales is a crucial understanding of the infiltration process since water transport will influence the infiltration time throughout a swale section. Water transport can be calculated through various hydraulic governing equations or simple volume balances, ensuring inflow equals outflow plus storage. This presented in the following chapter.

6.1 Water balance for a subcatchment

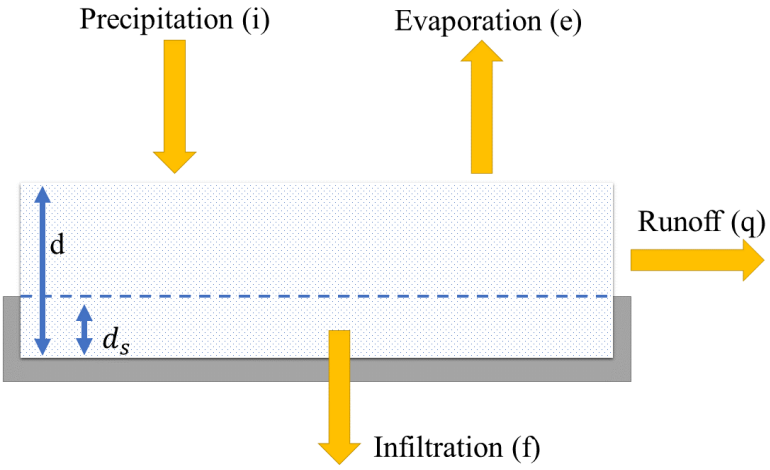

Figure 6.1. Nonlinear reservoir model of a subcatchment indicating in- and outflows including ponding depth (d) and depression storage (d_s), modified from Rossman [2016a].

The water balance of a subcatchment is defined by a nonlinear reservoir tank model in SWMM (Fig. 6.1). Rainfall acts as input, while connected subcatchments outflow also contribute to the total inflow of downstream subcatchments in conjunction. Outflow terms are defined by the evaporation rate, the infiltration rate and runoff rate (eq. 6.1). The parameters are expressed as flow rates per unit area ($\frac{\frac{m^3}{s}}{m^2} = \frac{m}{s}$).

$$\frac{\partial d}{\partial t} = i - e - f - q \tag{6.1}$$

Where,

$\frac{\partial d}{\partial t}$	Change in depth per unit of time	$[m \cdot s^{-1}]$
i	rate of rainfall	$[m \cdot s^{-1}]$
e	surface evaporation rate	$[m \cdot s^{-1}]$
f	infiltration rate	$[m \cdot s^{-1}]$
q	runoff velocity	$[m \cdot s^{-1}]$

Within a subcatchment, a LID control can be implemented to account for a percentage of the entire subcatchment area. LID is the SWMM equivalent of a SuDS. SWMM calculates the surface runoff differently than for a subcatchment when applying a vegetative swale as a LID control.

6.2 Water balance for a vegetative swale

SWMM expresses a vegetative swale as a trapezoidal channel able to convey and infiltrate surface runoff. SWMM applies the continuity equation for modelling the process of infiltration and transport within a single surface layer (eq.6.2), which is visualised in Figure 6.2.

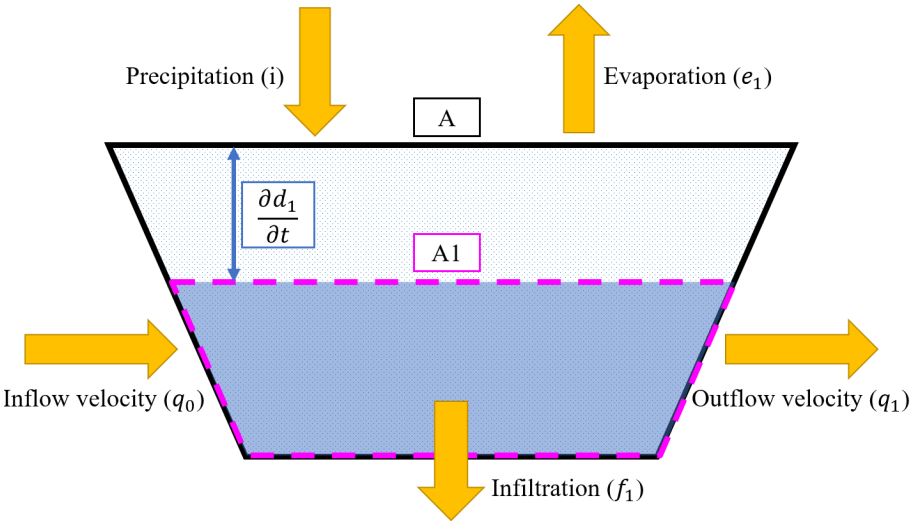

Figure 6.2. Conceptual mass balance model of a vegetative swale applied by SWMM.

The equation 6.2 describes water fluxes in the modelling of the water balance.

$$A_1 \frac{\partial d_1}{\partial t} = (i + q_0) \cdot A - (e_1 + f_1) \cdot A_1 - q_1 \cdot A \tag{6.2}$$

Where,

A_1	Surface area at water depth d_1	$[m^2]$
$\frac{\partial d_1}{\partial t}$	Change in water depth over time	$[m \cdot s^{-1}]$
i	Rain intensity	$[m \cdot s^{-1}]$
q_0	Inflow velocity	$[m \cdot s^{-1}]$
A	Surface area occupied by the swale across its full water height	$[m^2]$
e_1	Evaporation rate	$[m \cdot s^{-1}]$
f_1	Infiltration rate	$[m \cdot s^{-1}]$
q_1	Outflow velocity	$[m \cdot s^{-1}]$

Equation 6.2 incorporates the varying surface area as the depth of water varies within the swale. This is calculated through the use of geometry relations of area and depth of flow, allowing for the wetted cross-sectional area to be determined [Rossman, 2016b]. The wetted area will directly influence the infiltrated volume as illustrated in Figure 3.4. The volumetric outflow rate ($q_1 \cdot A$) is computed using the Manning equation.

6.3 Saint Venant equations

The one-dimensional Saint Venant equations are a set of partial differential equations, consisting of the conservation of mass and momentum (eq. 6.3 and 6.4). The equations are applied when modelling water transport within sewer networks in SWMM. The solution is specified as the fully dynamic or kinematic wave solution. SWMM applies these equations for calculating water transport in conduits to determine the spatial and temporal variation of water levels and discharge rates throughout the investigated system [Rossman, 2017].

Continuity equation:

$$\frac{\partial Q}{\partial x} + \frac{\partial A}{\partial t} = 0 \tag{6.3}$$

Where,

Q	flow discharge	$[m^3 \cdot s^{-1}]$
x	length	$[m]$
A	cross sectional area	$[m^2]$
t	time	$[s]$

Momentum equation:

$$\frac{\partial V}{\partial t} + V \cdot \frac{\partial V}{\partial x} + g \cdot \frac{\partial h}{\partial x} - g \cdot (S_0 - S_f) = 0 \tag{6.4}$$

Where,

V	Velocity	$[m \cdot s^{-1}]$
g	gravitational force	$[m \cdot s^{-2}]$
h	water depth	$[m]$
S_0	swale bed slope	$[m \cdot m^{-1}]$
S_f	friction slope	$[m \cdot m^{-1}]$

The dynamic wave analysis provides the most theoretically accurate results and should be applied for systems subjected to backwater effects, pressurised flow and flow regulations [Rossman, 2017]. The kinematic wave solution does not apply to the exact scenarios as the dynamic wave solution. Still, it can be an accurate and computationally efficient method, especially for long term simulations, if the limitations mentioned above are minimal.

Backwater effects, flow reversal or pressurised flow are not expected within the modelling scope of water transport in swales, which is why the kinematic wave solution is chosen.

6.4 Manning formula

Within SWMM, the Manning formula is applied for describing open channel flow, based on the assumption of uniform flow. It describes the volumetric flow rate as a function of the channel cross-sectional area, the manning coefficient, the energy gradient and hydraulic radius (eq. 6.5).

$$Q = A \cdot M \cdot R^{2/3} \cdot I^{1/2} \tag{6.5}$$

Where,

Q	Volumetric flow rate	$[m^3 \cdot s^{-1}]$
A	Cross sectional area	$[m^2]$
M	Manning coefficient	$[m^{1/3} \cdot s^{-1}]$
I	Energy gradient	$[m \cdot m^{-1}]$
R	Hydraulic radius	$[m]$

The Manning formula is a key governing equation in SWMM for computing surface runoff (q) from each subcatchment (sec. 6). This is done by obtaining a runoff flow rate per unit of the surface area combined with a subcatchments mass balance to solve the nonlinear differential equation. The Manning formula is also utilised in the kinematic wave approximation, to express the friction slope, for steady uniform flows.

In the following chapter, the sites under investigation will be presented, as well as the methods used and conduction of laboratory work.

Part III

Materials and methods

The following part describes the conducted field experiment and laboratory work. An introduction to the investigated locations and physical characteristics of investigated swales are given based on soil analysis and single ring infiltrometer tests.

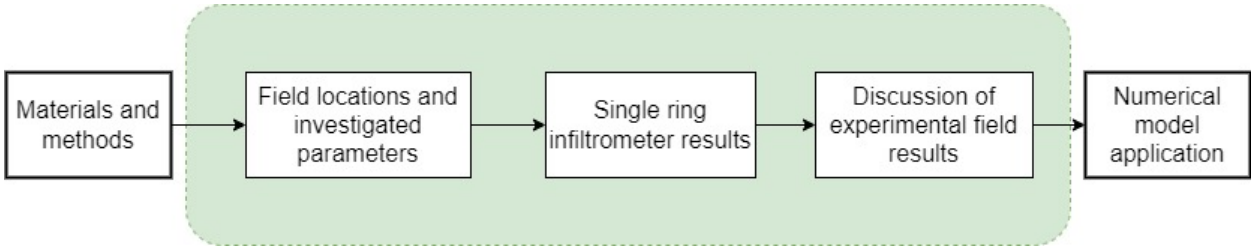

Field locations and investigated parameters 7

In the following chapter the two field locations of investigation are presented along with experiments conducted to determine physical soil properties, through soil sampling and single ring infiltrometer tests.

An investigation of two areas in Northern Jutland, Denmark (fig. 7.1) was conducted on three separate days in mid-March 2022. The two locations of investigation included:

1. Marshalls Allé, 9220 Aalborg East (red)
2. Skjoldet, 9230 Svenstrup South (blue)

Figure 7.1. Overview of field experiment locations in Northern Jutland, Denmark. Red indicates Marshalls Allé, 9220 Aalborg. Blue indicates Skjoldet, 9230 Svenstrup South.

The locations were chosen in cooperation with Niras as advisor on the initial comprehensive project plan, including the dimensioning of the investigated swales. For the dimensioning of swales and SuDS at the two locations, Niras applied a hydraulic model in MIKE URBAN to determine relevant water volumes in need of being handled within the vegetative swales.

7.1 Soil sampling and estimation of field-saturated soil hydraulic conductivity

At each location of investigation, loose soil samples were taken in order to investigate:

- Soil water content
- Organic matter content
- Grain size distribution

Soil samples were taken at a depth of 10-20 cm. Only one grain-size distribution was conducted for Marshalls Allé and Skjoldet respectively, based on the assumption of homogeneous soil conditions throughout the swale sections resulting in isotropic conditions. This assumption is taken because the same industrial contractor firm implemented the swales, applying a predetermined soil composition throughout the swale. A detailed description of the laboratory procedure and experiments mentioned above can be found in Appendix A.

7.2 Infiltrometer test protocol

In each swale section, one infiltrometer test was conducted. The infiltrometer test consisted of two runs, as seen in Figure 7.2.

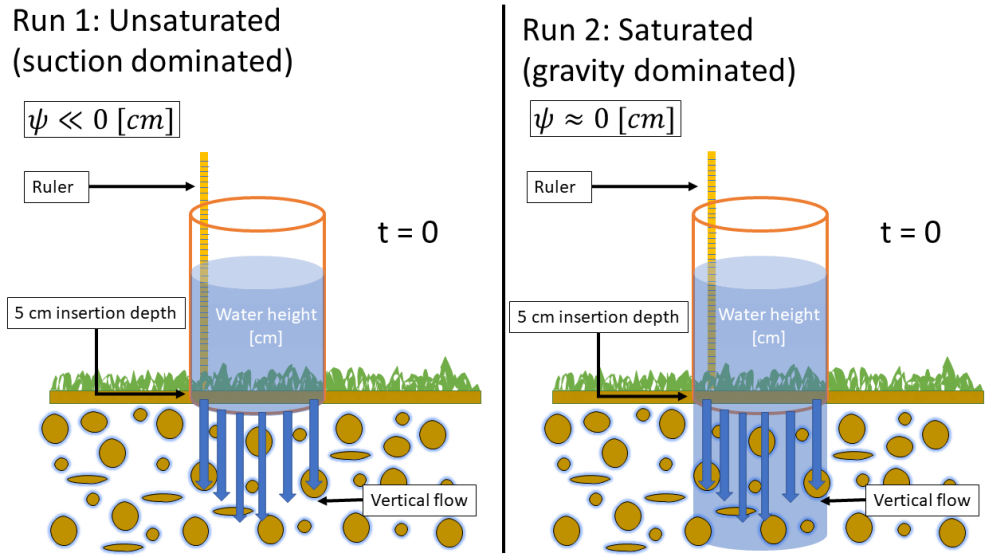

Figure 7.2. Initial assumptions for the two single ring infiltrometer runs. Run 1 shows unsaturated soil conditions, with the primary water transport mechanism of suction. Run 2 shows saturated soil conditions, with the primary infiltration mechanism of gravity. 5cm insertion depth into the topsoil, assuming vertical flow.

The SRI is used to estimate the hydraulic conductivity of the soil from measured infiltration data. By continuously pouring water into the SRI to a specified water height (35-40 cm), the experiment is run from the moment the water is at the chosen height and re-filled for the second run. The field experiment setup of the SRI run is shown in Figure 7.2 and the entire experiment procedure can be found in Appendix B.

Constant head setup

A SRI experiment is, in reality, a falling head setup since water infiltrates over time. This Master Thesis, however, treats the data as a constant head setup by calculating the saturated hydraulic conductivity at mean times, thus plotting the values against time, identifying the saturated hydraulic conductivity value when the infiltration rates become constant. The principle of saturated hydraulic conductivity calculation from gathered SRI test can be found in Appendix B.

7.3 Marshalls Allé

Investigated swales at Marshalls Allé consisted of three swale sections (fig. 7.3) with varying size and slope, as seen in Table 7.1. The swales are 1.5m wide and 20cm in-depth, with an applied Manning coefficient of 33.

Figure 7.3. Overview of Marshalls Allé and the three investigated swale sections.

The soil water content, organic matter, and soil classification were determined based on collected soil samples. The soil textural class of Marshalls Allé corresponds to a fine sand (USDA).

Table 7.1. Physical characteristics of swale sections investigated in Marshalls Allé.

Swale section nr.	Length [m]	Slope [‰]	Soil water content [%]	Organic matter [%]	Soil classification [USDA]
1	32	47.0	13.60	2.61	
2	21	26.6	8.01	1.10	Fine sand
3	26	21.0	11.34	2.06	

7.3.1 Niras specifications

Swales are implemented in Marshalls Allé to infiltrate the water volumes corresponding to a 10-year 10-minute box rain event with a climate projection factor of 1.4. Furthermore, a historical rain series of 28 years, with a climate projection factor of 1.4, did not result in overflows when the system was tested.

7.3.2 Field results

A total of six SRI runs were conducted, three each day, respectively the 8/3/2022 and 14/3/2022. The measured saturated hydraulic conductivity values can be seen from Table 7.2. Furthermore, the applied saturated hydraulic conductivities from Niras are also presented, indicating a 1 order magnitude difference from field measurements.

A soil texture analysis was performed for both field locations to estimate the theoretical saturated hydraulic conductivity for each swale section of investigation through grain-size analysis, organic matter content and water content (app. A). The theoretical saturated hydraulic conductivity values are compared to measured saturated hydraulic conductivity values obtained from the SRI run, to highlight the variation between direct and indirect determination (app. E.

Table 7.2. Overview of saturated hydraulic conductivities (K_s) for swale sections in Marshalls Allé. Measured single ring infiltrometer (SRI), applied K_s for projection by Niras and theoretical K_s values estimated from soil textural analysis. The calculation for the Kozeny-Carman empirical formula is applied with 10 °C water temperature, and best-fit values determined by Nielsen et al. [2018] for the Nielsen et al. model.

Section	**SRI K_s [m/s]**		**Niras K_s [m/s]**	**Theoretical K_s [m/s]**		
	8/3/2022	14/3/2022		USBR	Kozeny-Carman	Nielsen et. al 2018
1	7.16E-06	1.64E-05	3.40E-04	6.60E-08	3.10E-05	6.89E-04
2	1.14E-05	6.00E-05	4.33E-04	6.60E-08	3.10E-05	7.04E-04
3	7.82E-06	2.24E-05	4.33E-04	6.60E-08	3.10E-05	6.94E-04

7.4 Skjoldet

Investigated swales at Skjoldet consisted of two swale sections (fig. 7.4) with varying length and slope, as seen in Table 7.3.

Figure 7.4. Overview of Skjoldet and the two investigated swale sections.

The soil water content, organic matter, and soil classification were determined based on collected soil samples. The soil textural class of Skjoldet corresponds to a coarse sand (USDA) (tab. 7.3).

Table 7.3. Physical characteristics of swale sections investigated at Skjoldet.

Swale section nr.	Length [m]	Slope [‰]	Soil water content [%]	Organic matter [%]	Soil classification [USDA]
1	46	41.3	10.05	2.33	Coarse sand
2	40	62.5	13.58	1.10	

7.4.1 Niras specifications

Swales are implemented in Skjoldet to handle the water volumes corresponding to a 100-year box rain event. This is due to a railway being located downstream. The swales are implemented to only treat surface runoff from the road, so each swale section's infiltration capacity is based on the contributing road surface area connected. The hydraulic model applied by Niras was MIKE URBAN, with a safety coefficient of 1.4 for the rainfall.

7.4.2 Field results

A total of four SRI measurements were conducted the 9/3/2022 and 14/3/2022. Section 1 was implemented in 2018 with a soil composition of 50% soil from the area, and 50% washed sand.

Table 7.4. Overview of saturated hydraulic conductivities (K_s) for swale sections in Skjoldet. Measured single ring infiltrometer (SRI), applied K_s for projection by Niras and theoretical K_s values estimated from soil textural analysis.

Section	SRI K_s [m/s]		Niras K_s [m/s]	Theoretical K_s [m/s]		
	9/3/2022	14/3/2022		USBR	Kozeny-Carman	Nielsen et. al 2018
1	2.47E-05	3.00E-05	5E-05	1.68E-07	3.46E-05	2.57E-03
2	2.03E-05	9.50E-06	5E-05	1.68E-07	3.46E-05	9.26E-04

Niras applied a standard saturated hydraulic conductivity of 5E-05 m/s with lower values measured, except for section 2 on the 14/3/2022. A large difference in saturated hydraulic conductivities for swale section 2 is observed. This was caused by a heavily compacted soil and night frost, minimising the infiltration rate. Theoretical saturated hydraulic conductivities vary 4 orders of magnitude, dependent on the chosen formula and swale section. However, the Kozeny-Carman is close to the applied and measured values.

Single ring infiltrometer results

8

The results from the infiltration run in Skjoldet and Marshalls Allé will be presented as plots of the infiltration rates over time. Two unsaturated runs are conducted in each section of the swale, and will be shown in the same plot. Only one plot from Marshals Allé and Skjoldet will be shown, and the rest of the unsaturated runs is seen in Appendix C. The saturated runs are not shown, as only the average calculated saturated hydraulic conductivity of these are used as input in the modelling part. A three moving average is applied for the measured values, to indicate the trend of the infiltration rate while minimising large variations within the measured data.

A fitted Horton infiltration curve and equation for each measured SRI run is also presented. The fitted Horton's equation will be shown in a box with the same colour as the fitted run. The fitting constants will be used as parameter input for the infiltration model during numerical modelling in SWMM (Chp. 12). The initial infiltration rate (f_0) is set to the initial infiltration rate measured at the beginning of a SRI run. The infiltration capacity (f_c) is equal to the average of the calculated saturated hydraulic conductivities calculated based on the saturated run. While the decay rate is applied as fitting parameter performed using Excel problem solver, minimising the root mean squared error (RMSE) between measured and calculated points.

8.1 Marshalls Allé: Horton fits

When observing the data from SRI runs at Marshalls Allé section 1, it is clear that the Horton's fit explains the observed variation nicely. For the run conducted on the 8^{th} of March, the R^2-value is 0.92, and for the run conducted on the 14^{th} of March, the R^2-value is 0.95. The time of measurements varied between the two days, due to higher infiltration rates on the 14^{th}.

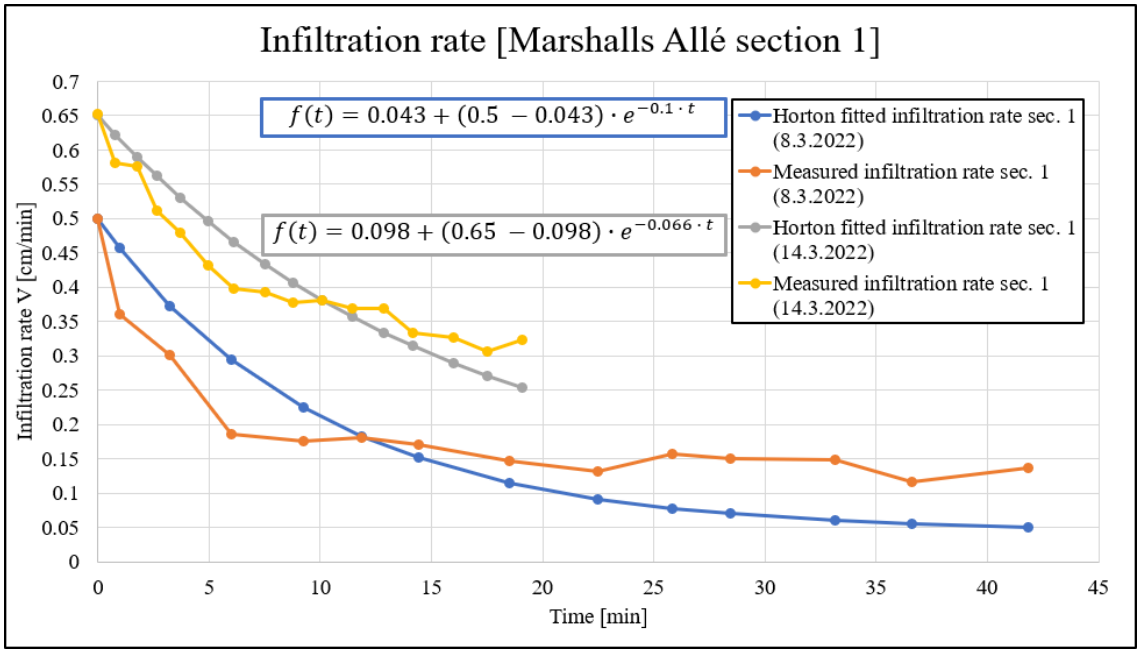

Figure 8.1. Infiltration measurements using single ring infiltrometer test and fitted Horton's infiltration. Both runs are unsaturated runs for section 1 at Marshalls Allé, with corresponding Horton fits. Infiltration rates are given in cm/min. The Horton's equation is presented colour coded to corresponding curve.

The infiltration rate is generally higher in the measurement taken the 14th of March compared to the 8th of March. Since there had been subzero temperatures leading up to the 8th, it is suspected that frost decreased the observed infiltration rates. Similarly, all the other SRI runs show the same pattern, except for section 2 in Skjoldet , where the first run on the 8th and 9th of March have lower infiltration rates than on the 14th and 15th of March.

In Table 8.1, the results from the fitted Horton equations is presented in m/s, alongside the the correlation between the fitted Horton equation and the measured data points.

Table 8.1. Fitting constants from Hortons infiltration equation for Marshalls Allé, along with R^2-values.

Marshalls Allé -	**Initial infil. rate** $\mathbf{f_0}$ $[m \cdot s^{-1}]$	**Saturated infil. rate** $\mathbf{f_c}$ $[m \cdot s^{-1}]$	**Decay rate** $\mathbf{c}$ $[h^{-1}]$	$\mathbf{R^2}$ -
Sec. 1 (8.3.2022)	8.33E-05	7.16E-06	6.0	**0.92**
Sec. 2 (8.3.2022)	6.25E-05	1.14E-05	1.8	**0.96**
Sec. 3 (8.3.2022)	5.33E-05	7.82E-06	2.3	**0.92**
Sec. 1 (14.3.2022)	10.8E-05	1.64E-05	3.9	**0.95**
Sec. 2 (14.3.2022)	30.0E-05	6.00E-05	4.0	**0.83**
Sec. 3 (14.3.2022)	10.0E-05	2.24E-05	0.7	**0.50**

8.2 Skjoldet: Horton fits

The SRI runs in Skjoldet were conducted on two separate days, in two sections of a swale, as described in chapter 7. In Figure 8.2 the results from the two runs in section 1 can be observed. The measured points seem to vary in consistency, however, with a high

coefficient of determination. The general trend seems to follow the Horton infiltration, which also can be noticed in the plot. With the exception of three measurement points on the 15_{th} being reduced followed by an increase. The reduction in infiltration rate is likely caused by a soil collapse within the soil column leading to a momentarily reduction in infiltration rates.

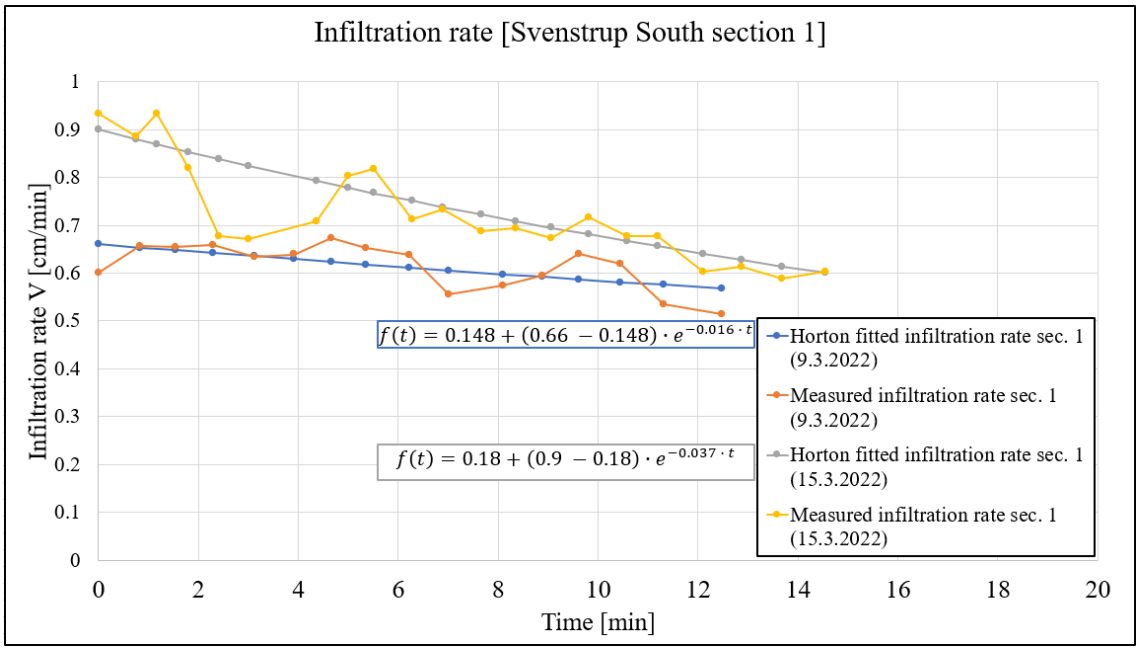

Figure 8.2. Infiltration measurements using single ring infiltrometer test and fitted Horton's infiltration. Both runs are unsaturated runs for section 1 at Skjoldet, with corresponding Horton fits. Infiltration rates are given in cm/min, but are transformed to m/s. The Horton's equation is presented colour coded to corresponding curve.

In Table 8.2, results from the fitted Horton equations can be seen for Skjoldet, alongside the R^2 values for the fits.

Table 8.2. Calculated fitting constants from Hortons infiltration equation for Skjoldet along with R^2-values.

Skjoldet -	**Initial infil. rate** $\mathbf{f_0}$ $[m \cdot s^{-1}]$	**Saturated infil. rate** $\mathbf{f_c}$ $[m \cdot s^{-1}]$	**Decay rate** $\mathbf{c}$ $[h^{-1}]$	$\mathbf{R^2}$ -
Sec. 1 (9.3.2022)	1.10E-04	2.47E-05	0.96	**0.75**
Sec. 2 (9.3.2022)	1.17E-04	2.03E-05	3.0	**0.81**
Sec. 1 (15.3.2022)	1.50E-04	3.00E-05	2.2	**0.72**
Sec. 2 (15.3.2022)	5.33E-05	9.50E-06	0.96	**0.79**

Initial infiltration rates and saturated infiltration rates are within the same order of magnitude, with the exception of swale section 2. In the following chapter, a discussion of the field results is presented.

Discussion of experimental field results 9

The following chapter presents a discussion of the SRI test results obtained from Marshalls Allé and Skjoldet. A comparison of applied and obtained saturated hydraulic conductivity values for the numerical modelling of the swales will be given, and how variation in values affect the determined infiltration capacities. A brief discussion of possible uncertainties associated with the field measurements is also given to highlight areas of caution when conducting infiltrometer tests.

9.1 Comparison of saturated hydraulic conductivities

Even though the swale soil composition of Marshalls Allé and Skjoldet is predetermined, allowing for a 'standard' conductivity value being applied, a theoretical soil composition often differs from reality. This is seen from the spatial variation observed between SRI runs and the predetermined saturated hydraulic conductivities, and the spatial variation within each field location (tab. 9.1). This spatial variability highlights the uncertainty of saturated hydraulic conductivity rates based on a single infiltrometer run, why several infiltration measurements should be taken to reduce the uncertainty interval of the geometric mean. According to Ahmed et al. [2015] 20 infiltration measurements should be taken to provide a specified level of uncertainty representing the geometric mean of the saturated hydraulic conductivity.

Equations used to calculate the theoretical saturated hydraulic conductivity were also implemented, to highlight the large variability between formulas and measured values. This is seen from Table 7.2 and 7.4 with theoretically determined values varying four orders of magnitudes in difference for both of the investigated locations with the use of the simple USBR equation. The choice of theoretical formula can minimise the theoretical saturated hydraulic conductivity variation between observed and calculated by implementing key physical properties into the equation. This is done with the Kozeny-Carmen equation applying the soil porosity while the Nielsen model, applies organic matter, total porosity and soil texture class fractions. The application of a theoretical saturated hydraulic conductivity formula should therefore be used as an indication of the expected value rather than an actual hydraulic conductivity value, as an initial step for the investigation of infiltration capacities.

When considering the results from Marshalls Allé and Skjoldet, the spatial variation can be observed between swale sections, however, a temporal variation is also observed. The temporal aspect of of the saturated hydraulic conductivity is observed when comparing

measured saturated hydraulic conductivity values to the measured values of Niras from the implementation of the Swales between 2018-2020 (tab. 9.1).

Table 9.1. Table showing the measured field results, the K_s used for dimensioning and the percentage difference between these.

Location	**Measured** K_s $[m \cdot s^{-1}]$	**Dimensioning** K_s $[m \cdot s^{-1}]$
Marshalls sec. 1	7.16E-06	3.40E-04
Marshalls sec. 2	1.14E-05	4.33E-04
Marshalls sec. 3	7.81E-06	4.33E-04
Skjoldet sec. 1	2.47E-05	5.00E-05
Skjoldet sec. 2	9.50E-06	5.00E-05

The decrease in saturated hydraulic conductivity from the implementation of the swales at Marshalls Allé can therefore indicate that a temporal effect also needs to be accounted for when simulating longer rain events, due to clogging effect of soil pores. This is also reported in Weiss et al. [2010], with infiltration capacities of observed swales decreasing exponentially with time until a constant long-term capacity is reached. The discrepancy in saturated hydraulic conductivities between measured and applied values result in the application of an inaccurate infiltration capacity for dimensioning, leading to over- or underestimation of a swale infiltration rates.

An uncertainty is also introduced, based on measurement position and climatic factors which may have influenced the saturated hydraulic conductivity. This temporal difference is also observed in the measured results. The runs conducted on the 8^{th} and 9^{th} of March display lower conductivities than the runs conducted on the 14^{th} and 15^{th}. Leading up to the first runs, there had been night frost, which may have affected the saturated hydraulic conductivity. When considering implementing SuDS solutions, the year-round applicability must be secured, why the lowest saturated hydraulic conductivity often is chosen.

9.2 Uncertainties

When conducting infiltrometer tests, there are uncertainties to account for. Two main points for discussion highlight possible discrepancies in the measured infiltration rates, compared to actual values.

- Infiltrometer setup
- Assumption of vertical flow

9.2.1 Infiltrometer setup

The SRI measurement technique is a simple method for determination of Horton's infiltration parameters. One of the key parameters regarding the Horton's equation, is the initial infiltration rate. The initial value is equal to the first measured hydraulic conductivity value measured at the beginning of the unsaturated run. The starting conditions therefore reflect the measured value. For the SRI run, the initial infiltration rate was noted when the SRI was filled to a certain water height. This allows initial infiltration

to occur during the 10-20 seconds, which it takes to fill the PVC pipe, as well as letting the water stabilise allowing to correctly measure the water level. Infiltration will occur from the beginning of the water pouring, resulting in a measured initial infiltration value lower, than the actual initial infiltration value. The procedure of the SRI procedure should as such be re-evaluated for further investigations. This could be done by filling the SRI without infiltration occurring, then measuring the initial infiltration rate at the beginning of the experiment. The lower initial infiltration rate results in an underestimation of a swales accumulated infiltration and thereby an over dimensioning of SuDS.

9.2.2 Assumption of vertical flow

When conducting the SRI test the assumption of vertical flow is applied. This however is a simplification of the infiltration process, as infiltration within a dry soil is dominated by suction and not gravity [Loll and Moldrup, 2000].

Furthermore, impermeable clay layers may be present, redirecting water flow. The implementation of a double-ring infiltrometer can lead to a reduction in lateral flow, however, a double-ring infiltrometer was not applied in the study, due to the large diameter of the ring not fitting within the investigated swales. However, Rice et al. [2014] state that double-ring infiltrometers also have been shown to be influenced by lateral flow, producing errors consistent with SRI.

The assumption of vertical flow can as such lead to an overestimation of the hydraulic conductivity during infiltrometer runs. This is a result of the vertical soil column obtaining saturation, but due to capillary suction forces of lateral surrounding soil, suction continues allowing a higher infiltration rate than would have occurred if complete vertical flow was obtained [Rice et al., 2014]. The overall influence of lateral flow increases for SRI with finer textured soils, as a greater capillary suction is associated with such soils. This results in a larger uncertainty of the saturated hydraulic conductivity within Marshalls Allé, than Skjoldet, due to difference in soil classifications. To account for lateral flow errors within SRI the correction method developed by Bouwer et al. [1999] can be applied to produce SRI measurements within a good estimate of large scale infiltration rates of soils with high permeability [Rice et al., 2014].

Although the measured values may contain uncertainties, they serve as input values for the numerical modelling part of this thesis. The numerical modelling will be presented in the following chapter.

Part IV

Numerical model application

The following part will explain the numerical modelling method applied in SWMM. Two model setups is elaborated upon, including differences and similarities. A comparison of application for swale infiltration investigation is applied based on the two model setups, to determine one model setup for further use when modelling swale systems in SWMM

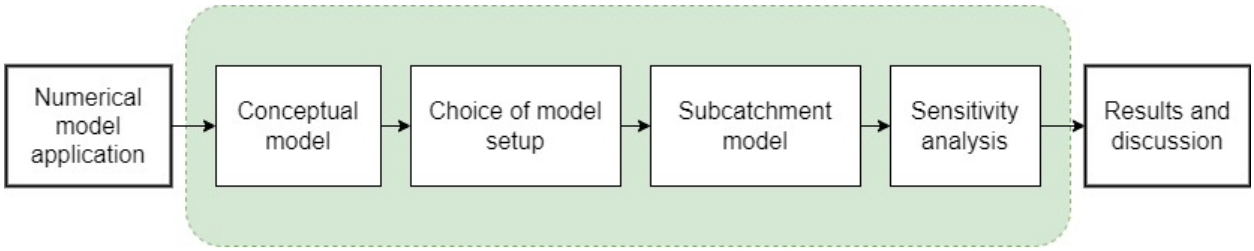

Conceptual model 10

Based on the system analysis, a conceptual model is created to represent the investigated swale systems of Marshalls Allé and Skjoldet (fig. 10.1). The model conceptualises the water transport and infiltration process within a defined subcatchment, including impervious road and pervious swale surface. The two primary overland flow calculations occurring in the conceptualisation, are based on the Manning formula. While the infiltration method applied in the conceptualisation is the Horton's method.

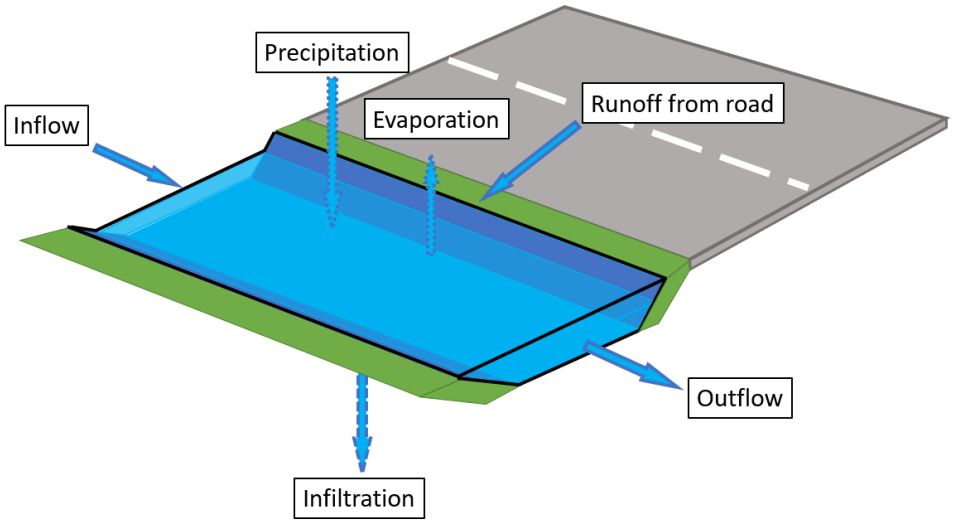

Figure 10.1. Conceptual model of representing the investigated swale system of Marshalls Allé and Skjoldet.

Swales investigated at Marshalls Allé and Skjoldet have been implemented to handle road surface runoff, why inflow to the swale consist of road runoff, upstream outflow and rain.

The mass balance for the water budget of the conceptual model is given in equation 10.1 based on the continuity equation of a swale and a subcatchment as presented in chapter 6. The parameters are expressed as flow rates per unit area ($\frac{\frac{m^3}{s}}{m^2} = \frac{m}{s}$).

$$\frac{\partial d}{\partial t} = (q_{in} + q_{road} + i) - (e + f + q_{out}) \tag{10.1}$$

Where,

$\frac{\partial d}{\partial t}$	Change in depth per unit of time	$[m \cdot s^{-1}]$
q_{in}	inflow velocity from upstream section	$[m \cdot s^{-1}]$
q_{road}	inflow velocity from road surface	$[m \cdot s^{-1}]$
i	rate of rainfall	$[m \cdot s^{-1}]$
e	surface evaporation rate	$[m \cdot s^{-1}]$
f	infiltration rate	$[m \cdot s^{-1}]$
q_{out}	runoff velocity from swale	$[m \cdot s^{-1}]$

SWMM utilises controlling equations as the numerical computational solver behind its calculations, and in this specific thesis, these equations will be presented as they provide understanding of the two main process when investigating swale infiltration:

1. Overland flow
2. Infiltration

The investigated systems are not influenced by high groundwater levels currently, however this can become a problem in the future. The possible groundwater influence is outside the scope of this thesis despite high groundwater levels having a direct impact on the soils infiltration rate. Similarly, any percolated water that may infiltrate the swale in a latter section, is also neglected. This means that any infiltrated water will be removed from the overall mass balance.

Within SWMM the runoff component operates on a collection of subcatchment areas that receive rain and generate runoff. The water routing method of SWMM transports runoff through a system of pipes and channels tracking flow rate and flow depth during a simulation, or by re-routing the overland flow from one subcatchment to another [Rossman, 2015].

The LID module is applied to model and investigate the infiltration efficiencies of swales in Marshalls Allé and Skjoldet respectively (eq. 10.2).

$$\text{Infiltration Efficiency} = \frac{\text{Infiltration Volume}}{\text{Total Runon Volume} + \text{Total rain Volume}} \tag{10.2}$$

In the following chapter, an overview of the different types of internal model setup is explained and applied values are given. Furthermore, the system understanding within each model setup is explained.

Choice of model setup 11

Within SWMM, two approaches capable of modelling infiltration are investigated:

- Node model
- Subcatchment model

A description of each model is given to determine limitations and capabilities of each setup. Finally one model setup will be chosen and applied for further analysis.

11.1 Node model

A node model consists of nodes connected by conduits. Subcatchments convey runoff to specific nodes, which then act as inlets and outlets for the conduits, while the conduits simulate a pipe drainage system (fig. 11.1). The conduits are defined in SWMM as different channels or pipes. The conduits are implemented with a trapezoidal cross-sectional geometry to represent a swale. The principle of the node model can be seen in Figure 11.1.

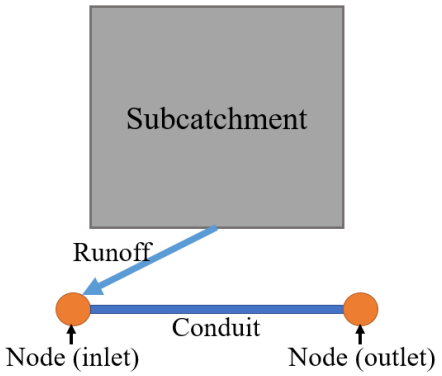

Figure 11.1. Figure showing the interaction of subcatchments and nodes.

Water transport is calculated based on the Saint Venaint equations, resulting in water velocities varying based on conduit slope, shape and roughness.

Infiltration in the node model, can only be modelled in a simplified manner, through a constant seepage rate, which is defined for each conduit, stating a constant infiltration rate. This however, limits the usage of the Horton infiltration model. The node model additionally lacks the ability to evenly distribute surface runoff from a subcatchment to the conduit, representing a swale, resulting in the net surface runoff being routed to the top of each swale section. The simplified system, when applying the node model, introduces inaccuracies which do not properly represent the physical characteristics of infiltration and water distribution into the swale, limiting the usage of the node model.

11.2 Subcatchment model

The SWMM subcatchment model has a setup consisting of individual subcatchments each representing the investigated swale sections, and the corresponding contributing road surface. The inflow to a subcatchment therefore relies entirely on rain and rerouted surface water from connected subcatchments (fig. 11.2). Each subcatchment will receive rain, followed by input from the adjacent roadside to each swale section. The runoff from an impervious subcatchment will be distributed evenly over the entire subcatchment in conjunction. This is particularly useful when modelling swales, where the swale conveys runoff from impervious areas such as roads, and the water is evenly distributed as it would be in reality. Furthermore, the length of the subcatchment is indirectly defined from the area and the width (fig. 11.2). Infiltrated water is removed from the system, swales thereby only convey water to the next subcatchment which has not infiltrated.

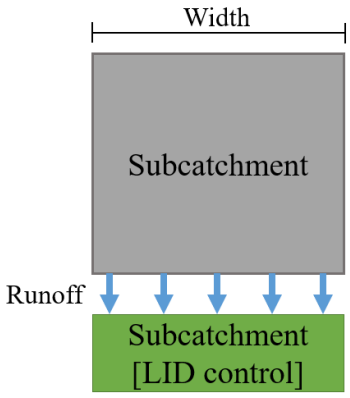

Figure 11.2. Figure showing the interaction off runoff between subcatchments

11.2.1 Assessment of the two model systems

An assessment of strengths, weaknesses and differences of the two model setups when constructing a conceptual model in SWMM, enables users to better understand results and usage of these (tab. 11.1).

Table 11.1. Table showing assessment of conceptual setup of different models in SWMM

	Subcatchment model	Node model
Considers saturated conditions	✓	✓
Considers unsaturated conditions	✓	✗
Underestimation of infiltration time	✓	✗
Overestimation of infiltration time	✗	✓

It is clear how the two model setups differentiate the conceptual understanding of the systems. The node model allows for hydraulic calculations with the application of the kinematic wave solution but represents the infiltration process as a constant seepage rate. Furthermore, the missing uniformly surface runoff distribution will result in overestimation of the infiltration time. The node model is not applied further for swale infiltration modelling in SWMM due to the lack of infiltration description. The subcatchment model is therefore applied.

This model is applied since it includes a more accurate description of the infiltration process, including unsaturated conditions through the Horton method. This is argued to be a lack in the current SVK spreadsheet dimensioning practice, why it should be incorporated rather than a constant seepage rate. The evenly distribution of subcatchment

runoff to downstream catchments is seen as a minor simplification when investigating the infiltration process but can have a significant influence on the net infiltration loss based on water travel times throughout the swale.

In the following chapter, a thorough description of the applied subcatchment model is given for the two field locations.

Subcatchment Model 12

A subcatchment is a delineated area within the model receiving rain and generating runoff, which flows into a drainage system to another subcatchment (fig. 12.1). SWMM applies a nonlinear reservoir model when calculating surface runoff over a catchment, which applies a conservation of mass from inflow and outflow rates as described in section 6.

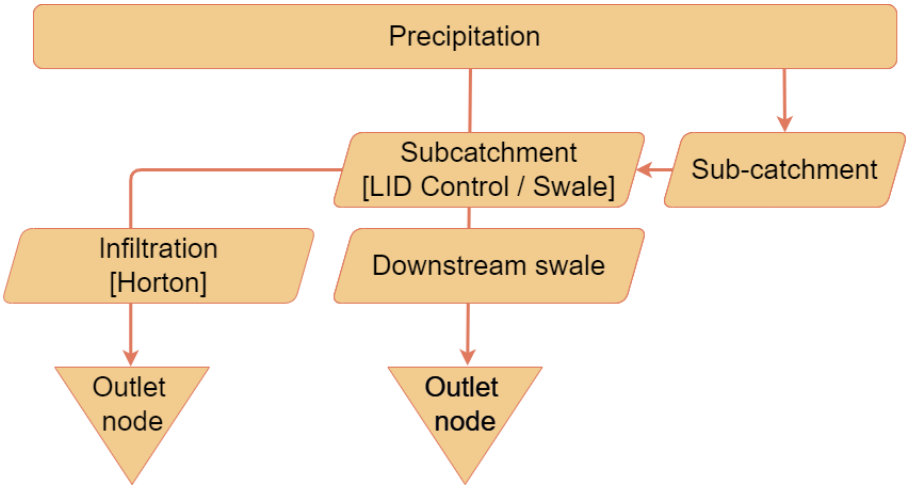

Figure 12.1. Conceptual setup of the subcatchment model in SWMM. Arrows indicate direction of water flow.

A subcatchment is conceptualised with a uniform slope, width and a rectangular surface. Under these assumptions the Manning's equation is applied to determine the volumetric flow rate of the surface runoff.

Subcatchments are applied for the modelling purpose of Marshalls Allé and Skjoldet, with each road section contributing to inflow to the swales. Roadside swales are also implemented as subcatchments with corresponding dimensions (tab. 12.1 and 12.2). Each road subcatchment has an applied surface slope of 2.5% equal to the roads transverse sectional slope. The cross sectional surface slope is applied since the entire road section is assumed to contribute to the corresponding swale section. The application of the lateral surface slope is thus deemed less relevant compared to the cross sectional slope, since it is the sectional slope which influences the water transport time to the adjacent swales on the impervious road subcatchment.

Overland flow routing from subcatchments is applied so the total runoff from a subcatchment is routed onto the downstream subcatchment. The overland flow re-routing simulates inflow to the downstream subcatchment by uniformly distributing the inflow over the subcatchment, as is done with rainfall as seen in Figure 12.2 [Rossman, 2016a].

The following subcatchment properties are used in the model setup of Marshalls Allé and Skjoldet respectively.

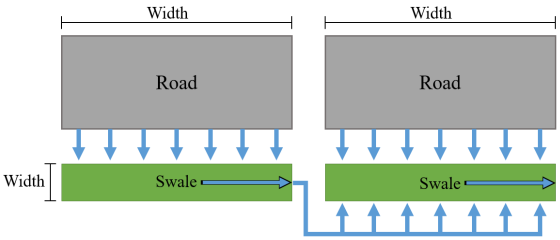

Figure 12.2. Figure showing the interaction off runoff between subcatchments in the Marshalls Allé setup.

Table 12.1. Subcatchment properties in SWMM applied for Marshall Allé.

Subcatchment Marshalls Allé	**Area** $[m^2]$	**Width** $[m]$	**Slope** [‰]	**Outlet**
Road1	306	51	25	Swale1
Road2	246	41	25	Swale2
Road3	252	42	25	Swale3
Swale1	48	1.5	47	Swale2
Swale2	31	1.5	27	Swale3
Swale3	54	1.5	21	Outlet

Table 12.2. Subcatchment properties in SWMM applied for Skjoldet.

Subcatchment Skjoldet	**Area** $[m^2]$	**Width** [m]	**Slope** [‰]	**Outlet**
Road1	500	50	25	Swale1
Road2	315	45	25	Swale2
Swale1	69	1.5	47	Outlet
Swale2	60	1.5	61	Outlet

12.1 Swale properties

In SWMM, the LID control for vegetative swale consists of two editors, the "LID Control Editor" and "LID Usage Editor" (fig. 12.3 and 12.4). The LID control editor allows for specific swale characteristics such as berm height, which is the height of the trapezoidal cross section and Manning surface roughness. The vegetative volume fraction is ignored and set to 0, since a low vegetation growth was observed. A Manning roughness of 0.03 is applied for all swales, based on previous hydraulic simulations from Niras. The longitudinal slope for each swale section varied and therefore several LID controls were established corresponding to the slope of each swale. A constant run over rise value of 1:3 was applied for Marshalls Allé while in Skjoldet a run over rise value of 1:4 was applied, indicating the slope of the side walls of a swales cross section for each interval of swale length [Rossman, 2016a].

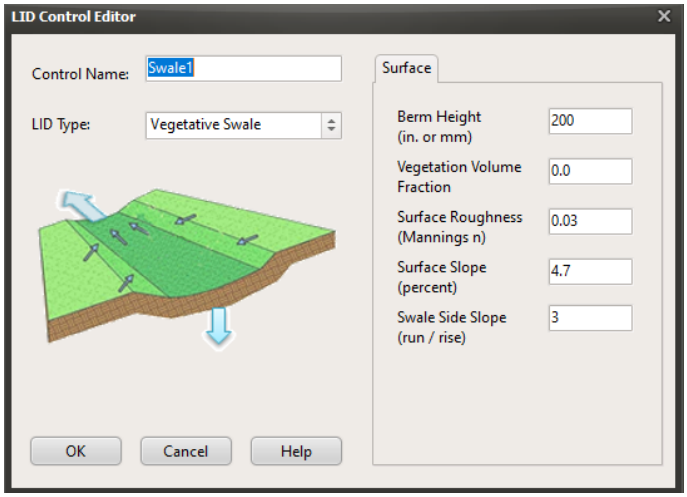

Figure 12.3. SWMM: LID control window.

The LID usage editor defines how a swale is implemented within the subcatchment. The LID control is set to occupy the full subcatchment, which allows the entire subcatchment to be defined as a vegetative swale. Each swale has a surface width of 1.5m and 20 cm depth. Furthermore, the LID usage editor allow to state a percentage of initially saturated conditions. This is however, not applicable for vegetative swales [Rossman, 2016a].

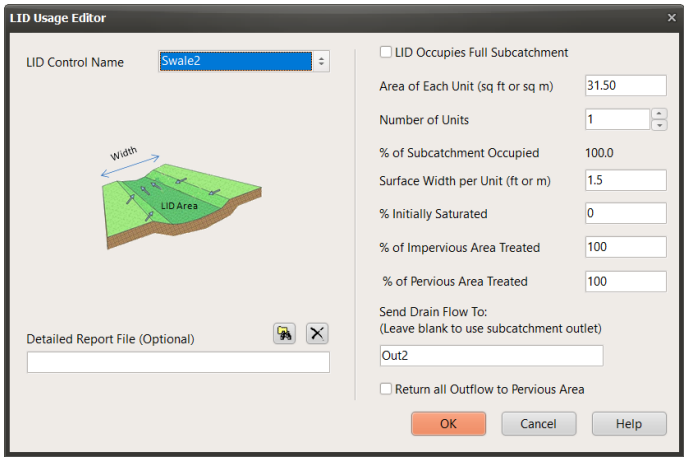

Figure 12.4. SWMM: LID usage editor window.

12.2 Evaporation

Evaporation occurs for water in the vegetative swales, however, Rossman [2016a] states that single event simulations are insensitive to the evaporation rate, why evaporation is not accounted for during such simulations. The evaporation rate during continuous events can influence the water budget significantly, especially during the summer half year. Evaporation is however, not applied in the SWMM model for continuous events, since the goal of the numerical modelling is to determine the infiltration loss independent of evaporation.

12.3 Depression storage

There is assumed no depression storage within the subcatchments, thereby neglecting the soils ability to contain a volume of water prior to the occurrence of runoff, promoting immediate runoff [Rossman, 2016a].

12.4 Horton's infiltration implemented in SWMM

The Horton infiltration parameters applied (tab. 12.3) are derived from the experimental field experiments described in Chapter 7. The results and Horton's fits is presented in Chapter 8. The estimation of drying time (T_{dry}) is presented in section 5.1.1.

Table 12.3. Table showing input to the Horton infiltration in the subcatchment mode.

Parameters	f_0 $[m \cdot s^{-1}]$	f_c $[m \cdot s^{-1}]$	k $[h^{-1}]$	T_{dry} $[days]$
Marshalls Allé				
Sec. 1	8.33E-05	5.00E-06	6.0	3.10
Sec. 2	6.25E-05	1.14E-05	1.8	2.46
Sec. 3	5.33E-05	7.82E-06	2.3	2.81
Skjoldet				
Sec. 1	1.10E-04	2.47E-05	0.96	1.51
Sec. 2	5.33E-05	9.50E-06	0.96	1.84

From Figure 12.5, the Horton infiltration editor in SWMM is presented. The minimum infiltration rate is based on the saturated hydraulic conductivity, obtained from the SRI runs. The calculated value is applied rather than the minimum measured infiltration rate from the SRI runs, since the infiltration curve did not flatten during infiltrometer runs.

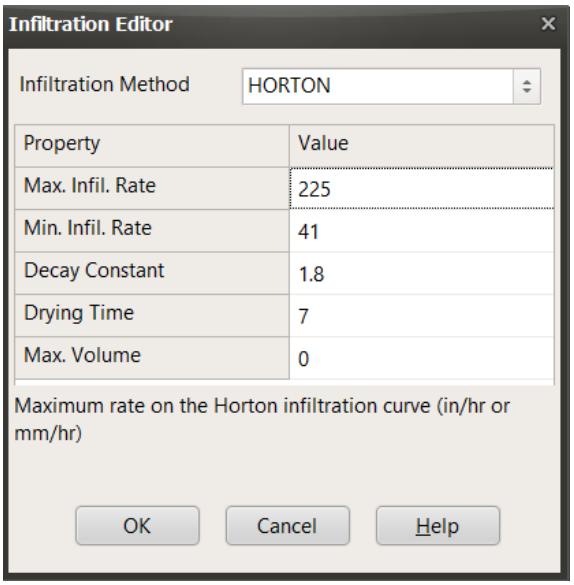

Figure 12.5. SWMM: Horton's infiltration editor.

The infiltration parameters in the Horton's method is therefore solely based on empirical

data obtained from SRI runs at Marshalls Allé and Skjoldet, with the exception of the decay rate, which is used as a fitting parameter.

Drying time is determined based on equation 5.5 in subsection 5.1.1. The max infiltration volume is set to 0, resulting in an infiltration volume per storm event, only dependent on the infiltration rate and with no theoretical maximum infiltration.

12.5 Rain events

For the numerical modelling of Marshalls Allé and Skjoldet, rain events corresponding to the applied dimensioning events used by Niras are applied (tab. 12.4). Niras applied a 10-year and a 100-year statistical box rain for Marshalls Allé and Skjoldet respectively, and a historical rain series from the Svenstrup rain gauge, for swale dimensioning. A CDS rain is applied in this thesis rather than a box rain to investigate the effect of varying rain intensity on the infiltration efficiency.

Table 12.4. Rain events applied for modelling surface runoff and infiltration in Marshalls Allé and Skjoldet. A climate projection factor of 1.4 is applied for all rain events.

Marshalls Allé	Skjoldet
10-year CDS event of 10 minutes	100-year CDS event of 10 minutes
10-year CDS event of 120 minutes	100-year CDS event of 120 minutes
10-year historic rain series	10-year historic rain series

12.5.1 CDS rain events

In order to test the dimensioning of the swales in Marshalls Allé and Skjoldet, CDS rain events with a statistical return period of 10 years and 100 years is applied. A 10- and 120-minute intensity is applied to investigate the effect of short duration rain events compared to longer events affect on infiltration in swales. The application of a 10-year and 100-year statistical event is described in Chapter 7.

12.5.2 Historical rain event

Coupled rain events within a short time span are critical for overflow as antecedent saturated conditions lower the initial infiltration rate. A historical rain series from Svenstrup, containing 10 years of measured rain data, is applied to the hydrologic model, to investigate the effect of infiltration efficiencies during coupled events of varying intensity. The rain gauge of the Svenstrup series is within a 9 km radius of both field locations, and therefore deemed representative as rain data input.

12.6 Selection of computational timestep and model discretisation

For the simulation of infiltration and water transport in SWMM, an appropriate time step is required, when evaluating surface runoff and infiltration. Three time steps are specified in SWMM [Rossman, 2016a]:

- Reporting step: visualisation of the results

- Dry step: there is neither rainfall nor ponding of water.
- Wet step: there is rainfall or ponded water.

Choosing the model discretisation is important when interpreting the results. When modelling synthetic rain such as CDS or box-rain, the period is often relatively small, in order of minutes to a few hours.

The time discretisation can therefore be set to a minimum, which equals the highest resolution of the result plots (fig. 12.6). The computation time does not increase significantly when modelling short rain series. However, when modelling historical rain series of 1, 10 or upwards of 30 years, the computational time significantly increases from a couple of seconds to hours depending on computational timestep. This computational time similarly increases with smaller timestep. A computational timestep of 1 second is applied during precipitation events (wet step) for CDS events, while 1 minute is applied for the historic rain series.

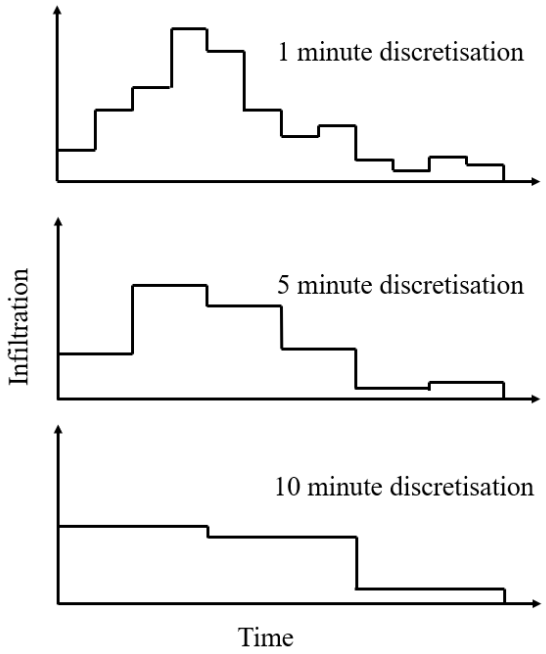

Figure 12.6. Conceptual model of peak differences in infiltration between reporting step visualisation

In the following section, a sensitivity analysis of governing infiltration parameters and physical swale properties is conducted.

Sensitivity analysis of governing infiltration parameters 13

In the following chapter, the subcatchment model's sensitivity to specific input parameters is investigated. This is an essential step in model assessment since no calibration data was obtained, why the numerical results in SWMM are analysed to determine parameter sensitivity. Investigation of parameter sensitivity will indicate the relative importance and effect of variation within parameter values.

13.1 Parameter description for sensitivity analysis

Parameters investigated in the sensitivity analysis include input parameters to the Horton infiltration model and swale physical properties.Infiltration parameters include:

- Initial infiltration rate
- Saturated hydraulic conductivity
- Decay rate

Physical properties of the swale, include:

- Manning number
- Swale slope

13.2 Sensitivity analysis result

The sensitivity analysis is conducted using equation 13.1, which determines model sensitivity to the parameter of investigation. The relative sensitivity is based on model output change relative to parameter input change, with the model output being the infiltration efficiency as presented in equation 10.2. The investigated parameter values are increased/decreased with a 25% increment in a range of -75% and 75%.

$$S = \frac{\frac{\Delta x}{x}}{\frac{\Delta p}{p}} \tag{13.1}$$

Where,

S	Relative Sensitivity	[/]
Δx	Change in model output	[/]
x	Initial model output	[/]
Δp	Change in parameter value	[/]
p	Initial parameter value	[/]

The sensitivity analysis was conducted using the standard model setup described in section 4.3. Three rain events were applied to investigate parameter sensitivity based on varying intensities and single versus coupled events. The rain events consist of a 10-year CDS rain event with a duration of 10 minutes, a 10-year CDS rain event with a duration of 120 minutes and a 1-year historic rain series from the Svenstrup series ranging from the 9th of May 2021, until the 24th of April 2022.

Figure 13.1 shows the sensitivity of the parameters when analysing a 10-year CDS rain event with a duration of 10 minutes.

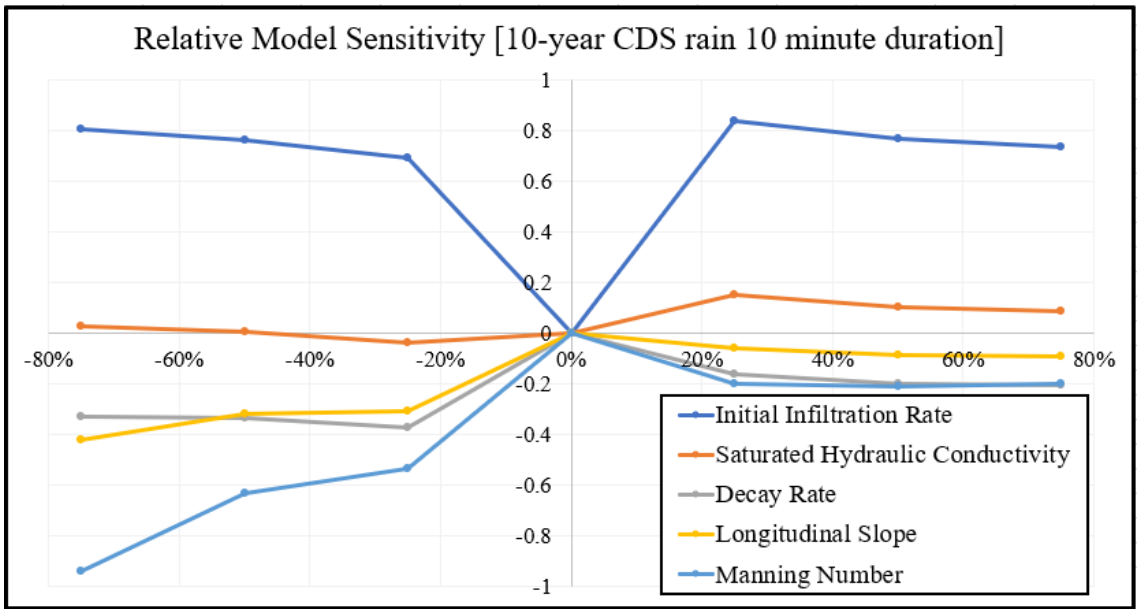

Figure 13.1. Model sensitivity of investigated parameters for a 10 year CDS rain with a duration of 10 minutes. Parameters are changed in the interval from -75% to 75%. The y-axis displays relative sensitivity.

As shown in Figure 13.1, the parameters to which the model is most sensitive are the initial infiltration rate and the manning number. When the parameters are changed by 25%, the initial infiltration rate differs from the other parameters. The sensitivity to the manning number increases with a decrease in manning roughness. The saturated hydraulic conductivity has the lowest relative sensitivity when analysed using a rain event with a 10-minute duration. This is caused by the hydraulic conductivity not reaching saturation within this period, therefore, not affect the model result.

To further investigate the effect of relative model sensitivity, a 10-year CDS rain with a 120-minute duration is investigated (fig. 13.2). It is noticeable how the model has a larger sensitivity to saturated hydraulic conductivity when compared to Figure 13.1, since the duration of the rain event is long enough to reach saturated conditions.

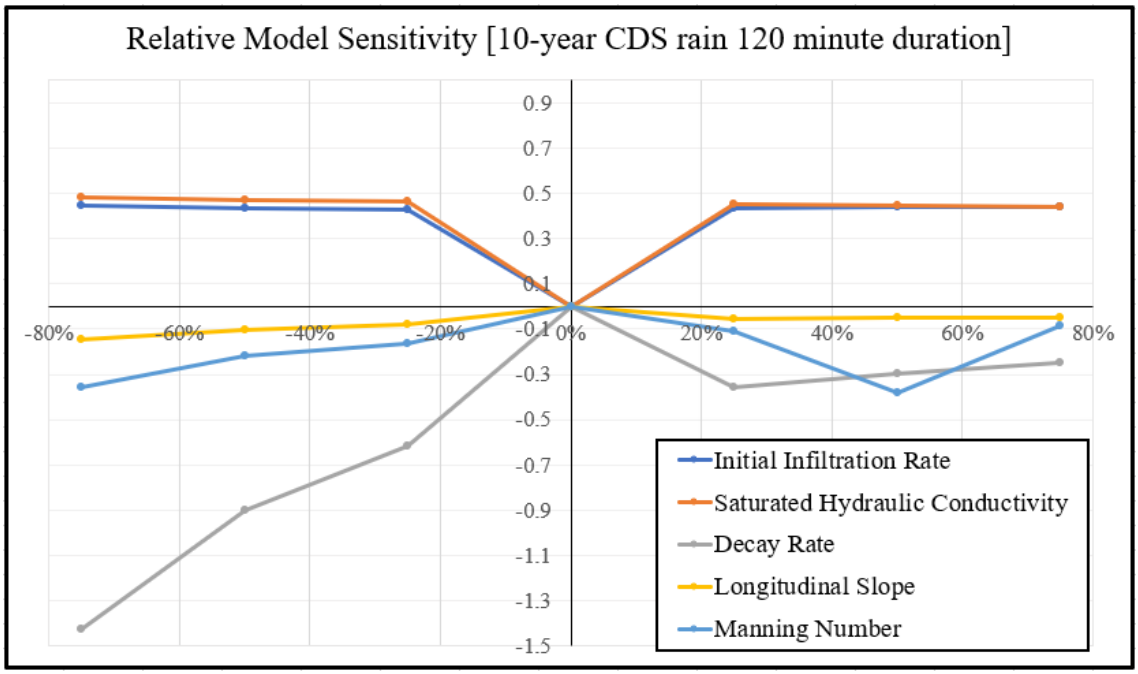

Figure 13.2. Model sensitivity of investigated parameters for a 10 year CDS rain with a duration of 10 minutes. Parameters are changed in the interval from -75% to 75%. The y-axis displays relative sensitivity.

Investigated parameters are shown to have varying sensitivities when compared to the 10-minute duration, noticeably the decay rate. The high sensitivity is related to a slower decrease in infiltration rates from the initial infiltration rate to the infiltration capacity, resulting in larger infiltrated volumes.

When considering the historical rain series, it is noticeable how the model sensitivity to parameters are almost equal, with the exception of saturated hydraulic conductivity and decay rate (fig. 13.3). The recovery rate is furthermore, investigated for the historic rain series, describing the time from infiltration capacity to initial infiltration rate.

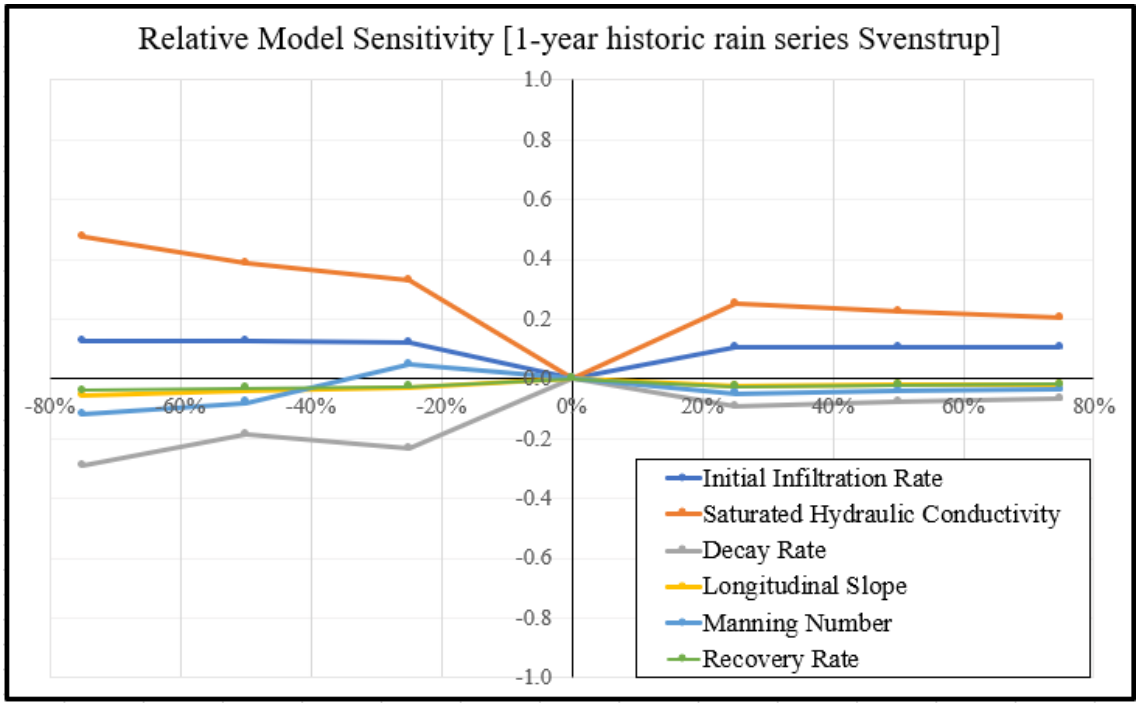

Figure 13.3. Model sensitivity of investigated parameters for a 1 year historic rain series from the Svenstrup rain gauge. Parameters are changed in the interval from -75% to 75%. The y-axis displays relative sensitivity.

The relative sensitivity of the saturated hydraulic conductivity and decay rate, highlights the effect of simulating coupled rain events. When multiple events are applied the infiltration rate decreases and may not reach initial conditions, resulting in a lower starting point for the next event. One parameter expected of having a high sensitivity was the recovery rate. It is however, observed that the recovery rate does not affect the infiltration efficiency as expected, indicating that the recovery rates are sufficiently low and capable of reaching initial infiltration rates between rain events.

Being conscious of the sensitivity of input values allows the modeller to determine which values should be defined based on field measurements to decrease possible model uncertainty. The discussion of the parameters is presented in the following section.

13.3 Discussion of relative parameter sensitivity

The relative sensitivity of the infiltration efficiency, when varying input values of the Horton's infiltration and swale slope, a clear trend of parameter influence is observed in Figure 13.1 and 13.2. The influence of each parameter is briefly discussed in the following.

Initial infiltration

The initial infiltration has the highest relative sensitivity when investigated using a 10-minute rain event. When the duration increases to 120 minutes, as seen in Figure 13.2, the relative sensitivity decreases. This parameter is key when dimensioning swales because of its effect on overall infiltration efficiency, highlighted in this sensitivity analysis. It should therefore be implemented when modelling coupled rain events. However, the initial

infiltration rate has a low sensitivity for the historical analysis, indicating that the duration between events are sufficiently long or short for the infiltration rate to have a minimal effect on infiltration efficiencies.

Manning number
The Manning's roughness coefficient has the second-highest sensitivity when investigated with a rain duration of 10 minutes shown in Figure 13.1. Mainly when the parameter is decreased, the sensitivity is observed to increase. This is caused by the overall infiltration efficiency decrease as a result of increased runoff, as a result of a smaller Manning roughness. However, when modelling with a duration of 120 minutes, the relative sensitivity of the manning number is observed to be less sensitive to reduction in Manning, but more sensitive to an increased Manning number. The Manning roughness experiences a relative small sensitivity, during the historic analysis indicating the roughness is less sensitive for coupled events than short intense rain events (fig. 13.1).

Decay rate
In the 10-minute rain event, the model seems to have a relatively constant sensitivity to this parameter, caused by its short duration. There is no significant effect of an increase or decrease in this parameter. Especially when analysed during a 120-minute rain duration, as shown in 13.2, the decay rate has a sensitivity almost linearly with the decrease in parameter value. The decay rate indicates the decrease from the initial infiltration rate to the infiltration capacity, being dependent on initial soil moisture content. A decrease will prolong periods with infiltration near the initial infiltration rate. This parameter value is determined by field experiments, and can be seen to impact the infiltration efficiency of a swale significantly. This is also the case for the historic analysis, where the decay rate becomes more sensitive than most other parameters when decreased

Saturated hydraulic conductivity
When considering the saturated hydraulic conductivity, it is not observed to affect the infiltration efficiency in the 10-year CDS rain with a duration of 10 minutes. This amounts to a low model sensitivity to this parameter, as observed in Figure 13.1. However, when considered during a rain event with a 120-minute duration, the saturated hydraulic conductivity is observed to have a more considerable model impact. This is caused by the extent of the rain event, allowing the infiltration capacity to reach saturation, which is why this parameter value will affect the overall result. In Figure 13.2, the model sensitivity to this parameter seems to be equal to the initial infiltration rate. A similar tendency of sensitivity is observed with the historic analysis. Here it is observed to have the highest sensitivity. The relative sensitivity underlines the importance of representative saturated hydraulic conductivity values when investigating infiltration efficiencies.

Swale Slope
The longitudinal slope of the swale affects the overall result, and the model displays a sensitivity to this parameter as seen in Figure 13.1. The model shows sensitivity, especially when the value is decreased, which would result in slower water transport and, therefore, more infiltration. However, when analysed using a 10-year CDS rain event with a duration of 120 minutes, as depicted in Figure 13.2, the sensitivity to this parameter decreases and is the least sensitive parameter. Similar results are observed in the historic analysis, with swale slope having a negligible relative sensitivity, compared to other parameters. Despite

the relative low sensitivity, the parameter is further investigated based on the difference in infiltration efficiencies. This is done, since the swale slope is a physical parameter able of easily being incorporated in a numerical model, when dimensioning swales.

Recovery rate

The drying time is not considered when modelling CDS rain events since there are no coupled rain events. In the sensitivity analysis of the historical rain event shown in Figure 13.3, the sensitivity of this parameter is observed to be very small. This may indicate that the two field locations are characterised by sandy soil resulting in a quick drying time, thereby not significantly affecting the overall results.

Part V

Results and discussion

The following part will serve as an elaboration of the modelled results. The investigated parameters are based on a sensitivity analysis highlighting certain parameters. The discussion will elaborate on the overall infiltration efficiencies found in the results and compare these results with existing practice utilising the SVK spreadsheet.

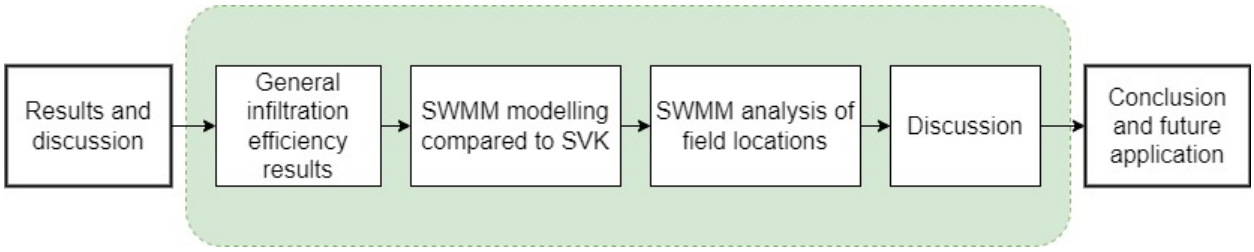

General infiltration efficiency results 14

The case studies, Marshalls Allé and Skjoldet, are presented with varying CDS rain events for the setup, and subsequently a historical rain event.

All general results presented are modelled through the use of the standard subcatchment model. The standard model is described in section 4.3, and is applied to analyse a swale system consisting of one swale with a connected subcatchment. In the general results, the following investigations are performed:

- Effect of swale slope
- Effect of saturated hydraulic conductivity

14.1 Effect of swale slope

In Figure 14.1 and 14.2 the results of infiltration efficiencies are presented, based on varying slope, rainfall duration and statistical return periods, while figure 14.3 investigates the effect of the saturated hydraulic conductivity in regards to the infiltration efficiency.

From Figure 14.1 an overall decrease in infiltration efficiency is observed with an increase in slope. Similar, a decreasing tendency is seen in the infiltration efficiency as the statistical return period of a rain-event is increased. It is noticeable how a small slope results in higher infiltration efficiencies, while slopes above 10‰ result in similar infiltration efficiencies.

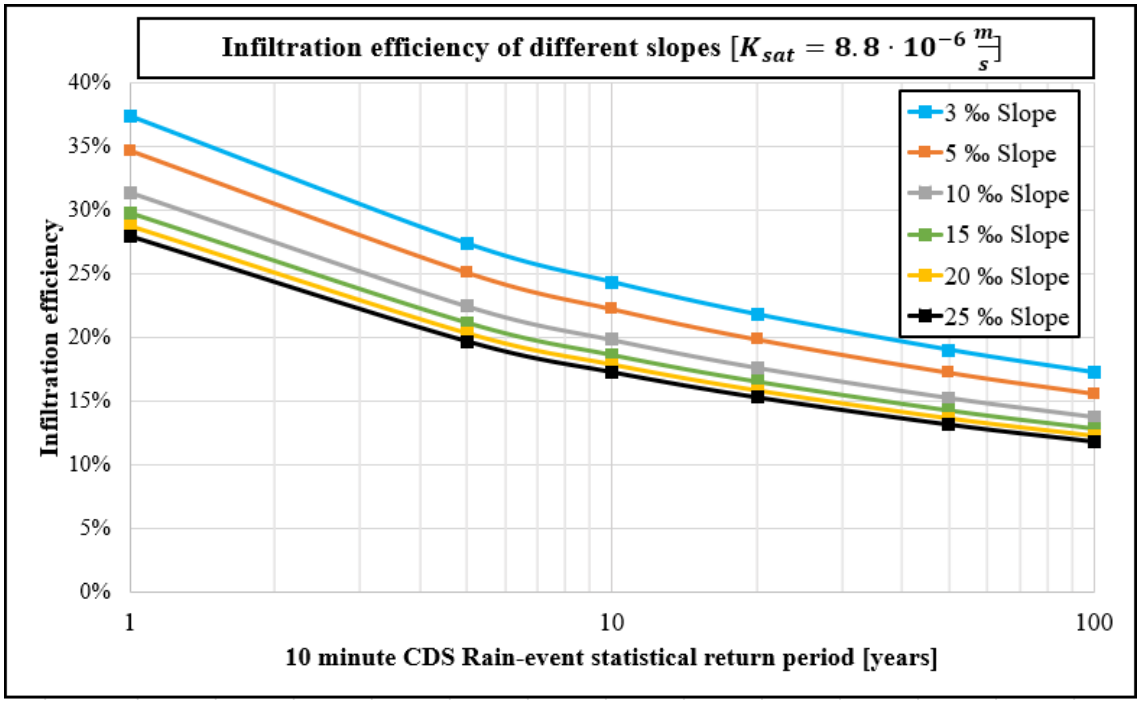

Figure 14.1. Infiltration efficiencies dependent on varying swale slope. Results are based on a varying a 1, 5, 10, 20, 50 and 100 year return period. The CDS rain events all have a duration of 10 minutes. Horton infiltration is applied.

To further investigate the effect of slope on rain events with longer duration, the setup is modelled with a duration of 120 minutes for the same statistical return periods. This can be seen in Figure 14.2. It is noticeable how the effect swale slope becomes less relevant, with decreasing infiltration efficiencies primarily being a result of increased statistical return periods.

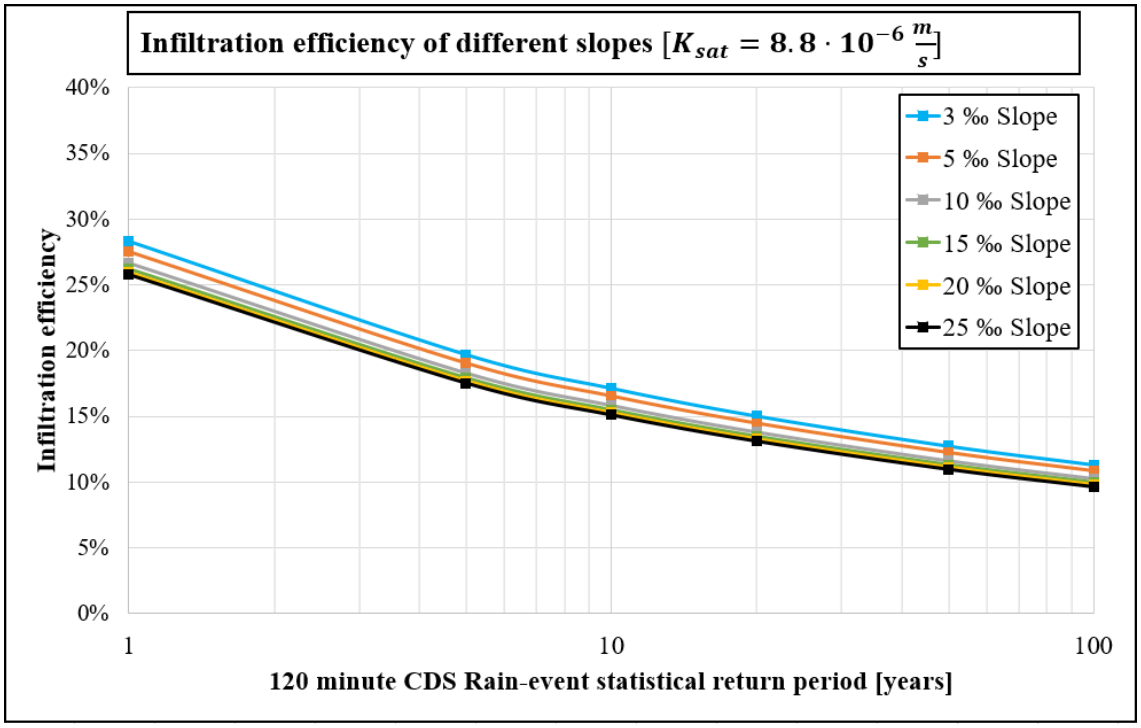

Figure 14.2. Infiltration efficiencies dependent on varying swale slope. Results are based on a varying a 1, 5, 10, 20, 50 and 100 year return period. The CDS rain events all have a duration of 120 minutes. Horton infiltration is applied.

Swales are typically constructed with minimum 5‰ longitudinal slope, since this is the minimum slope of the road. The longitudinal slope of 5‰ is therefore applied as a constant slope value in the following investigation of the saturated hydraulic conductivities effect on infiltration efficiency.

14.2 Effect of saturated hydraulic conductivity

The range of saturated hydraulic conductivities are investigated in order to highlight uncertainty related to local variability in saturated hydraulic conductivity, affecting the infiltration efficiency.

In Figure 14.3 the infiltration efficiency of a swale with varying saturated hydraulic conductivity is presented. Infiltration efficiency range from 4-55% efficiency, when considering both the high end and the low end of the saturated hydraulic conductivity range, during a 1 year statistical return period.

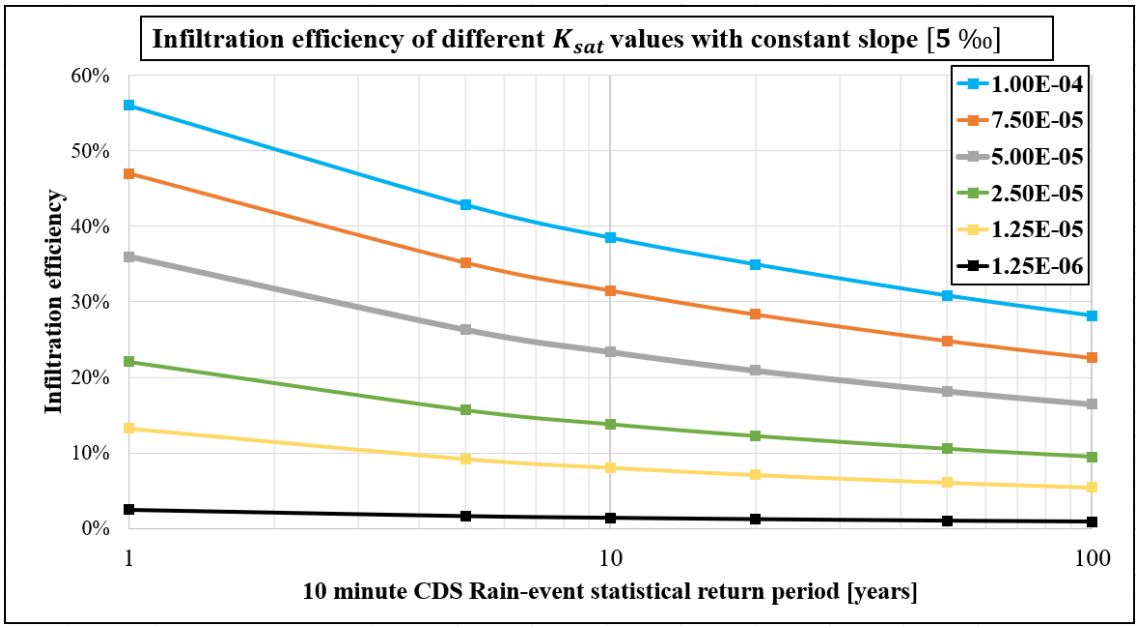

Figure 14.3. Infiltration efficiency as a function of varied saturated hydraulic conductivities and constant swale slope. Results are based on a varying a 1, 5, 10, 20, 50 and 100 year return period. The CDS rain events all have a duration of 10 minutes. A constant seepage rate is applied.

The general trend in Figure 14.3, indicates a decrease in infiltration efficiencies with a corresponding decrease in saturated hydraulic conductivity. The greatest variation between infiltration efficiency occurs at high saturated hydraulic conductivity values and low statistical return periods, as seen on the figure. With the modelled 100-year CDS rain, the highest saturated hydraulic conductivity has an infiltration efficiency of 28%, while the lowest is $< 1\%$.

The results are confirmed by the sensitivity analysis indicating that saturated hydraulic conductivity greatly influences the overall infiltration efficiencies of vegetated swales.

The current practice of applying a saturated hydraulic conductivity value for scenarios where an unsaturated hydraulic conductivity may be dominating can thus influence the determined overall infiltration of a swale. This is investigated in the following chapter.

SWMM modelling compared to SVK

15

The following results highlight the discrepancies related to the current practice of using the SVK spreadsheet, neglecting slope and infiltration method. Firstly, the effect of implementing swale slope, while modelling different CDS rain events will be presented. Secondly, the effect of implementing Horton infiltration opposed to the constant seepage rate defined in SVK is modelled in SWMM to highlight variation in emptying time, infiltration rate and runoff.

The constant seepage rate in the SVK swale is defined as the average hydraulic conductivity from the SRI run in Marshalls Allé. The initial infiltration and saturated hydraulic conductivity in the swale which is modelled with slope and Horton infiltration, is based on average Horton parameter values obtained from the SRI test at Marshalls Allé.

15.1 The effect of implementing slope

In Figure 15.1, two swales are modelled in SWMM. One representing a swale with a longitudinal slope of 0‰ and one swale that has a longitudinal slope of 5‰. Both swales are modelled with a constant seepage rate of 5E-05 $\frac{m}{s}$. The swale is implemented with a 5‰ slope being the standard longitudinal slope of roads.

The difference between infiltration- and runoff-time in the two swales highlights the the difference in emptying time between the existing practice implementing 0‰ slope compared to the minimum slope applied in reality of 5‰.

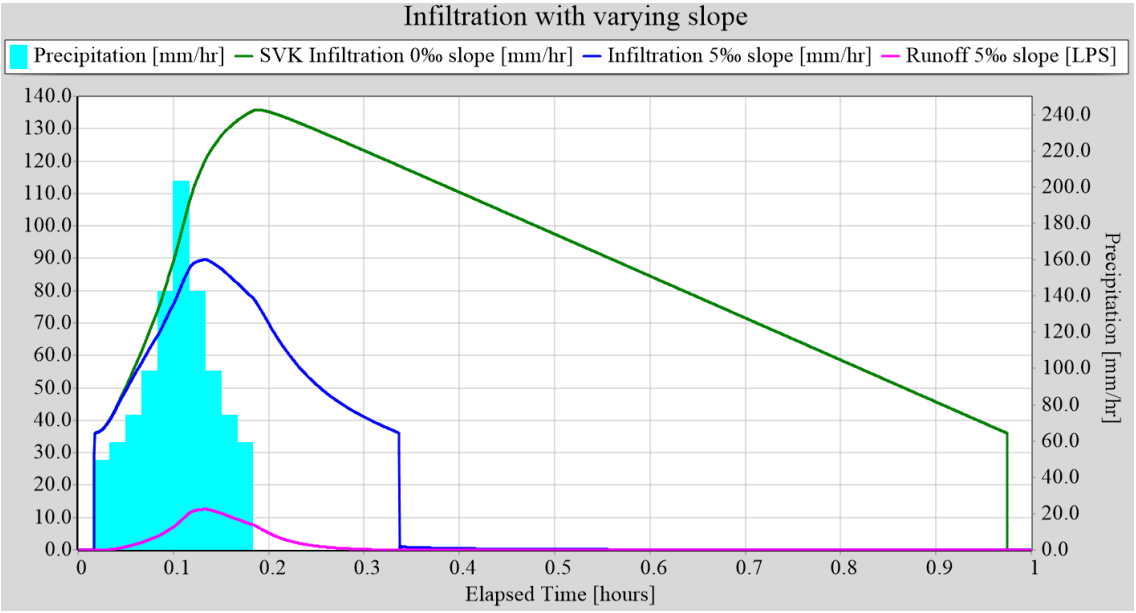

Figure 15.1. Infiltration with varying slope and constant seepage rate of 5E-05. A 10-year CDS rain with a duration of 10 minutes is applied. Green corresponds to a swale with 0‰, also called SVK 0‰. Blue corresponds to a swale with 5‰, also called SWMM 5‰. Pink is surface runoff from the swale incorporating slope (blue).

Runoff only occurs in the swale with a slope of 5 ‰, while a slope of 0 ‰, does not result in water transport and thereby runoff, hence the entire volume is infiltrated. The emptying time is defined as the time of bulk water volume to infiltrate, and can be seen to vary significantly between the two swales. Including a slope of 5‰ decreases the emptying time from 1 hour to 20 minutes (tab. 15.1).

To analyse the implemented SVK approach in SWMM, an identical setup for a swale with no slope has been conducted in the SVK spreadsheet to compare the emptying time (tab. 15.1). The SWMM setup produces similar emptying times to the SVK spreadsheet, indicating the implementation in SWMM is a comparable solution to SVK.

Table 15.1. Emptying time variation between the SVK spreadsheet and SWMM setup with presented emptying time, infiltration loss, applied K_s and slope.

Parameters	Ks [m/s]	Slope [‰]	Emptying time [min]	Infiltration efficiency [%]
SVK 0‰ slope	5E-5	0	58	100
SWMM 5‰ slope	5E-5	5	20	23
SVK Spreadsheet	5E-5	0	63	100

The infiltration efficiency is considerably reduced to 23% of the swale incorporating slope indicating a large runoff volume caused by water transport, compared to a 100% infiltration efficiency.

The implementation of swale slope decreases the infiltration efficiency, thus producing runoff. The investigation of implementing a constant seepage rate or Hortons infiltration method is thus important to understand the difference in infiltrated volume during rain events.

15.2 The effect of implementing an infiltration method

A comparison of infiltration rates between two swales with varying infiltration methods is shown in Figure 15.2. The green graph depicts the SVK calculation modelled with a constant seepage rate, while the blue graph depicts the revised method incorporation the Horton infiltration. A constant slope of 0‰ is applied for both scenarios.

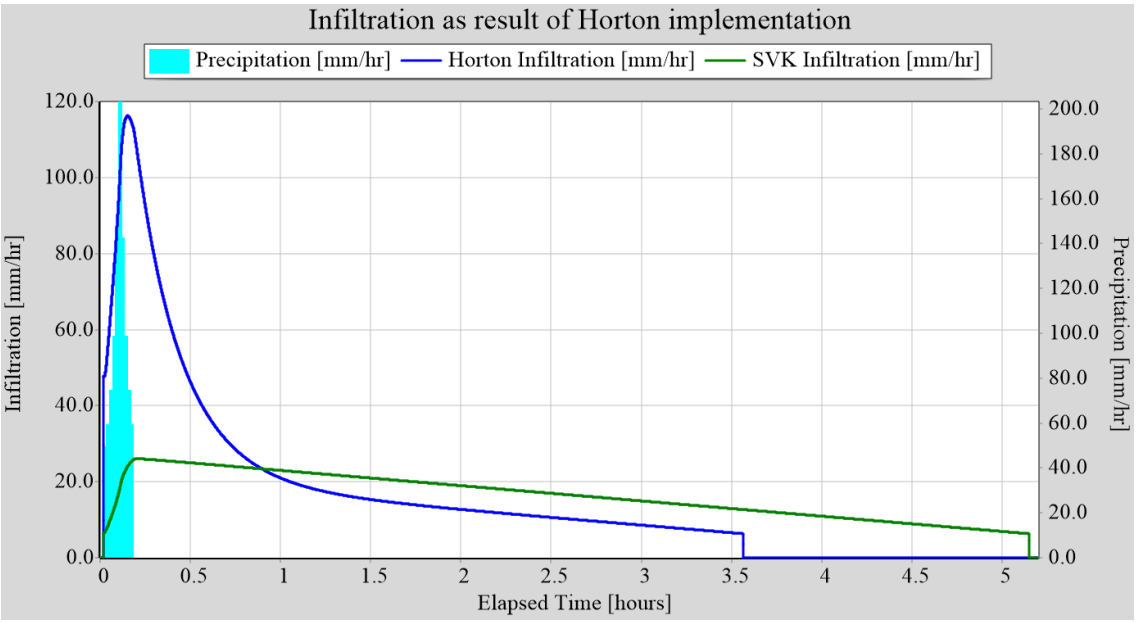

Figure 15.2. Infiltration rate and emptying time comparison between the implementation of Horton's method (blue) versus a constant seepage rate (green). Rain is depicted on the right side axis.

From Figure 15.2, varying emptying times are noticeable with approximately 1.5 hours difference between the Horton's infiltration compared to a constant seepage rate. This is caused by the initial infiltration, which decreases to the same saturated hydraulic conductivity as in the SVK setup, which has a constant saturated hydraulic conductivity from the beginning of the rain event. In Table 15.2, the specifications for each model setup can be seen.

Table 15.2. Comparison of emptying times between Horton's infiltration and constant seepage rate. Input values of hydraulic conductivities and slope are also presented.

Parameters	Initial K [m/s]	Ks [m/s]	Slope [‰]	Emptying time [min]	Infiltration efficiency [%]
Swale 1 Horton infiltration	6.6E-5	8.8E-6	0	214	100
Swale 2 Constant seepage rate (SVK)	8.8E-6	8.8E-6	0	309	100

The emptying time when comparing Horton infiltration with a constant seepage rate increases from 214 til 309 minutes, which is a 44 % increase. This increase in emptying time when modelling without an infiltration method highlights an uncertainty related to the SVK spreadsheet of overestimating infiltration times by disregarding an initial infiltration rate.

15.3 Numerical modelling compared to existing practice

Combining the implementation of slope and infiltration model allows a comparison of the revised swale dimensioning practice in SWMM with the existing practice in SVK. In Figure 15.3, two swales are modelled. The green line represents the SVK practice of a constant seepage rate and 0‰ slope, while the blue line represents a swale modelled with 5‰ slope and Horton infiltration.

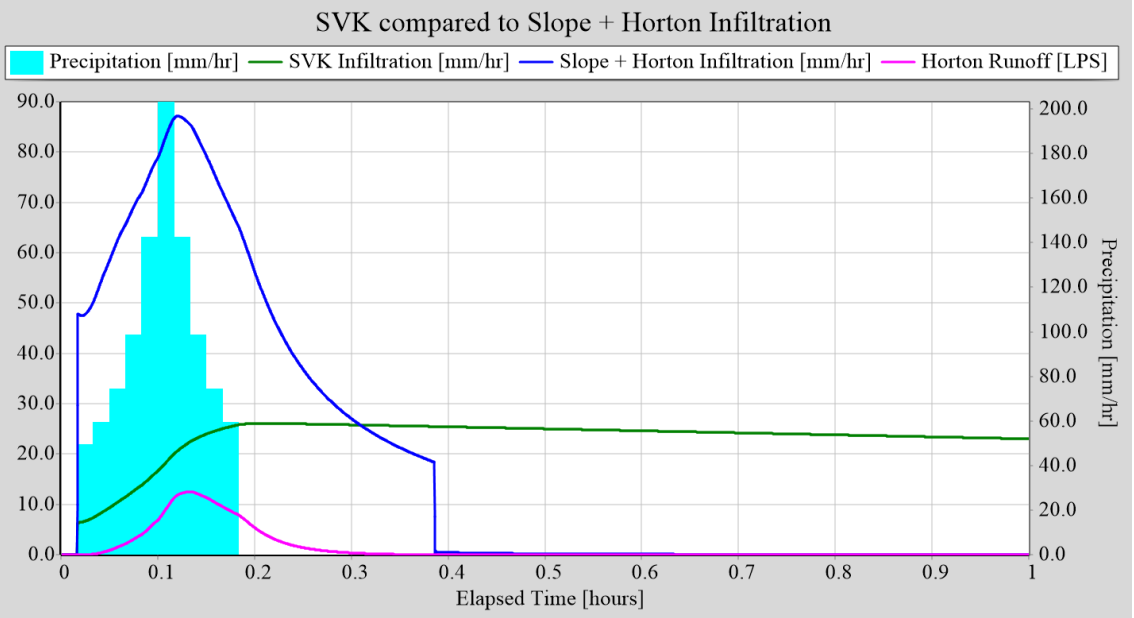

Figure 15.3. Results from implementing both slope and Horton infiltration, compared to SVK practice. Rain is depicted on the right side axis.

In Table 15.3, the results of the modelling is presented. It is observed that the SVK swale infiltrates 100% of the rain event, while the SWMM swale infiltrates 22%.

The swale with 5‰ slope and Horton infiltration has an emptying time of 23 minutes compared to the SVK swale having an emptying time of 309 minutes. Indicating dimensioning without slope can lead to large volumes of water not accounted for, caused by runoff as a result of longitudinal slope.

Table 15.3. Values for modelled swales with implemented slope, emptying time and infiltration efficiency. SVK versus SWMM implementation.

Parameters	Initial K [m/s]	Ks [m/s]	Slope [‰]	Emptying time [min]	Infiltration efficiency [%]
SWMM swale	6.6E-5	8.8E-6	5	23	22
SVK swale	8.8E-6	8.8E-6	0	309	100

SWMM analysis of field locations 16

In the following sections, the results of infiltration efficiencies, total infiltration volumes and total runoff volumes are presented for Marshalls Allé and Skjoldet based on the combination of swale slope and infiltration method versus the SVK practice.

16.1 Infiltration efficiency

16.1.1 Marshalls Allé

The model results of the three swale sections resulted in infiltration efficiencies >5% for both CDS events and infiltration efficiencies exceeding 35% within all swales for a 10-year historic series (tab. 16.1). Swale 1 has the highest infiltration efficiency. Swale 1 and 3 have decreasing infiltration efficiencies from a 10-minute to a 120-minute CDS rain, while swale 2 infiltration efficiency increases.

Table 16.1. Infiltration efficiencies for two CDS dimensioning events and one historical rain series in Marshalls Allé. Values are presented for all swale sections.

Subcatchment	**Infiltration efficiency [%]**		
Marshalls Allé	CDS 10 year 10 min	CDS 10 year 120 min	10 year historic
Swale1	10.5	7.9	49.7
Swale2	5.6	6.5	39.3
Swale3	6.2	5.5	36.0

16.1.2 Skjoldet

The model results of the two independent swale sections produced approximately 3 times higher infiltration efficiencies in swale 1 compared to swale 2, for both CDS events. Swale 1 additionally produces the highest infiltration efficiency for the historic rain event (tab. 16.2).

Table 16.2. Infiltration efficiencies for two CDS dimensioning events and one historical rain series in Skjoldet. Values are presented for all swale sections.

Subcatchment	**Infiltration efficiency [%]**		
Skjoldet	CDS 100 year 10 min	CDS 100 year 120 min	10 year historic
Swale1	13.0	16.8	68.0
Swale2	4.2	5.1	35.8

The results indicate smaller infiltration efficiencies for the statistical return periods when compared to the 10 year historic series.

16.2 Total infiltration and runoff volumes

In Table 16.3 and 16.4 SWMM results for infiltration efficiency, total runoff volume and total infiltration volume are presented. The results are presented based on three rain events, with varying length and intensity. This is done for Marshalls Allé and Skjoldet. The historic rain series results are presented with the unit of mm per event, due to the large infiltrated volume over ten years. Events have an applied separation time of 2.5 hours, with events determined based on infiltration and runoff events within SWMM. Average event times are applied for the total volumes for each field location.

It can be observed that the total infiltrated volume and total runoff volume increase with increasing intensity. Furthermore, it is apparent that based on the modelling results infiltration occurs within the swale system. A significant runoff is also produced when implementing Horton's infiltration and slope gradient, compared to a 100% infiltration efficiency in the SVK spreadsheet.

Within a dimensioning 10-year 10 minute and 120 minute event it is observed that 6.6-7.4% and 8.6-10.9% of the total inflow infiltrates in Marshalls Allé and Skjoldet respectively. This is increased for the 10-year historic event, with 41 and 51% of the total inflow infiltrating.

Table 16.3. SWMM results for Marshalls Allé with given infiltration efficiency, total infiltration volume and total runoff volume. Total volumes for the historic event is presented in $\frac{mm}{event}$ during the 10-year period. For CDS events total volumes are presented in mm and the infiltration efficiency is given in %.

Swale values	**Rrain events**		
	CDS 10-year 10 min	**CDS 10-year 120 min**	**10 year historic**
Marshalls Allé Infiltration Efficiency [%]	**7.43**	**6.63**	**41.67**
Total infiltration volume [mm] and [$\frac{mm}{event}$]	47.40	107.71	27.96
Total runoff volume [mm] and [$\frac{mm}{event}$]	655.87	1586.92	62.62

Table 16.4. SWMM results for Skjoldet with given infiltration efficiency, total infiltration volume and total runoff volume. Total volumes for the historic event is presented in $\frac{mm}{event}$ during the 10-year period. For CDS events total volumes are presented in mm and the infiltration efficiency is given in %.

Swale values	**Rain events**		
	CDS 100-year 10 min	**CDS 100-year 120 min**	**10 year historic**
Marshalls Allé Infiltration Efficiency [%]	**8.6**	**10.95**	**51.9**
Total infiltration volume [mm] and [$\frac{mm}{event}$]	47.70	144.07	19.09
Total runoff volume [mm] and [$\frac{mm}{event}$]	592.78	1383.10	26.43

In the following chapter, a discussion of the results are conducted.

17 Discussion

17.1 The effect of swale slope on infiltration efficiency

One of the goals of this thesis was to investigate the effect of swale slope on infiltration efficiency. When the slope effect was investigated for a single swale system with varying rain duration, the results indicate that infiltration occurs even in swales constructed with a large slope, as seen in Figures 14.1 and 14.2. This was also reported by Fox et al. [1997] who determined a decrease in infiltration efficiency due to an increase in slope in their experimental analysis.

Surprisingly a contradiction to the general assumption of all water becoming run-off during large statistical return periods is questioned based on the results in Figures 14.1 and 14.2. It is observed that for a 100-year rain event, approximately 12-17% of the total inflow infiltrates, highlighting infiltration also occurring during high-intensity rain events.

From Figure 14.1 and 14.2 it can be observed that the statistical return period has a larger influence on infiltration efficiencies than the swale slope. Longer rain duration results in the initial infiltration rate decreasing towards soil saturation before the actual statistical intensity occurs. The increase in soil moisture leads to larger run-off volumes, lowering infiltration efficiencies. It is observed that with the 10-minute duration, the soil does not reach saturation, which is why a higher efficiency is observed than in the 120-minute duration. Hence, swale slope will have a larger effect when analysing short-duration rain events.

The slope effect was insensitive to the infiltration efficiencies in the sensitivity analysis (chp.13). This corresponds to the result of Figure 14.2, however, from Figure 14.1 the results indicate swale slope influencing overall infiltration efficiency when considering short-duration rain events. This is observed for slope values smaller than 10‰. From the swale slope values of 3-5‰ a larger difference in infiltration efficiencies is observed compared to slope values above 10‰. Applying Horton's infiltration, where an increase of the swale slope from 5‰ to 25‰ results in approximately a 5% decrease in infiltration efficiency of a 10-year 10-minute statistical return period, increasing the total run-off from the swale to connected SuDS.

A generalised tendency of swale slope and infiltration efficiencies are difficult to obtain due to infiltration efficiencies varying greatly based on various influencing parameters and not solely on the swale slope. A generalised impact of slope on swale infiltration is difficult to attain in practice, which is why a standard model setup can be an approach to investigate possible correlations. When the effect of swale slope is implemented in the SWMM standard model setup, the comparison and variation between the SVK method

and the SWMM practice are highlighted. In Figure 15.3 a model setup consisting of Horton's infiltration produces significantly shorter swale emptying times, reduced infiltration efficiency and run-off volumes compared to the implemented SVK assumptions of constant seepage rate and 0‰ swale slope.
The current practice of the SVK spreadsheet results in 100% infiltration efficiencies with long emptying times due to the neglection of water transport and thereby run-off, which in reality is false. The influence of swale slope within the model setup is evident. Compared to the SVK calculations, the incorporation of a 5‰ swale slope compared to 0‰ highlights that for the same system, the calculated infiltration efficiency is reduced by 78%. Applying the current SuDS dimensioning practice will, therefore, overestimate the actual infiltration occurring within a vegetative swale due to the neglection of the swale longitudinal slope and infiltration method.

Based on the results presented in figures 14.1, 14.2 and 15.3 a general indication is seen for the effect of swale slope on infiltration efficiencies is observed. The individual variation of swale slope is less significant when compared to the effect of implementing slope versus no slope. The current application of applying 0‰ the slope is, therefore, a crude overestimation of actual infiltration efficiencies since the effect of swale slope significantly decreases infiltration efficiencies from 0‰ to 5‰. However, a general tendency is observed of decreasing infiltration efficiencies with increasing swale slope. Contradictory results are presented in the meta-study of slope effect on infiltration rate, as studies found infiltration efficiencies increasing with increasing slope. This result highlights the discrepancy between a conceptualised model and reality, which may be affected by other parameters.

The article by Fox et al. [1997] generally highlights the uncertainties related to the relationship between slope angle and infiltration rate change in the real world, as soil parameters also vary greatly, which may affect infiltration in different soils. One parameter influencing the general infiltration efficiency was the rain intensity observed when comparing synthetic and historical events.

17.2 Comparing synthetic and historical events for swale dimensioning

When comparing infiltration efficiencies within Marshalls Allé and Skjoldet, the difference between historical rain data and synthetically created rain is evident, including the spatial variation between swale sections (tab. 16.1 and 16.2). Applying a synthetic 10-year CDS rain results in an average infiltration efficiency for Marshalls Allé of 6.6-7.4% while modelling the 10-year historic rain series results in an overall infiltration efficiency of 41.6% as seen in Table 16.3.

When Niras dimensioned the swales, the criteria was that they could handle a 10-year, 10-minute box rain. However, this was tested with a CDS rain of the same return period and duration, which amounted to an average infiltration efficiency of 7.4% compared to the expected 100%. This large discrepancy highlights uncertainties when dimensioning swales with slope utilising the SVK spreadsheet and the difference in applying a CDS versus a box rain.

Similar results occur for Skjoldet, with 51.9% infiltration efficiency for the simulated 10-year historical series. The lower infiltration efficiencies experienced with CDS rain are due to the high rain intensity. There is no certainty that the historic rain series contains a rain event equivalent to a 10 year return period in intensity. On the contrary, the historical rain series could, statistically, however, also contain several high-intensity rain events such as 10-, 20- or higher statistical return period events.

It is evident when using a 10 year CDS rain as a dimensioning rain for the swale systems in Marshalls Allé and Skjoldet smaller total infiltrated volumes compared to the total run-off volumes (tab. 16.3 and 16.4), are observed when compared to the historic infiltration. The historic rain series results in approximately 50% of the total inflow being infiltrated per event. Based on the numerical results, the current practice of implementing a statistical return period for swale dimensioning purposes is therefore questioned since they indicate that swales are not particularly effective in handling high intensities but are well equipped for reducing smaller rain events seen for the historic rain series.

This becomes especially relevant when considering the future effect of climate change. The increase in high-intensity rainfall events must be implemented in future SuDS dimensioning. However, the higher intensities will reduce the overall infiltration efficiencies of implemented swale systems, as indicated by Tables 16.3 and 16.4. Therefore, an argument can be made that vegetative swales should not be implemented for such statistical rare events, such as the dimensioning synthetic rain events, but dimensioned to reduce total run-off volumes from everyday rain events, as seen in the historic rain series. Swales should have the capability of containing volumes corresponding to the peak intensity of a rain event but do so to act as transport swales to connected water retention basins. The current SuDS dimensioning practice needs a revision regarding applied rain events for dimensioning, but also a revision from the current lumped SVK spreadsheet to a dynamic numerical model.

17.3 Revising the current dimensioning practice of swales

The saturated hydraulic conductivity plays an essential role in infiltration efficiencies, especially during large return periods, as seen in Figure 14.3. The influence of the saturated hydraulic conductivity indicates the importance of determining the soil properties accurately as a variation of 1-order of magnitude results in an infiltration efficiency decrease of 30%. A standard interval of saturated hydraulic conductivity from 1E-04 $\frac{m}{s}$ to 1E-05 $\frac{m}{s}$ is given for the locations of Marshalls Allé and Skjoldet. The predetermined saturated hydraulic conductivity will often vary from the planning value to the implemented value, resulting in an uncertainty of the actual swale saturated hydraulic conductivity. This was observed in both field locations, having lower saturated hydraulic conductivities than the applied values for dimensioning of the SuDS, resulting in lower swale infiltration efficiencies.

Based on Figure 14.3 and 14.1 indicating decreasing infiltration efficiencies with increasing slope and decreasing saturated hydraulic conductivity, the actual infiltration within the two field locations is overestimated, with infiltration efficiencies varying approximately 40% when comparing the measured saturated hydraulic conductivities to the expected

interval. The determination of the saturated hydraulic conductivity should be based on field infiltration measurements rather than theoretical or predetermined values to calculate accurate infiltration efficiencies of investigated SuDS.

Based on Figures 15.2 and 15.1 it is also apparent that the current swale dimensioning practice simplifies key parameters influencing the actual infiltration and runoff volumes. Therefore, the authors of this thesis suggest a revision of the SVK spreadsheet to incorporate aspects such as swale slope and Horton's infiltration. A distributed numerical model such as SWMM increases the complexity of SuDS dimensioning practice but is still argued to be within practical engineering capabilities due to the relative few input parameters required. The proposed revision of the SVK spreadsheet for swale dimensioning in SWMM allows time-dependent simulations capable of processing historic rain series for dimensioning purposes while investigating multiple swale systems at once and the interaction between coupled swale sections, to differentiate between varying hydraulic conductivity profiles, as presented in Table 8.1.

Applying SWMM for the investigation of swale infiltration efficiencies also incorporates simplifications of the natural system, especially regarding the transport and routing of surface run-off. The coupling of subcatchments in SWMM may result in imprecise modelling results caused by re-routing overland flow between subcatchments. This is caused by run-off from one swale to another being evenly distributed throughout the downstream swale, as done with the rain, resulting in a theoretical underestimation of the total infiltration time. The simplification of water transport is still considered an improvement in swale infiltration investigations due to the current practice of SVK not implementing transport altogether.

Part VI

Conclusion and future application

The purpose of this part is to summarise the most significant conclusions made in the project and to elucidate the further development and future applications of the hydrodynamic model and swale infiltration practice. Finally a brief comment is given focusing on aspects to include within swale infiltration modelling for future studies.

18 Conclusion

In the sensitivity analysis, key parameters were investigated to determine their influence on infiltration efficiency. The results clearly indicate discrepancies between the current practice for swale dimensioning utilising the SVK spreadsheet and the suggested revision applying the Storm Water Management Model: SWMM. The discrepancy of the results when the SVK spreadsheet is compared to SWMM may stem from several differences, both methodically, parameterisation and conceptual understanding of the system.

The investigation conducted in this thesis leads to the following conclusions:

- The modelled infiltration efficiencies, indicate that the current practice utilising the SVK spreadsheet, overestimates infiltration related to the dimension-giving rain events significantly.
- Based on the results, it is evident that the implementation of swale slope and infiltration method influences the swale infiltration efficiency and emptying time significantly. The current practice of neglecting swale slope and application of constant seepage rate in the SVK spreadsheet should, therefore, be revised for more accurate SuDS dimensioning.

Future perspectives in swale infiltration modelling

19

19.1 Aspects to include

Pollutant control is an option in SWMM, allowing for pollutant decay and removal analysis. This was, however, not the scope of this thesis but can add a benefit to environmental engineering practices.

The maintenance and operation of the swales were similarly not included in the scope of this thesis. However, a study by Weiss et al. [2010] states that the overall efficiency changes over time. Therefore, this perspective would be essential to include when modelling historical rain series, where the swale might expect to decrease in infiltration efficiency based on soil pores clogging with fine sediments.

The saturated hydraulic conductivity may vary throughout the year, caused by temporal changes. This was not considered in the modelling of this thesis but should be incorporated if measurements of the saturated hydraulic conductivity is taken throughout the year.

Throughout this thesis, the modelled results are solely based on input parameters as neither calibration nor validation data were available. In future studies of infiltration efficiencies of vegetative swales using SWMM, calibration and validation data should be included, as this adds certainty to the results presented.

19.2 Optimising swale design in SWMM

The optimisation of swale design in SWMM could be achieved by altering the way SWMM 'understands' the model setup. Combining the node and subcatchment models could create a tool capable of modelling more precise setups than each model. This could be achieved by connecting nodes, which act as inlets and outlets, to a subcatchment where a LID control constitutes 100% of the subcatchment area. This would ensure the water transport to be described by the kinematic wave solution rather than the Manning equation while applying an infiltration method through the LID module.

Bibliography

Aalborg Kommune, Miljø- og Energiforvaltningen, 2016a. *Hydrauliske forudsætninger, LAR-metodekatalog.* `https://www.aalborg.dk/media/15028438/introduktion-lar-metodekatalog.pdf`. Downloaded: 15-02-2022.

Aalborg Kommune, Miljø- og Energiforvaltningen, 2016b. *Render og grøfter, LAR-metodekatalog.* `https://www.aalborg.dk/media/15028448/render-groefter.pdf`. Downloaded: 15-02-2022.

Ahmed, F., Gulliver, J. S. and Nieber, J. L., 2015. *Field Infiltration Measurements in Grassed Roadside Drainage Ditches: Spatial and Temporal Variability.* Journal of Hydrology, 530, 604–611. doi: https://doi.org/10.1016/j.jhydrol.2015.10.012.

Arnbjerg-Nielsen, K. and Sørup, H. J. D., 2019. *Validering af eksisterende dimensionspraksis for LAR-anlæg ved hjlæp af langtidssimuleringer.* EVA : Erfaringsudveksling i vandmiljøteknikken, 32 (1), 16–22. ISSN 1901-3663.

Blohm, F. J. A., 2016. *Determination of Hydraulic Conductivities through grain size analysis.* Boston College, Dissertation.

Bouwer, H., Back, J. T. and Oliver, J. M., 1999. *Predicting Infiltration and Ground-Water Mounds for Artificial Recharge.* Hydrologic Engineering, 4 (4), 350–353. doi: https://doi.org/10.1061/(ASCE)1084-0699(1999)4:4(350).

Carrier, W. D., 2003. *Goodbye, Hazen; Hello, Kozeny-Carman.* Journal of Geotechnical and Geoenvironmental Engineering, 129 (11), 1054–1056. doi: https://doi.org/10.1061/(ASCE)1090-0241(2003)129:11(1054).

Davis, A. P., Stagge, J. H., Jamil, E. and Kim, H., 2012. *Hydraulic performance of grass swales for managing highway runoff.* Water Research, 46, 6775–6786. doi: https://doi.org/10.1016/j.watres.2011.10.017.

EEA, cited January 2022. *European Environment Agency - Precipitation change.* URL `https://www.eea.europa.eu/data-and-maps/data/external/euro-cordex-new-high-resolution`.

Fox, D. M., Bryan, R. B. and Price, A. G., 1997. *The influence of slope angle on final infiltration rate for interrill conditions.* Geoderma, 80, 181–194. doi: PH:S0016-7061(97)00075-X.

Gregersen, I. B., Rasmussen, S. H., Madsen, H. and Arnbjerg-Nielsen, K., 2015. *Dimensionering af LAR-anlæg (notat version 2.0).* The Water Pollution Committee of The Society of Danish Engineers.

Jensen, M. B., 2004. *Hydrological conditions for contaminant leaching through highway swales.* Water Air and Soil Pollution, 158 (1), 169–180. doi: https://10.1023/B:WATE.0000044851.30151.e0.

Kale, V. and Sahoo, B., 2011. *Green-Ampt Infiltration Models for Varied Field Conditions: A Revisit.* Water Resources Management, 25, 3505–3508. doi: https://doi.org/10.1007/s11269-011-9868-0.

Loll, P. and Moldrup, P., 2000. *Soil Characterzation and Polluted Soil Assessment.* Aalborg University.

Mein, R. G. and Larson, C. L., 1973. *Modeling Infiltration during a Steady Rain.* Water Resources Research, 9 (2), 384–394. doi: https://doi.org/10.1029/WR009i002p00384.

Nielsen, J. E., Karup, D., de Jonge, L. W., Ahm, M., Bentzen, T. R., Rasmussen, M. R. and Moldrup, P., 2018. *Can the Volume Ratio of Coarse to Fine Particles Explain the Hydraulic Properties of Sandy Soil?* Soil Science Society of America, 82 (5), 1093–1100. doi: https://doi.org/10.2136/sssaj2018.02.0083.

Nielsen, K. T., Nielsen, J. E., Uggerby, M. and Rasmussen, M. R., 2020. *Moddelling of Subsurface Throughflow in Urban Pervious Areas.* 25 (12), 1–2. doi: https://doi.org/10.1061/(ASCE)HE.1943-5584.0001990.

Parnas, F. E. Å., Abdalla, E. M. and Muthanna, T. M., 2021. *Evaluating three commonly used infiltration methods for permeable surfaces in urban areas using the SWMM and STORM.* Hydrology Research, 52 (1), 160–175. doi: https://doi.org/10.2166/nh.2021.048.

Rawls, W. J., Brakensiek, D. L. and Miller, N., 1983. *Green-Ampt Infiltration Parameters From Soil Data.* Journal of Hydraulic Engineering, 109 (1), 62–70. doi: 0.1061/(ASCE)0733-9429(1983)109:1(62).

Rawls, W. J., Ahuja, L. R., Brakensiek, D. L. and Shirmohammadi, A., 1993. *Handbook of hydrology, Chapter 5, Infiltration and Soil Water Movement.* McGraw Hill. ISBN: 0-07-039732-5, 1st Edition.

Rice, R. C., Milczarek, M. and Keller, J., 2014. *A Critical Review of Single Ring Cylinder Infiltrometers with Lateral Flow Compensation.* 14th Biennial Symposium on Managed Aquifer Recharge.

Rossman, L. A., 2017. *Storm Water Management Model Reference Manual - Volume 2 Hydraulics, Chp. 1, 2, 4.* `https://nepis.epa.gov/Exe/ZyPDF.cgi?Dockey=P100S9AS.pdf`. Downloaded: 15-04-2022.

Rossman, L. A., 2016a. *Storm Water Management Model Reference Manual - Volume 1 Hydrology, Chp. 1, 3, 4.* `https://nepis.epa.gov/Exe/ZyPDF.cgi?Dockey=P100NYRA.txt`. Downloaded: 15-04-2022.

Rossman, L. A., 2016b. *Storm Water Management Model Reference Manual - Volume 3 Water quality, Chp. 6.* https://nepis.epa.gov/Exe/ZyPDF.cgi/P100P2NY.PDF?Dockey=P100P2NY.PDF. Downloaded: 25-04-2022.

Rossman, L. A., 2015. *Storm Water Management Model User's Manual Version 5.1.* https://www.epa.gov/sites/default/files/2019-02/documents/epaswmm5_1_manual_master_8-2-15.pdf. Downloaded: 11-04-2022.

Rujner, H., Leonhardt, G., Perttu, A., Marsalek, J. and Viklander, M., 2016. *Advancing green infrastructure design: Field evaluation of grassed urban drainage swales.* In Proceedings of the 9th International Conference on Planning and Technologies for Sustainable Management of Water in the City, Lyon, France, 28. June - 1. July.

Rushton, B. T., 2001. *Low-impact parking lot design reduces runoff and pollutant loads.* Journal of water resources planning and management, 127, 172–179. doi: https://10.1061/(ASCE)0733-9496(2001)127:3(172).

Shafique, M., Kim, R. and Kyung-Ho, K., 2018. *Evaluating the Capability of Grass Swale for the Rainfall Runoff Reduction from an Urban Parking Lot, Seoul, Korea.* Environmental Research and Public Health, Vol. 15, 1–13. doi: https://doi.org/10.3390/ijerph15030537.

Trenberth, K. E., 2011. *Changes in precipitation with climate change.* Climate Research, 47, 123–138. doi: 10.3354/cr00953.

UN, cited January 2022. *2021 floods: UN researchers aim to better prepare for climate risks.* URL https://unric.org/en/2021-floods-un-researchers-aim-to-better-prepare-for-climate-risks/.

United States Environmental Protection Agency, 2003. *Protecting Water Quality from Urban Runoff.* United States Environmental Protection Agency.

Weiss, P. T., Gulliver, J. S. and Erickson, A. J., 2010. *The Performance of Grassed Swales as Infiltration and Pollution Prevention Practices.* Minnesota University.

Winther, L., Linde, J.J., Jensen, H. T., Mathiasen, L.L. and Johansen, N.B., 2011. *Afløbsteknik, Chapter 5 Rain and rainwater runoff.* Polyteknisk Forlag. ISBN:978-87-502-1015-3, 6st Edition.

Laboratory methods for soil sample analysis

A

In the following appendix, an overview of the procedure for collecting, transporting and analysing the collected soil samples at the two field locations: Marshalls Allé and Skjoldet is presented. The soil samples were brought back to the laboratory to investigate the:

- Grain size distribution
- Soil water content
- Organic matter

Methods applied follow appertaining standards further described in the standard DS/CEN ISO/TS 17892-4, DS/CEN ISO/TS 17892-1, DS 204 and DS/EN 1997-2, Eurocode 7: Geotekning - Del 2, Nationalt Anneks N.

A.1 Grain Size Distribution

Before the initial sieving, loose soil samples from the two locations is sieved in a 2 mm sieve to exclude large particles. Then approximately 100g of the remaining soil is put into a sieving tower, where soil particles are filtered through 8 different mesh widths (fig. A.1):

1. 1 mm
2. 0.5 mm
3. 0.25 mm
4. 0.2 mm
5. 0.125 mm
6. 0.075 mm
7. 0.063 mm

One grain size distribution is conducted per location (two in total), to indicate the grain size distribution for all swale sections within the area of investigation. This is based on the assumption of homogeneity of soil composition from the construction phase of the swales.

Figure A.1. Grain size distribution done in a sieving tower.

The soil samples are air-dried for one week at room temperature (22 °C) before the grain size distribution started. After 20 minutes of sieving, content from each sieve is weighed and noted. The bottom sieve contains particles <0.063 mm with silt, clay and partially fine sand fractions. The fractions of each category are distributed based on the assumption of even distribution (1/3 for each fraction). A total of 100% for the weight distribution is not obtained due to loss of soil material during the weighing process (tab. A.1, A.2).

Table A.1. Grain size distribution of soil based on sieving tower results from Marshalls Allé. Total percentage 99.75%.

Marshalls Allé				
Depth	**Clay**	**Silt**	**Fine sand**	**Coarse sand**
cm	<0.002 mm	0.002-0.02 mm	0.02-0.2 mm	0.2-2 mm
Weight distribution [%]				
10-20	3.22	3.22	61.92	31.38

Table A.2. Grain size distribution of soil based on sieving tower results from Skjoldet. Total percentage 99.78%.

Skjoldet				
Depth	**Clay**	**Silt**	**Fine sand**	**Coarse sand**
cm	<0.002 mm	0.002-0.02 mm	0.02-0.2 mm	0.2-2 mm
Weight distribution [%]				
10-20	1.78	1.78	39.87	56.35

From the grain size distribution a cumulative weight for grain size diameter classes is acquired (tab. A.3):

Table A.3. Grain sizes corresponding to a cumulative weight.

Depth	**Location**	**d10**	**d50**	**d60**
cm		mm	mm	mm
10-20	Skjoldet	0.078	0.287	0.357
	Marshalls Allé	0.063	0.170	0.210

Figure A.2 shows the collection method for the loose soil sampling, which purpose was to be analysed in the sieving tower. The soils were taken in approximately 10-15cm depth in both locations. This was done in order to classify the topsoil, where the initial infiltration will take place. The analysed soils were used to compose a grain size distribution graph and later classify the soil based on the distribution.

Figure A.2. Collection of loose soil samples from Marshalls Allé for further laboratory analysis.

In figure A.3 the two USDA soil texture classes of Marshalls Allé (red dot) and Skjoldet (blue dot) are shown. Both soils are classified as sandy, although Skjoldet contains a larger percentage of coarse sand compared to Marshalls Allé, which has a higher percentage of fine sand, as seen in table A.4.

Table A.4. Table showing the grain size percentages used to determine the soil texture class.

Grain distribution		**Marshalls Allé**	**Skjoldet**
Coarse sand	[%]	31.80	56.35
Fine sand	[%]	61.92	39.87
Clay	[%]	3.22	1.78
Silt	[%]	3.22	1.78

The grain distributions shown in Table A.4 was used to classify the soils of Marshalls Allé and Skjoldet as seen in Figure A.3.

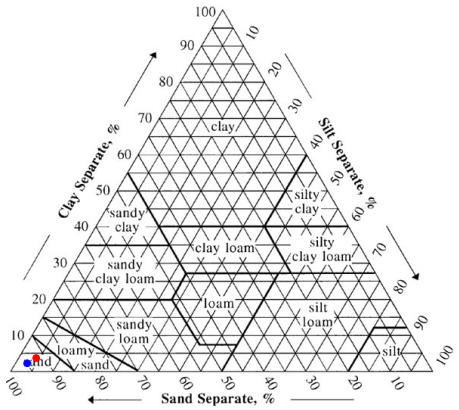

Figure A.3. Collection of loose soil samples from Marshalls Allé for further laboratory analysis. Red dot represents soil from Marshalls Allé, while the blue dot represents soil from Skjoldet.

A.2 Soil water content

Loose soil samples were collected from a 10-15 cm depth of the location before the infiltration runs. Enough soil is collected to produce 3 samples for investigation in the laboratory. A total of 3 x 3 (Marshalls Allé) + 3 x 2 (Svenstrup) were collected during the period (8-9 March).

Soil samples were stored in plastic bags in the shade to minimise water evaporation during infiltration runs. It is assumed that no water is lost during the storage and transportation of soil samples to the laboratory.

The soil water content was determined based on the AAU guide. The soil was stored in a 105 °C oven for a minimum of 24 hours. When the samples have been stored for a minimum of 24 hours, the samples were cooled in a desiccator. When the samples are cooled to room temperature, the weight is noted, and the soil water content is calculated.

A.2.1 Marshalls Allé

In Table A.5 weight information and water content for each sample is presented. Three samples are taken for each location to take an average value.

Table A.5. Soil water content for samples taken at Marshalls Allé on the 8/3/2022.

Location	**Tara nr.**	**Tara weight**	**Tara + wet**	**Tara + dry**	**Dry**	**Water content**	
[-]	[-]	[g]	[g]	[g]	[g]	[g]	[%]
Marshalls	71	4.17	146.58	128.57	124.40	18.01	**14.48**
Allé	76	4.21	122.28	109.26	105.05	13.02	**12.39**
Sec. 1	108	4.31	139.36	122.85	118.54	16.51	**13.93**
Marshalls	83	4.18	111.11	103.61	99.43	7.50	**7.54**
Allé	86	4.22	126.71	117.58	113.36	9.13	**8.05**
Sec. 2	85	4.21	143.42	132.6	128.39	10.82	**8.43**
Marshalls	90	4.19	155.64	140.28	136.09	15.36	**11.29**
Allé	91	4.2	178.74	160.31	156.11	18.43	**11.81**
Sec. 3	92	4.18	189.58	171.33	167.15	18.25	**10.92**

A.2.2 Skjoldet

In Table A.6 weight information and water content for each sample is presented. Three samples are taken for each location.

Table A.6. Soil water content for samples taken at Skjoldet on the 9/3/2022.

Location	**Tara nr.**	**Tara weight**	**Tara + wet**	**Tara + dry**	**Dry**	**Water content**	
[-]	[-]	[g]	[g]	[g]	[g]	[g]	[%]
Skjoldet Sec. 1	84	4.15	163.88	149.64	145.49	14.24	**9.79**
	88	4.18	165.4	150.64	146.46	14.76	**10.08**
	89	4.17	164.67	149.7	145.53	14.97	**10.29**
Skjoldet Sec. 2	93	4.26	141.26	125.49	121.23	15.77	**13.01**
	94	4.31	153.57	135.37	131.06	18.20	**13.89**
	97	4.3	153.6	135.44	131.14	18.16	**13.85**

A.3 Organic matter

After soil water content determination, samples were stored for four days at room temperature (22 °C) with a cloth on top to minimise moisture entering the samples. Then the samples were placed in a 550 °C oven for 24 hours to determine organic matter content. The samples are cooled to 350 °C and placed in a desiccator for four hours. Then the samples were weighed, and the organic matter content was determined with the assumption of no water entering the dried soil during the four days of storage.

A.3.1 Marshalls Allé

In table A.7 information on organic matter content (%) for soil samples collected at Marshalls Allé on the 8/3/2022.

Table A.7. Organic matter content (%) from loose soil samples taken from Marshalls Allé on the 8/3/2022.

Location	**Organic matter content**
[/]	[%]
Marshalls Allé Sec. 1	2.70
	2.59
	2.55
Marshalls Allé Sec. 2	1.04
	1.15
	1.12
Marshalls Allé Sec. 3	2.07
	2.27
	1.85

A.3.2 Skjoldet

In table A.8 information on organic matter content (%) for soil samples collected at Skjoldet on the 9/3/2022.

Table A.8. Organic matter content (%) from loose soil samples taken from Skjoldet on the 9/3/2022.

Location	**Organic matter content**
[/]	[%]
Skjoldet Sec. 1	2.18
	2.33
	2.48
Skjoldet Sec. 2	2.33
	2.36
	2.56

Single ring infiltrometer procedure

B

This appendix describes the procedure applied for the field single ring infiltrometer experiments.

Two PVC pipes with a diameter of 250mm, were cut to a similar length and used as a single ring infiltrometer to gather infiltration rates from the sites of investigation. Having two pipes allowed for multiple runs to be conducted simultaneously. The pipes were hammered 5cm into the topsoil with the use of a rubber hammer and a wooden slab. A ruler was taped to the inner side of the pipe, enabling continuous measurements of the water head during infiltration runs. This can be seen on figure B.1. This setup was used in every infiltrometer test combined with a stopwatch to note the corresponding time interval.

B.1 Sampling procedure

Sampling run procedure

1. Insert PVC pipe 5cm into topsoil
2. Fasten ruler to inside of pipe
3. Fill pipe with water to a certain height
4. Start timer
5. Log measurements as water proceeds to infiltrate

Two infiltration rates were collected by filling the pipes with water to a pre-determined water level. The first infiltration rate represents unsaturated soil conditions. The second infiltration rate represents saturated soil conditions.

The chosen water level varied between 35cm and 40cm. The level was noted, and a timer was started. In the unsaturated run, the time was noted each time the water level decreased by 0.5cm, which can be seen in table B.1. However, in the second run, the saturated run, the time intervals were kept at certain intervals, and the water level was noted after a specific amount of time. Results from Skjoldet - section 2, from the infiltrometer runs on the 14^{th} of March 2022, can be seen in Table B.1. The results shown are an example of an infiltration run. The remaining infiltration results were treated in Microsoft Excel, allowing for easy comparison.

Figure B.1. Setup of the single ring infiltrometer. Ruler attached to the inner side of the pipe. Insertion depth kept at 5cm into the topsoil.

Table B.1. Results from infiltrometer runs in Skjoldet - section 2, from the 14th of March 2022. Both unsaturated and saturated results are shown.

Skjoldet - Section 2			
Unsaturated run [cm]	**Time [min:sec]**	**Saturated run [cm]**	**Time [min:sec]**
40	0	50	0
39.5	2:22	49.5	2
39	3:33	48.8	4
38.5	5:17	48.2	6
38	6:59	47.6	8
37.5	9:20	47.1	10
37	11:20	45.8	15
36.5	13:07	44.5	20
36	14:58	43.5	25
35.5	16:48	42.1	30
35	18:53	39.8	40
34.5	20:45		
34	22:54		
33.5	25:03		
33	27:07		

B.2 Calculating the saturated hydraulic conductivity (Ks) - example

The K_s is calculated based on the Darcy velocity (Chp.4, eq. 3.5), where the infiltration velocity (v) is directly derived from the measured decrease in hydraulic head over time.

An example of this can be seen in the following, where the principle of Darcy is used, with the average water depth, insertion depth and infiltration rate velocity to calculate K_s. These terms are highlighted in figure B.2. The example given will relate to the data in table B.1 from the unsaturated run, from measurement numbers 1 and 2.

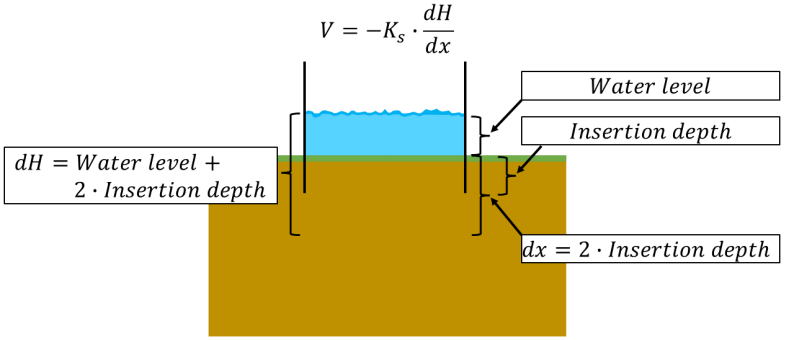

Figure B.2. Figure showing the principle for Darcy calculations.

$$\text{Average water level} = \frac{39.5cm + 39cm}{2} = 39.25cm$$

$$\text{Soil column length (dx)} = 2 \cdot \text{insertion depth} \Longrightarrow 2 \cdot 5cm = 10cm$$

$$\text{Time step}(\Delta t) = (3\,\text{min} + \frac{33\,\text{sec}}{60\text{sec/min}}) - (2\,\text{min} + \frac{22\text{sec}}{60\,\text{sec/min}}) = 1.18\text{min}$$

$$\text{Infiltration rate (V)} = \frac{\Delta H}{\Delta t} \Longrightarrow \frac{39.5cm - 39cm}{1.18\text{min}} = 0.42254\frac{cm}{\text{min}}$$

$$\frac{dH}{dx} = \frac{(\text{Soil column length} + \text{Average water level})}{\text{Soil column length}} \Longrightarrow \frac{10cm + 39.25cm}{10cm} = 4.93\frac{cm\ H2O}{cm\ soil}$$

$$K_{\text{sat}} = \frac{V}{\frac{dH}{dx}} \Longrightarrow \frac{0.42254\frac{cm}{min}}{4.93\frac{cm\ H20}{cm\ soil}} \Longrightarrow K_{sat} = 0.086\frac{cm}{min}$$

This procedure was conducted in Microsoft Excel for all data points in order to quickly process measurements as well as being able to visually inspect the data easily.

Infiltration Results: Skjoldet and Marshals Allé

C

C.1 Skjoldet results

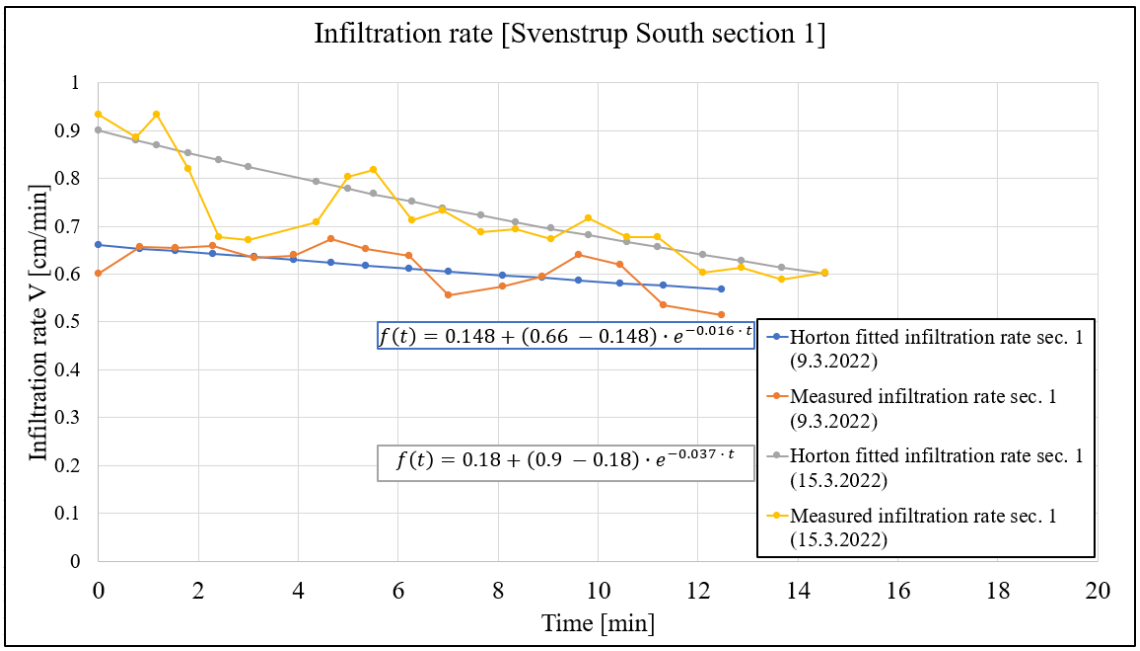

Figure C.1. Infiltration measurements using single ring infiltrometer test and fitted Horton's infiltration for Skjoldet. Both runs are unsaturated runs for section 1, with the Horton equation fitted to the infiltrometer measurements. Infiltration rates are given in cm/min. The Horton's equation is presented colour coded to corresponding curve.

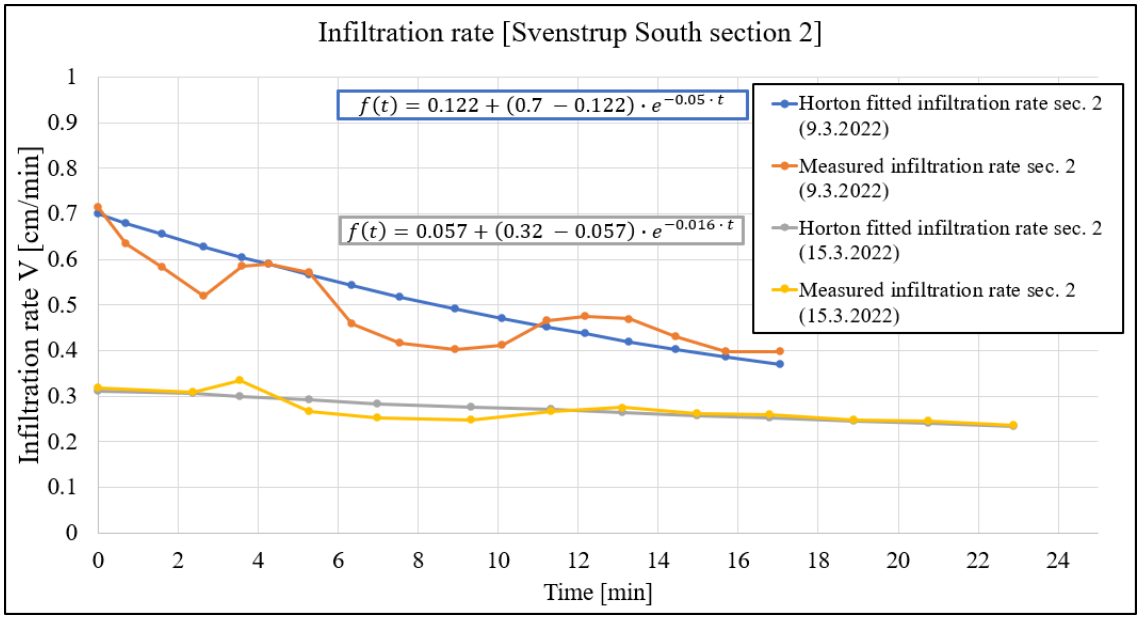

Figure C.2. Infiltration measurements using single ring infiltrometer test and fitted Horton's infiltration for Skjoldet. Both runs are unsaturated runs for section 2, with the Horton equation fitted to the infiltrometer measurements. Infiltration rates are given in cm/min. The Horton's equation is presented colour coded to corresponding curve.

C.2 Marshalls Allé results

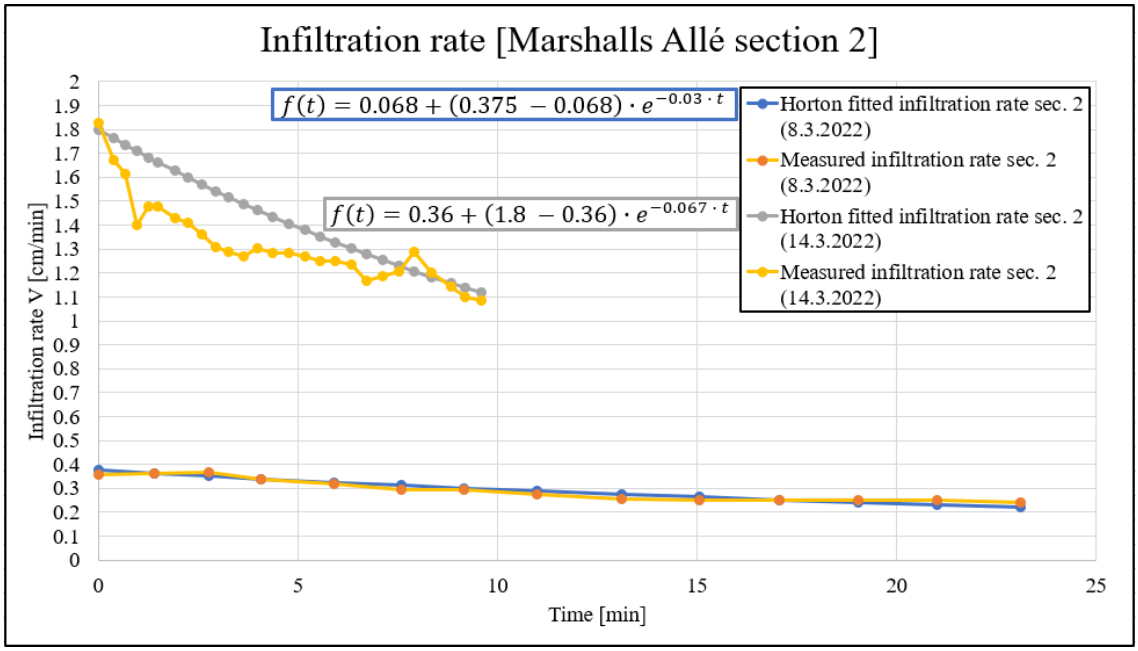

Figure C.3. Infiltration measurements using single ring infiltrometer test and fitted Horton's infiltration for Marshalls Allé. Both runs are unsaturated runs for section 2, with the Horton equation fitted to the infiltrometer measurements. Infiltration rates are given in cm/min. The Horton's equation is presented colour coded to corresponding curve.

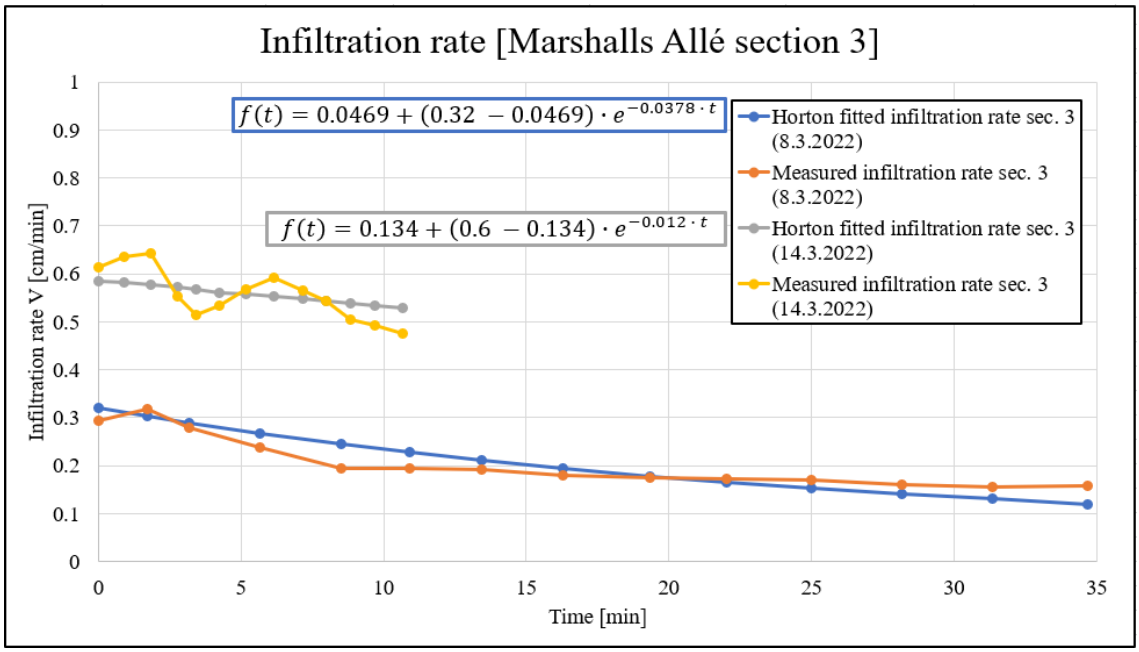

Figure C.4. Infiltration measurements using single ring infiltrometer test and fitted Horton's infiltration for Marshalls Allé. Both runs are unsaturated runs for section 3, with the Horton equation fitted to the infiltrometer measurements. Infiltration rates are given in cm/min. The Horton's equation is presented colour coded to corresponding curve.

Non-linear regression for determination of suction head

D

An empirical relationship based on a non-linear regression, applied by a power function in Excel, has been chosen for the determination of suction head as a function of saturated hydraulic conductivity. The relation has been based on Rawls et al. [1983] who published a comprehensive compilation of Green-Ampt parameters, based on soil water data for approximately 1200 soils in the United States. From D.1 the power function applied for determination of suction head is presented and the corresponding R^2-value.

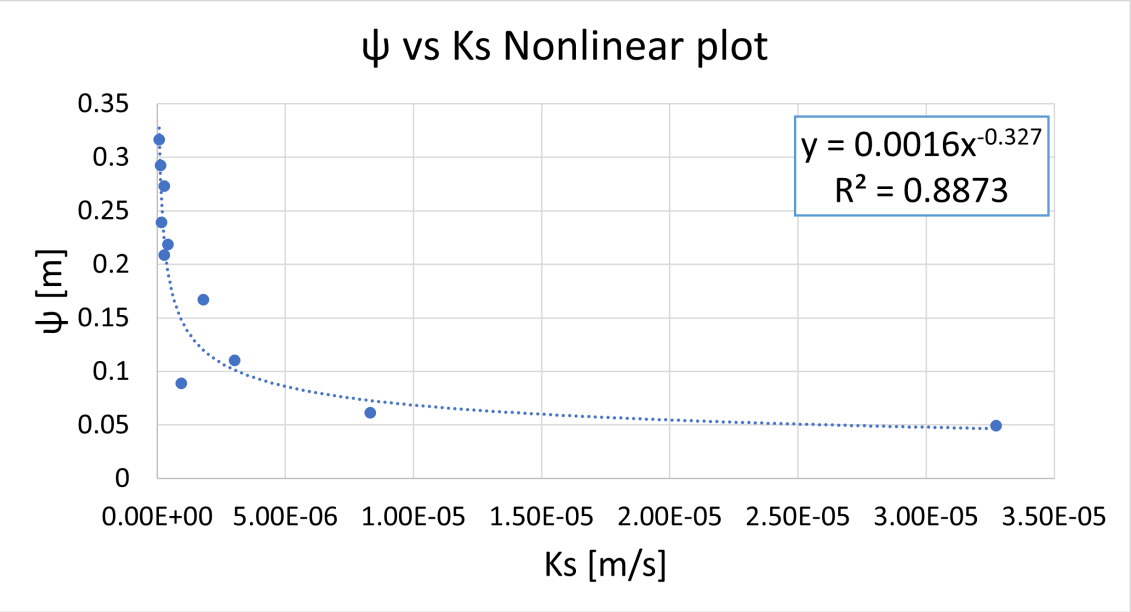

Figure D.1. Non-linear regression based on values from Rawls et al. [1983], presenting the relation between suction head (ψ) and saturated hydraulic conductivity (K_s).

Calculation of empirical saturated hydraulic conductivities

E

In the following appendix, empirical saturated hydraulic equation are presented. Three empirical formulae are applied:

1. The U.S Bureau of Reclamation (USBR) [Blohm, 2016]
2. Kozeny-Carman [Carrier, 2003]
3. Nielsen et. al. [Nielsen et al., 2018]

Units are presented in the unit applied for calculations. A comparison for Ks values is afterwards applied. Values within a parentheses indicates the applied value for calculations of constants. Other values applied are presented within the master thesis.

USBR

$$K_s = \beta \cdot \frac{g}{v} \cdot d_{20}^{2.3} \tag{E.1}$$

Where,

K_s	Saturated hydraulic conductivity	$[cm/s]$
β	Fitting parameter $(4.8 \cdot 10^{-4})$	[/]
g	gravitational constant	$[\frac{m}{s^2}]$
v	kinematic viscosity $(10 \circ C)$	$[\frac{mm^2}{s}]$
d_{20}	diameter corresponding to 20% cumulative diameter	$[mm]$

Kozeny-Carman

$$K_s = \beta \cdot \frac{\rho \cdot g}{\mu} \cdot \frac{n^3}{(1-n)^2} \cdot d_{10}^2 \tag{E.2}$$

Where,

K_s	Saturated hydraulic conductivity	[cm/s]
β	Fitting parameter $(\frac{1}{180})$	[/]
ρ	Density	$[kg/m^3]$
g	gravitational constant	$[\frac{m}{s^2}]$
μ	kinematic viscosity $(10 \circ C)$	$[Pa \cdot s]$
n	Porosity	$[\frac{cm^3 pores}{cm^3 soil}]$
d_{10}	diameter corresponding to 10% cumulative diameter	$[mm]$

Nielsen et. al.

$$K_s = A \cdot \phi \cdot (\frac{CS + B \cdot FS}{CL + R_D \cdot OM})^P_{NC} \tag{E.3}$$

Where,

K_s	Saturated hydraulic conductivity	$[cm/s]$
A	Fitting parameter (3.1)	[/]
ϕ	Total porosity	$[m^3/m^3]$
CS	The fraction of coarse sand	$[\frac{kg}{kg}]$
B	Particle size 20-200µm (0.25)	$[m]$
FS	The fraction of fine sand	$[\frac{kg}{kg}]$
CL	The fraction of clay	$[\frac{kg}{kg}]$
R_D	The relative density (2.65)	[-]
OM	The fraction of organic matter	$[\frac{kg}{kg}]$
P_{NC}	The pore network connectivity (1.8)	[-]